



HAL
open science

Microbial metabolic activity in metal(loid)s contaminated sites impacted by different non-ferrous metal activities

Hao Li, Jun Yao, Ning Min, Geoffrey Sunahara, Jianli Liu, Miaomaio Li, Bang Liu, Wancheng Pang, Ying Cao, Ruofei Li, et al.

► To cite this version:

Hao Li, Jun Yao, Ning Min, Geoffrey Sunahara, Jianli Liu, et al.. Microbial metabolic activity in metal(loid)s contaminated sites impacted by different non-ferrous metal activities. *Journal of Hazardous Materials*, 2023, 459, pp.132005. 10.1016/j.jhazmat.2023.132005 . hal-04189888

HAL Id: hal-04189888

<https://univ-pau.hal.science/hal-04189888>

Submitted on 25 Mar 2024

HAL is a multi-disciplinary open access archive for the deposit and dissemination of scientific research documents, whether they are published or not. The documents may come from teaching and research institutions in France or abroad, or from public or private research centers.

L'archive ouverte pluridisciplinaire **HAL**, est destinée au dépôt et à la diffusion de documents scientifiques de niveau recherche, publiés ou non, émanant des établissements d'enseignement et de recherche français ou étrangers, des laboratoires publics ou privés.

Journal of Hazardous Materials

New insights on the effect of non-ferrous metal mining and smelting activities on microbial activity characteristics and bacterial community structure

--Manuscript Draft--

Manuscript Number:	HAZMAT-D-23-01105R2
Article Type:	Research Paper
Keywords:	Mining and smelting activities; Heavy metal(loid)s pollution; Microbial metabolic activities; Bacterial community; Phenotypes
Corresponding Author:	Jun Yao, Ph.D China University of Geosciences Beijing School of Water Resources and Environment Beijing, CHINA
First Author:	Hao Li
Order of Authors:	Hao Li Jun Yao, Ph.D Ning Min Geoffrey Sunahara Robert Duran
Suggested Reviewers:	<p>Fei Wang Beijing Normal University wangfei@ustb.edu.cn Research areas: 1. Environmental behavior and biological effects of environmental pollutants (nanoparticles, organic pollutants, heavy metals); 2. Environmental functional nanomaterials; 3. Phosphorus behavior in lake water; 4. Mining pollution mechanism and restoration</p> <p>Huilun Chen University of Science and Technology Beijing chenhuilun@ustb.edu.cn Main research directions: Environmental toxicology expert, research direction is the environmental toxicological effects of pollutants such as mining area pollutants, pesticides and heavy metals.</p> <p>Yi Wang Anhui Agricultural University wangyi@ahau.edu.cn Main research direction: Environmental risk and management of toxic pollutants. New pesticide creation, pesticide residues, fluorescent sensors, agricultural product quality and safety.</p> <p>Bin Chen Beijing Normal University chenb@bnu.edu.cn Research direction: Environmental risk and management of heavy metal pollution in industrial activity polluted sites.</p> <p>Zhi Dang South China University of Technology chzdang@scut.edu.cn Research directions: 1. Research on environmental geochemistry and biogeochemical processes (migration, transformation, enrichment and fate) of heavy metals and harmful elements in ecosystems; 2. Research on chemical forms, bioavailability and toxicology of heavy metals in the environment; 3. Bioremediation technology for soil and water polluted by organic pollutants.</p>

	<p>Wenshen Su Sun Yat-sen University shuwensheng@m.scnu.edu.cn Research direction: Ecological restoration of mining wasteland, vegetation characteristics of heavy metal anomaly areas in China, succession of heavy metal contaminated soil ecosystem and molecular ecological characteristics, etc.</p>
	<p>Rongbing Fu Tongji University furongbing@tongji.edu.cn Research direction: 1. Research on pollution hydrogeology and environmental process and effect of pollutants in site system; 2. Research and application of site environmental survey methodology; 3. Research and engineering of risk control and collaborative remediation technology for contaminated soil and groundwater; 4. Research on prevention and control system and treatment technology of heavy metal pollution; 5. Comprehensive diagnosis and repair technology and application of water environment.</p>
	<p>Deyi Hou Tsinghua University houdeyi@tsinghua.edu.cn Research direction: 1. Development and optimization of green and sustainable remediation technology; 2. Life-cycle modeling of secondary pollutants during remediation of contaminated sites; 3. Sustainability assessment of environmental remediation; 4. Impact of environmental policy and environmental management on green and sustainable restoration.</p>
	<p>Shengguo Xue Central South University sgxue@csu.edu.cn Main research directions: Remediation of nonferrous metal smelting sites, lateritic soil technology of aluminum industry, emergency management of environmental emergencies, remediation of heavy metal pollution environment, and ecological reconstruction of mine wasteland</p>
	<p>Hefa Cheng Peking University hefac@pku.edu.cn Research directions: Migration and transformation of organic pollutants at the mineral-water interface, geochemical behavior of typical heavy metals in environmental media, remediation of groundwater pollution, and systematic analysis of environmental problems in China's water resources and energy utilization.</p>

Dear Editor,

We wish to submit the attached revised manuscript (HAZMAT-D-23-01105R2)

“New insights on the effect of non-ferrous metal mining and smelting activities on microbial activity characteristics and bacterial community structure” by Li et al., to be considered for publication in the *Journal of Hazardous Materials*.

No conflict of interest exists with the submission of the present work. This manuscript was approved by all authors for publication. I declare on behalf of my co-authors that the work described was original research and has not been published previously or is not under consideration for publication elsewhere.

Mining and smelting activities pose potentially serious heavy metal(loid)s problems to their surrounding ecosystems and residents. Studies on microbial metabolic activities, community structure, and adaptation in the soils proximal to non-ferrous metal mining and smelting areas are still lacking. Here geochemical and microbial characteristics of soil taken from sites surrounding inactive and active nonferrous metal mine smelting facilities were studied by analyzing microbial enzyme activity, microcalorimetry, and high-throughput sequencing of 16S rRNA gene barcoding. We hypothesize that the microbial communities in soils proximal to nonferrous metal mining and smelting sites are influenced by these neighboring activities.

The research aims were to 1) Determine the microbial metabolic activity and bacterial communities structure characteristics in contaminated soil around active and inactive nonferrous metal mining and smelting sites in Southwest China, and 2) Identify and compare the main factors affecting the microbial characteristics of the studied nonferrous metal-contaminated sites. The present study provides new insights into soil microbial characteristics after environmental disturbances from different mining and smelting activities.

This revised paper has 10811 total number of words, 0 Tables, and eight Figures.

We deeply appreciate your consideration of our manuscript, and we look forward to receiving comments from the reviewers. I hope this paper is suitable for publication in your journal. If you have any queries, please contact me at the address below. Thank you and with best regards,

Yours sincerely,

Jun Yao, Ph.D.

Professor,
School of Water Resources and Environment,
Research Center of Environmental Sciences and Engineering,
China University of Geosciences (Beijing), 100083, PRC.

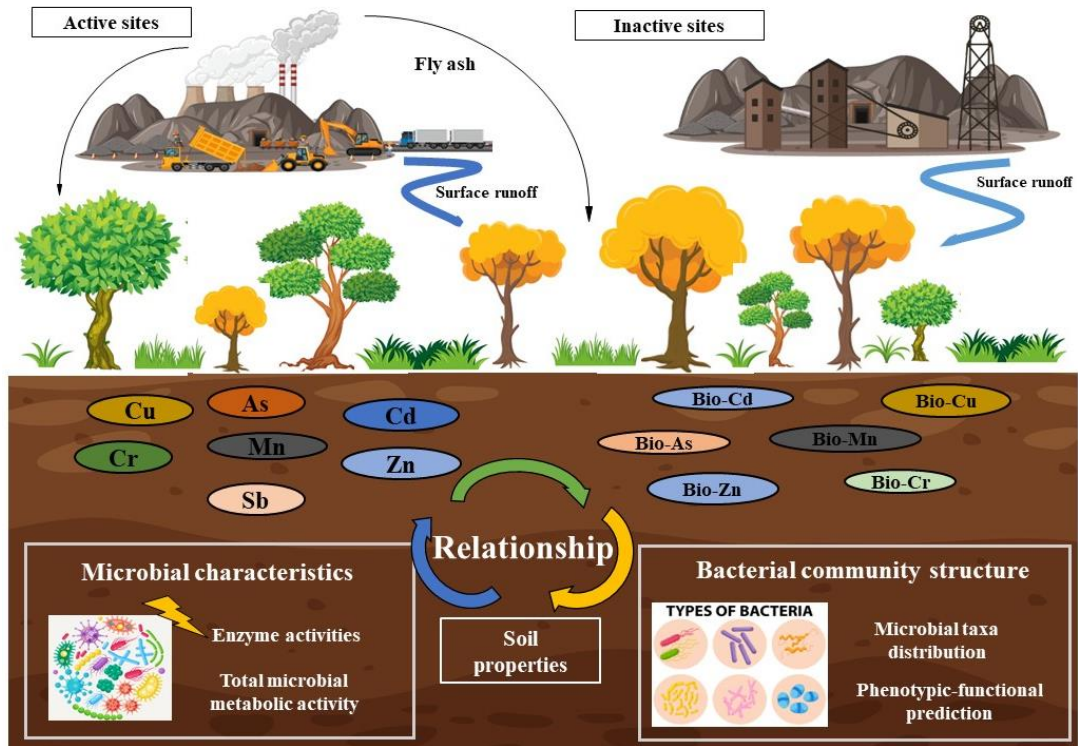
☎ +86-10-82321958

yaojun@cugb.edu.cn

Environmental Implication

Mining and smelting activities can bring hazardous trace metal(loid)s pollution to their surrounding locale. Studies on microbial metabolic activities, community structure, and adaptation in the soils proximal to metal smelting areas are lacking. Geochemical and microbial studies were undertaken on soils from sites surrounding active and abandoned nonferrous metal mine smelters. High throughput studies showed that many soil bacterial groups exhibited different response patterns to each heavy metal(loid), implying that the microbial communities were shaped jointly by aerial fugitive multiple trace metal(loid)s and possibly microbes. The present studies provide a comprehensive and theoretical basis for the future bioremediation of non-ferrous metal-contaminated sites.

Graphical abstract



1 **Highlights**

- 2 ● Soils around nonferrous metal-contaminated sites were barren and heterogeneous.
- 3 ● Microbial characteristics differed among different research sites.
- 4 ● Acid phosphatase and microcalorimetric total heat indicated microbial activity.
- 5 ● As, Cd, and Cu are the main factors affecting bacterial composition.
- 6 ● *Actinobacteriota*, *Proteobacteria*, and *Chloroflexi* were the dominant phyla.

Response to the Reviewers

Dear Editor and Reviewers:

Thank you for your comments on our manuscript HAZMAT-D-23-01105R2 “New insights on the effect of non-ferrous metal mining and smelting activities on microbial community structure and function” by Li *et al.*

We found your comments valuable and very helpful for improving the quality of our paper, as well as providing significant guidance to our research. We have carefully followed your comments and have made corrections. Revised parts are marked in red in the main text. The main corrections in the paper and our responses to the Reviewers’ comments are stated below. We sincerely hope that the present revised manuscript meets your approval.

Comments from the Reviewers:

Reviewer #1: The authors have revised the manuscript according to my comments. I suggest it can be accepted by the journal.

Response: Thank you for this recommendation.

Reviewer #2: I think that the revised manuscript could be published in JHM.

Response: Thank you for this recommendation.

Reviewer #3: I find that the authors have put considerable efforts into addressing the reports of the referees. As a result, the paper is very much improved and I have no problem in recommending it for publication.

Response: Thank you for this recommendation.

Reviewer #4: The quality of the revised manuscript has been improved a lot, with point by point author responses to the reviewers' comments and suggestions. Thus, I recommend it be accepted for publication.

Response: Thank you for this recommendation.

Reviewer #5: The revised manuscript is in good shape, and I am ready to recommend acceptance once the authors address the following minor comments:

Response: Thank you for your suggestions. We hope that the following corrections to the main text will address the Reviewer's comments.

Comment 1: The authors should pay attention to that the size of characters marked on the map in figure S2, figure S3, and figure 1 is not consistent, and the map of China is distorted. Please make corresponding amendments.

Response: Thank you for your suggestions. We have made the corrections according to this Reviewer's comments.

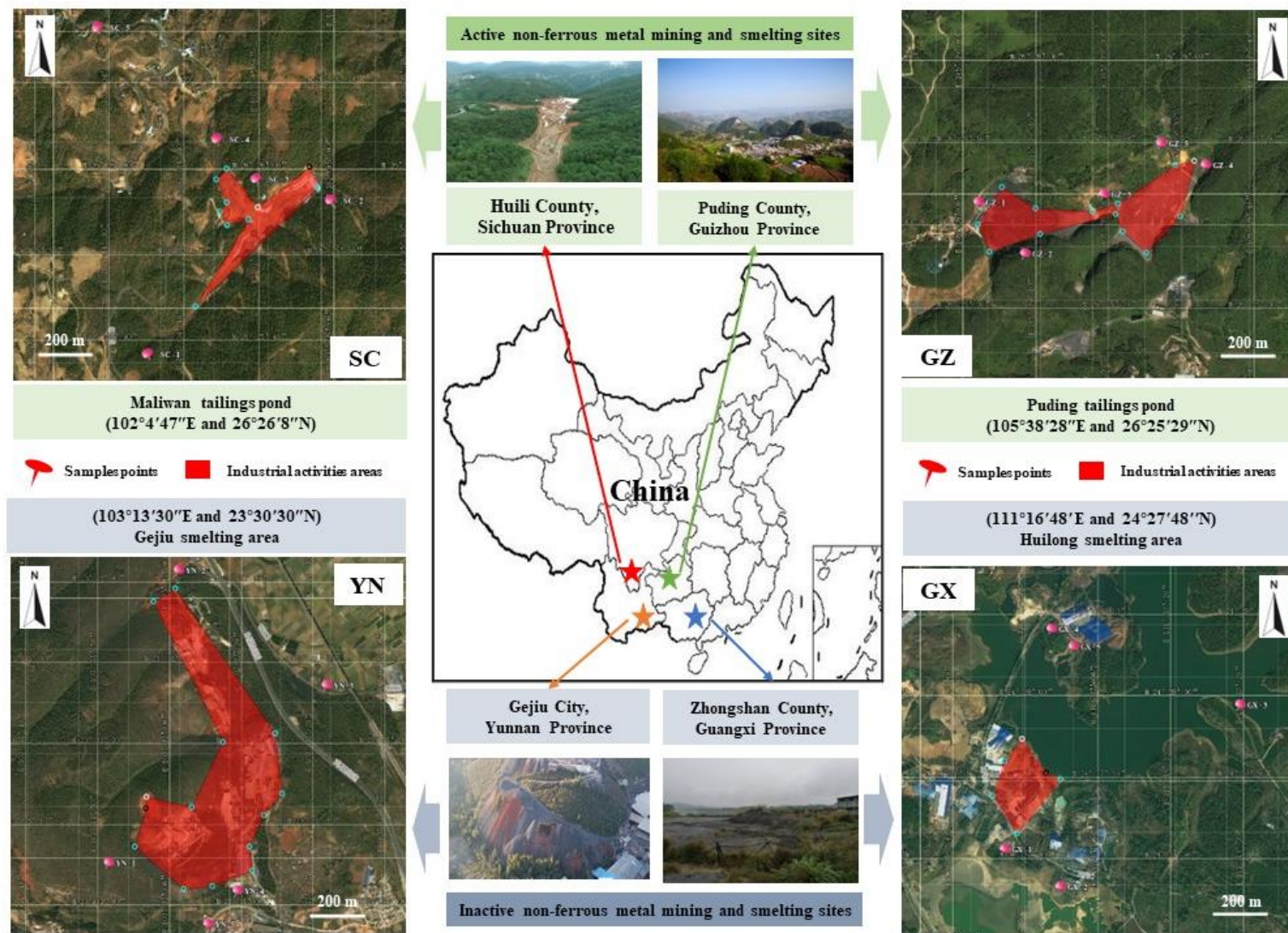
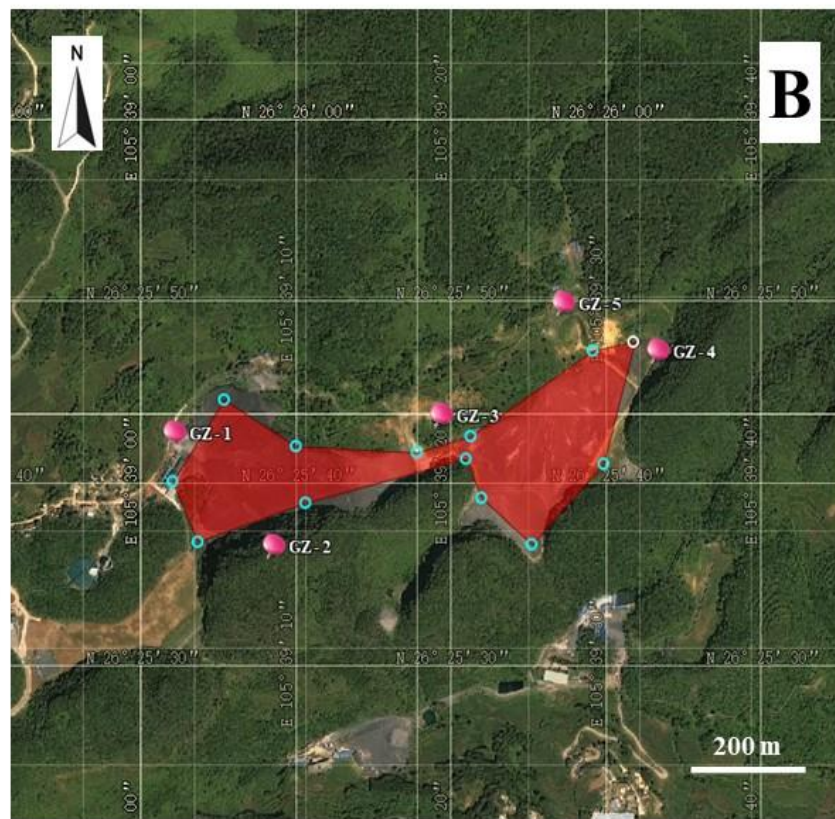
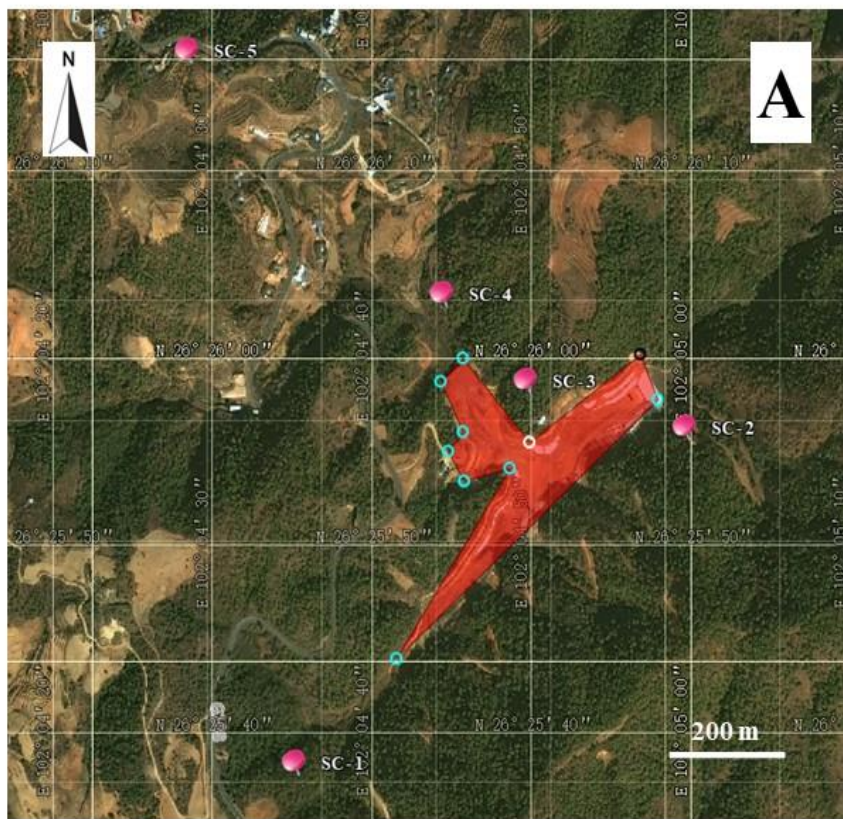


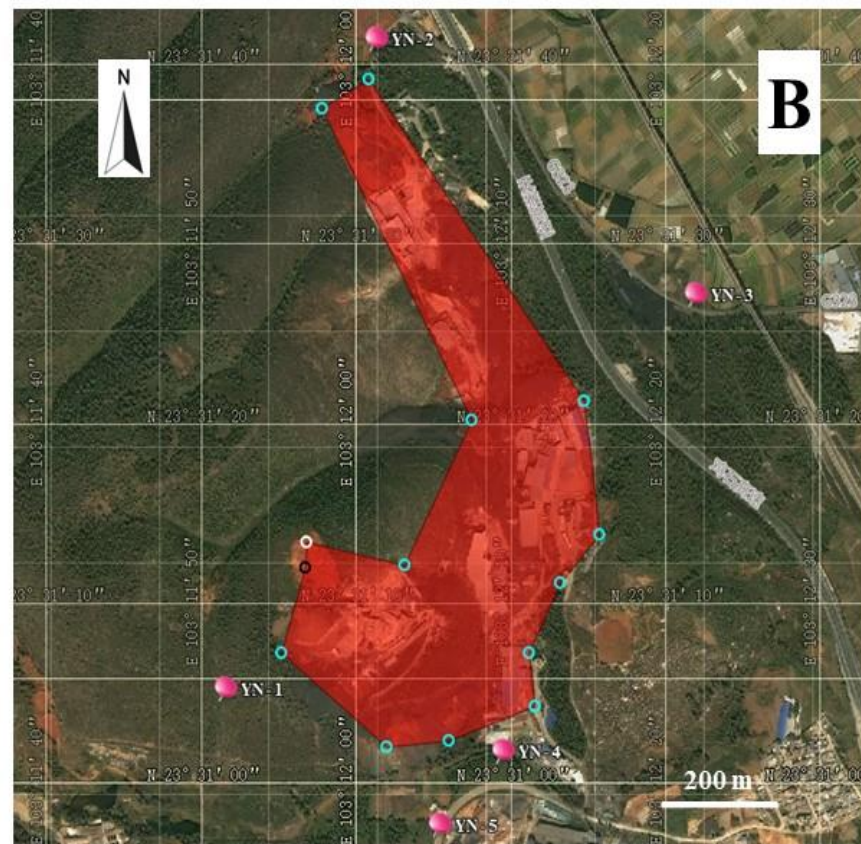
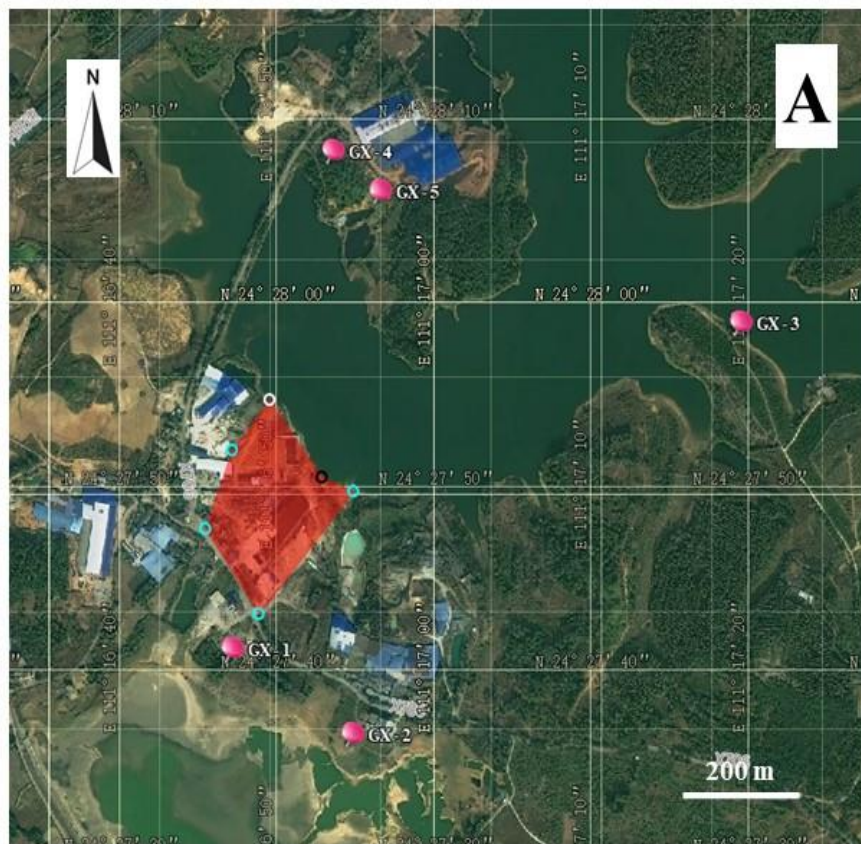
Fig. 1. Locations and photos of four non-ferrous metal mining and smelting activities affected areas in Southwest China. The distributions of sampling points of active sites (SC and GZ) and inactive sites (YN and GX) are shown in the top and bottom panels, respectively (also see Supplementary Information, Figs. S1 and S2).



 Samples points
  Industrial activities areas

 Samples points
  Industrial activities areas

Fig. S1. The distributions of sampling points of active sites (SC and GZ) are shown in the left (A) and right (B) panels, respectively.



 Samples points
  Industrial activities areas


 Samples points
  Industrial activities areas

Fig. S2. The distributions of sampling points of inactive sites (GX and YN) are shown in the left (A) and right (B) panels, respectively.

Comment 2: It is suggested that the importance and necessity of phenotypic-functional prediction of bacterial communities should be raised in the part of introduction.

Response: Thank you for your suggestions. We have made the corrections according to this Reviewer's comments.

Line 82-87 (Introduction) now reads: Phenotypic plasticity is widespread in the biological world, but relatively few studies have been conducted in the field of microorganisms (Ward et al., 2017). Phenotypic predictive research based on soil bacterial communities is important for understanding the adaptability of microbial populations, as well as for protecting the ecological environment and maintaining species coexistence (Zhang et al., 2019b).

We added a new reference.

Line 818-820:

Ward, T., Larson, J., Meulemans, J., Hillmann, B., Lynch, J., Sidiropoulos, D., Spear, J., Caporaso, G., Ran, B., Knight, R., 2017. BugBase predicts organism level microbiome phenotypes. bioRxiv. <https://doi.org/10.1101/133462>.

Comment 3: Line 544. Please correct the "microbial" to "bacterial".

Response: Thank you for your suggestions. We have made the corrections according to this Reviewer's comments.

Line 554: 3.7. *Phenotypic-functional prediction of **bacterial** communities*

Other minor modifications marked in red in the article

1 New insights on the effect of non-ferrous metal mining and smelting activities
2 on microbial activity characteristics and bacterial community structure

3

4

5 Hao Li^a, Jun Yao^{a,*}, Ning Min^a, Geoffrey Sunahara^{a,b}, Robert Duran^{a,c}

6

7

8 ^a School of Water Resources and Environment, Research Center of Environmental Science
9 and Engineering, China University of Geosciences (Beijing), 29 Xueyuan Road, Haidian
10 District, 100083, Beijing, China

11 ^b Department of Natural Resource Sciences, McGill University, 2111 Lakeshore Drive, Ste-
12 Anne-de-Bellevue, Quebec, H9X 3V9, Canada

13 ^c Universite de Pau et des Pays de l'Adour, E2S-UPPA, IPREM 5254, BP 1155, 64013 Pau
14 Cedex, France

15

16

17

18

19 * Corresponding author. School of Water Resources and Environment, Research Center of
20 Environmental Science and Engineering, China University of Geosciences (Beijing), 29
21 Xueyuan Road, Haidian District, 100083 Beijing, China, E-mail: yaojun@cugb.edu.cn (J.
22 Yao), Tel: +86-10-82321958.

23

24 **Abstract**

25 Mining and smelting activities have brought potentially serious heavy metal(loid) pollution to
26 their surrounding locale. However, studies on microbial metabolic activities, community
27 structure, and adaptation in soils proximal to non-ferrous metal mining and smelting areas are
28 still lacking. Here the effects of biotic and abiotic characteristics of soil taken from sites
29 surrounding inactive and active nonferrous metal mine smelting facilities on microbial
30 enzyme activity, microcalorimetry, and high-throughput sequencing of 16S rRNA gene
31 barcoding were studied. Data indicated that the soils were heavily polluted by toxic
32 metal(loid)s, of which As and Cd are the main contaminants. Microbial acid phosphatase
33 activity and microcalorimetric total heat value were sensitive metabolic indicators in the
34 studied areas. *Actinobacteriota* had the highest relative abundance, followed by
35 *Proteobacteria*, *Chloroflexi*, and *Acidobacteria*. Microbial metabolic activity and bacterial
36 community structure and phenotype varied between inactive and active sites ($p < 0.05$). Such
37 analyses indicated that electrical conductivity, total As, Cu, and Mn contents, and
38 bioavailable As, Cu, Cd, and Mn concentrations were key factors determining microbial
39 activities, bacterial community structure, and phenotypes. Knowledge of microbial adaptation
40 to heavy metal stressors is important for better understanding the aerial transfer of fugitive
41 heavy metals (and possibly microbes) and for designing future strategies for improved soil
42 bioremediation.

43 **Keywords:** Mining and smelting activities, Heavy metal(loid)s pollution, Microbial
44 metabolic activities, Bacterial community, Phenotypes

45 **1. Introduction**

46 Industrial activities including mining and smelting, production of used Pb-acid batteries,
47 tanneries, and dye production, and agriculture are key sources of potentially toxic metal
48 pollution causing serious global environmental issues and have drawn considerable scientific
49 attention (Hu et al., 2021; Guo et al., 2021b). In recent decades, the long-term large-scale
50 non-ferrous metal mining and smelting activities in China have produced a large amount of
51 waste gas and water, as well as waste residues, carrying a variety of toxic heavy metal(loid)s
52 (e.g., As, Cr, Cu, Ni, Pb, and Zn) (Li et al., 2020; Ke et al., 2022; Zeng et al., 2022). These
53 environmental contaminants have invaded farmland and forests causing continuous damage
54 to their surrounding environments (Li et al., 2020; Guo et al., 2021b).

55 The soil ensures important ecosystem services, including material cycling, information
56 transfer, energy flow, and the microbial-mediated biogeochemical cycling of key
57 metal(loid)s (Liu et al., 2021). In environments contaminated by tailings and smelting waste,
58 excess heavy metals can affect microbial metabolic activities in soil (Chun et al., 2021). Soil
59 microbial activities are involved in the storage and cycling of nutrients in the soil (Batista et
60 al., 2020). Soil enzyme activities (phosphatase, invertase, and urease) have been used as
61 biochemical markers (biomarkers) of soil microbial nutrient (C, N, and P) effects and
62 metabolic activity (Chae et al., 2017; Aponte et al., 2021). Other soil biomarkers such as
63 fluorescein diacetate hydrolase (FDA) reflect the total microbial activity (Schnurer and
64 Rosswall, 1982), whereas isothermal microcalorimetry can be used as a quantitative and real-
65 time measure of the total metabolic activity of microbial communities in soil (Herrmann et

66 al., 2014). Microbial enzymatic and total metabolic activities are considered sensitive and
67 effective indicators of soil health in mining and smelting ecosystems (Vinhai-Freitas et al.,
68 2017; Yuan et al., 2021).

69 As important components of soil, microbial communities also play a key role in the
70 ecological functions of energy and nutrient cycling (Guo et al., 2021a; Li et al., 2022b).

71 Bacteria are important members of the soil ecosystem, interacting with plants or fungi to
72 change and adapt to the soil environment (Chun et al., 2021). Therefore, soil microbial
73 characteristics can be used as potential indicators of ecosystem health (Li et al., 2020).

74 Although tailings and smelting sites are often described as metal-rich and nutrient-poor
75 environments, certain microorganisms can tolerate highly toxic environmental conditions by

76 developing specific survival strategies for their growth on contaminated sites (Chun et al.,
77 2021). These strategies include detoxification, metal resistance, and cellular oxidative stress

78 responses (Jiang et al., 2021). Many heavy metal-resistant microorganisms (e.g., dominant
79 soil phyla including *Actinobacteria*, *Proteobacteria*, *Chloroflexi*, and *Acidobacteriota*) can be

80 found in various polluted environments (Li et al., 2020; Yin et al., 2023). Differences in

81 microbial community structure between active and inactive nonferrous metal smelting sites

82 have been reported earlier (Liu et al., 2018). Phenotypic plasticity is widespread in the

83 biological world, but relatively few studies have been conducted in the field of

84 microorganisms (Ward et al., 2017). Phenotypic predictive research based on soil bacterial

85 communities is important for understanding the adaptability of microbial populations, as well

86 as for protecting the ecological environment and maintaining species coexistence (Zhang et

87 al., 2019b).

88 The soil properties including the bioavailable and total contents of heavy metal(loid)s may
89 vary greatly between different mining and smelting sites (Liu et al., 2021; Yin et al., 2023).
90 Earlier studies show that the total concentrations of As, Cd, Co, Cr, Cu, Mn, Ni, and Pb are as
91 important as their bioavailable contents by influencing the soil microbial community
92 structure (Yin et al., 2023). The exchangeable (EXC) content of heavy metal(loid)s is often
93 regarded as the bioavailable fraction in soil, using the European Community Bureau of
94 Reference (BCR) sequential extraction procedure (Zhu et al., 2018). The pollution load index
95 (PLI) and contamination factor (CF) can be used to assess the pollution degree of heavy
96 metal(loid)s in soil (Rinklebe et al., 2019). Although complex interactions between soil
97 properties, heavy metal(loid)s, microbial metabolic activities, and microbial communities
98 have been reported (Yan et al., 2020), few studies have addressed how these important factors
99 (heavy metal(loid)s and soil properties) and processes affect microbial metabolic activities
100 and bacterial communities in contaminated soils surrounding active and inactive nonferrous
101 metal mining and smelting sites.

102 Most nonferrous metal smelting and collection activities in Southwest China are located in
103 karst landforms, so mobile heavy metals are often highly diffusible and can disperse within
104 the environment, especially through runoff or atmospheric deposition. Long-term mining and
105 smelting of non-ferrous metals have caused serious damage to the health of the local soil
106 environment (Liu et al., 2022a; Zhang et al., 2020). Compared to active nonferrous metal
107 smelting sites, microbial communities present in mine tailings at inactive or abandoned
108 facilities can adapt (by long-term natural attenuation) to their nonferrous metal(loid)s-
109 containing environments (Liu et al., 2018). Therefore, there are few studies on the microbial

110 characteristics and bacterial community structure of the surrounding soil caused by the non-
111 ferrous metal activities in different states (inactive and active).

112 Here we hypothesize that the microbial communities in soils proximal to nonferrous metal
113 mining and smelting sites are influenced by these neighboring activities. The research aims
114 were to 1) Determine the microbial metabolic activity and bacterial communities structure
115 characteristics in contaminated soil around active and inactive nonferrous metal mining and
116 smelting sites in Southwest China, and 2) Identify and compare the main factors affecting the
117 microbial characteristics of the studied nonferrous metal-contaminated sites. The results
118 described here will provide new insights into soil microbial characteristics after
119 environmental disturbances from different mining and smelting activities.

120 **2. Materials and methods**

121 *2.1. Study areas*

122 The soil samples were collected in triplicate from the topsoil (depth of 0-20 cm) of forest land
123 proximal to two active, and two inactive sites non-ferrous metal mining and smelting sites
124 (Fig. 1). It was assumed that the forest land surrounding the smelter sites were not influenced
125 by extraneous anthropogenic factors such as agricultural tilling, use of chemical and
126 biological fertilizers, domestic hazardous waste, and roadside emissions.

127 The active Lumaolin Pb-Zn tailing pond (GZ) was located in Puding County, Guizhou
128 Province (105°38'28"E, 26°25'29"N) (Figs. 1 and S1). The metal minerals are mainly
129 sphalerite, smithsonite, and galena. The site GZ started production after 2008. Samples were
130 collected from five representative points (GZ-1, GZ-2, GZ-3, GZ-4, and GZ-5). Additional

131 information is provided in Supplementary Information (Text S1.1). The active Maliwan Cu-
132 Ni tailing pond (SC) was located in Huili County, Sichuan Province (102°4'47"E, 26°26'8"N)
133 (Figs. 1 and S1). The tailings are mainly copper-nickel beneficiation smelting slag, nickel-
134 iron processing plant waste, and calcium sulfate slag. Samples were collected from five
135 representative points (SC-1, SC-2, SC-3, SC-4, and SC-5).

136 The inactive Gejiu Pb smelting site (YN) was located in Gejiu City, Yunnan Province
137 (103°13'30"E, 23°30'30"N) (Figs. 1 and S2). A large amount of waste residue was stored at
138 this smelting area typical of the lead smelting industry. Samples were collected from five
139 representative points (YN-1, YN-2, YN-3, YN-4, and YN-5). The inactive Huilong As
140 smelting site (GX) was located in Zhongshan County, Guangxi Province (111°16'48"E,
141 24°27'48"N) (Figs. 1 and S2). This site opened operations (producing metal arsenic, arsenic
142 trioxide, and other products) in 1994 but stopped production in 2003. Samples were collected
143 from five representative points (GX-1, GX-2, GX-3, GX-4, and GX-5).

144 All samples were collected using sterile tools and placed in biological storage bags (□ 1 kg
145 per sample), stored in ice packs, and quickly transported to the laboratory. Each collected soil
146 sample was divided into two sub-samples for subsequent testing, one of which was air-dried
147 (for 10 d) at room temperature, sieved (100-mesh) to remove rocks, animal, and plant debris,
148 etc., and stored at 4°C for geochemical and microbial analyses, and the other aliquot was
149 stored at -80°C for high-throughput sequencing. All chemicals and reagents were purchased
150 from commercial sources and were at least analytical grade purity.

151 ***2.2. Geochemical analyses and heavy metal(loid) pollution assessment***

152 The electrical conductivity (EC, expressed as $\mu\text{S}/\text{cm}$) and the pH of the soil were determined
153 in the slurry with the soil-to-water ratio of 1:2.5 and 1:5, respectively. The soil moisture
154 content (MC, as %) was measured by drying the soil sample in an oven ($105 \pm 2^\circ\text{C}$) for 8 h
155 until the weight remains constant (Li et al., 2020). The soil total organic carbon (TOC, mg/g)
156 in soil was determined using a TOC instrument (Shimadzu SSM-5000, Japan) (Zhu et al.,
157 2018). To determine the total amount of heavy metal(loid)s in soil, the following digestion
158 steps were taken. The air-dried soil sample was ground and sieved, and 0.100 g of pretreated
159 soil sample was weighed, and then added into a digestion tube containing $\text{HNO}_3\text{-HCl}$ (1:3,
160 volume/ volume). The tube was placed in a $140\text{-}180^\circ\text{C}$ heater for 2 h. If a solid residue
161 remained in the tube, a 2 mL volume of HF was added until a white sediment was formed.
162 The digested residue was then dissolved in a 1% HNO_3 solution and made up to 50 mL in a
163 volumetric flask. All experimental data were corrected by subtracting the blank group of
164 mixed acids prepared using the same digestion steps described above. The recovery rate of
165 total As, Cd, Cr, Cu, Fe, Mn, Ni, Pb, Sb, V, and Zn concentration in soil was between 92.5%
166 and 107.5%, and the relative standard deviation (RSD) was $< 5\%$. The concentrations of As,
167 Cd, Cr, Cu, Fe, Ni, Pb, Sb, V, and Zn were measured using an inductively coupled plasma
168 atomic emission spectrometer, with the detection limits of 0.03, 0.002, 0.004, 0.002, 0.002,
169 0.009, 0.03, 0.03, 0.004, and 0.005 mg/kg, respectively. The quality assurance and quality
170 control procedures are described in Text S1.2.

171 The bioavailable metal(loid) contents (EXC, Exchangeable fraction) (expressed as mg/g or
172 as % of total) were determined by using 0.11 M acetic acid solution of the BCR sequential
173 extraction method, as described in Text S1.2. The pollution load index (PLI) and

174 contamination factor (CF) were used to assess the pollution degree of heavy metal(loid)s in
175 the soil (Rinklebe et al., 2019). The calculation of these indices is described in Text S2.

176 **2.3. Microbial metabolic activity characteristics**

177 **2.3.1. Microcalorimetric measurements**

178 The total metabolic activity of microorganisms was measured using a Model TAM-IV (Fig.
179 S3) isothermal multichannel microcalorimeter (TA Instruments, Delaware, USA), as
180 described earlier (Herrmann et al., 2014). This technique provides qualitative and quantitative
181 information on microbial metabolic processes by generating power-time curves based on
182 microbial growth processes (see Text S3). Using the power-time curve, a variety of
183 thermodynamic parameters can be obtained, including peak time (T , expressed as h), total
184 heat (Q , J/g), growth rate (k , h^{-1}), and peak power (P , $\mu\text{W/g}$) (Zhu et al., 2018). The research
185 data calculated using microcalorimetry are similar to conventional microbiological methods
186 and can provide more detailed information on complex biological processes.

187 **2.3.2. Soil enzyme activity measurements**

188 Fluorescent diacetate hydrolase (FDA, expressed as mg fluorescein/g) was measured as a
189 reflection of the overall microbial activity. The following soil enzyme activities involved in
190 the metabolic cycling of nutrient elements (C, N, and P) were measured, as described by
191 others (Chae et al., 2017; Li et al., 2022a): invertase (INV; hydrolyzes sucrose to fructose and
192 glucose, expressed as mg glucose/g), urease (UA; hydrolyzes urea to carbon dioxide and
193 ammonia, mg NH_4/g), and acid phosphatase (APA; catalyzes the release of phosphate by
194 hydrolysis, mg p -nitrophenyl phosphate/g). Methodological details of the enzyme assays are

195 described in Text S4.

196 **2.4. DNA extraction, 16S rRNA gene sequencing**

197 Genomic DNA was extracted from the selected samples by 1% agarose gel electrophoresis,
198 and the V3-V4 hypervariable region fragment of the 16S rRNA gene was amplified by the
199 polymerase chain reaction (PCR). The primer sequence was 338F (5'-ACT CCT ACG GGA
200 GGC AGC AG-3') and 806R (5'-GGA CTA CHV GGG TWT CTA AT-3'). The 2% agarose
201 gel electrophoresis was used to verify the qualified PCR amplification. The PCR product was
202 further purified with E.Z.N.A.TM Gel Extraction Kit (OMEGA Bio-Tek Inc., USA). Bacterial
203 sequencing was carried out on the Illumina MiSeq platform of Majorbio Bio-Pharm
204 Technology Co., Ltd (Shanghai, China).

205 **2.5. Data processing and statistical analyses**

206 The raw sequencing data were optimized using Fastp software (v0.19.6,
207 <https://github.com/OpenGene/fastp>; accessed 22-March-2023) to filter raw reads. The raw
208 pair-end reads were processed with Flash software (v1.2.11)
209 (<https://ccb.jhu.edu/software/FLASH/index.shtml>; accessed 22-March-2023). During the
210 merging process, the allowable error rate for the pairing of overlapping regions was ≤ 0.2 and
211 resulted in high-quality sequences. Bacterial community diversity indexes, including alpha
212 (α) richness and diversity indices (Ace, Chao, Coverage, Shannon, Sobs, and Simpson) were
213 calculated using the "vegan" package. The calculation of the beta (β) diversity of the
214 microbial community was based on Bray Curtis distance similarity. The Analysis of
215 Similarity (ANOSIM) was used to analyze the availability of sample groupings. Hierarchical

216 clustering and principal coordinates analysis (PcoA) was used to analyze the differences in
217 bacterial communities among samples. Spearman's correlation and distance-based
218 redundancy (db-RDA) analyses were processed using the vegan package in R version 3.4.2 to
219 identify important environmental variables affecting bacterial community structure.
220 Differences between groups were considered significant at $p < 0.05$. Data were expressed as
221 the average \pm standard deviation (SD) unless otherwise stated. BugBase is a microbiome
222 analysis tool to identify high-level phenotypes in microbiome samples and enable phenotype
223 prediction. SPSS 22.0 software was used to calculate the statistical tests, as described in Text
224 S5.

225 **3. Results and discussion**

226 ***3.1. Geochemical characterization of the studied soils***

227 The geochemical properties of the soil from the different site soils are shown in Fig. S4 and
228 Tables S1-S4. The soil pH of sites GX, GZ, and YN was either weakly acidic or weakly
229 alkaline, whereas the SC soil was acidic (pH 4.84 – pH 5.89). These acidic and alkaline pH
230 signatures are typical of forest soils surrounding contaminated sites such as non-ferrous metal
231 smelting sites and tailing ponds (Zhao et al., 2020). The MC and EC values of sites GX, GZ,
232 SC, and YN differed greatly because the soil structure around the polluted sites was
233 heterogenous and complex (Zhao et al., 2020). The TOC contents of all samples were lower
234 than the average generic local soil background level (CNEMC, 1990), which agrees with the
235 fact that the surrounding soils of non-ferrous metal-contaminated sites are often nutrient-poor
236 (Batista et al., 2020). The large differences in soil properties are consistent with the high

237 degree of soil heterogeneity in the affected areas surrounding the studied mining and smelting
238 activities.

239 **3.2. Heavy metal(loid) contents**

240 The total heavy metal contents of soils sampled from the four study sites are summarized in
241 Fig. 2A and Tables S5-S9. The average total contents of As, Cd, Cr, Cu, Fe, Ni, Pb, Sb, V, and
242 Zn in the soil exceeded the local soil background value (CNEMC, 1990), especially the total
243 As, Cd, and Pb content that exceeded the standard values of Grade II for agricultural land.
244 This observation is not surprising given that nonferrous metal smelter sites are enriched with
245 nonferrous metal ores.

246 In soils from the inactive sites (respectively YN and GX), the average total contents (mg/kg)
247 of Cd (17.61 ± 19.72 and 18.14 ± 35.52), Cu (19913.52 ± 11650.05 and 756.99 ± 647.79),
248 and Ni (94.14 ± 13.61 and 782.63 ± 997.05) were higher than those from the active areas (SC
249 and GZ) (Fig. 2A). The average contents (mg/kg) of Cu (19913.52 ± 11650.05), Fe (91468.16
250 ± 30496.68), Pb (1234.48 ± 1053.83), and Sb (27.46 ± 8.14) in the YN site were higher than
251 in the other sites, whereas As (2985.16 ± 1214.52 mg/kg) in SC site was higher than that in
252 the other sites. Such results are consistent with earlier reports that As, Cd, Cu, Pb, Sb, and Zn
253 (especially As, Cu, and Cd) are the major heavy metal pollutants in nonferrous metal mining
254 and smelting areas (Liu et al., 2022a; Yin et al., 2023).

255 In the inactive site soils (respectively YN and GX), the average bioavailable metal contents
256 (mg/kg) of As (3.51 ± 3.29 and 3.70 ± 6.47), Cd (5.37 ± 8.54 and 9.25 ± 20.53), Cu ($88.66 \pm$
257 50.34 and 51.03 ± 111.35), Fe (56.01 ± 81.58 and 264.10 ± 574.69), Sb (0.22 ± 0.12 and 0.16

258 ± 0.23), and Zn (135.78 ± 176.17 and 136.39 ± 301.36) were significantly higher (Fig. 2B,
259 Table S10) than the active sites (respectively SC and GZ) as evidenced by As (0.44 ± 0.16
260 and 0.55 ± 0.03), Cd (0.89 ± 0.51 and 0.06 ± 0.05), Cu (0.19 ± 0.16 and 1.50 ± 0.37), Fe
261 (1.66 ± 1.21 and 3.26 ± 1.13), Sb (0.14 ± 0.06 and 0.09 ± 0.05), and Zn (115.08 ± 125.53 and
262 1.80 ± 0.36). In addition, the average bioavailable contents (mg/kg) of Cr (6.37 ± 1.43), Ni
263 (2.67 ± 2.61), Pb (54.32 ± 97.46), and V (0.08 ± 0.08) were highest in the soils from the YN
264 area.

265 The correlation analyses (Tables S11-S14) show that the total contents of Cd, Cu, Mn, and Ni
266 were significantly and positively correlated ($p < 0.05$) with their bioavailable metal contents.
267 The TOC had a significant positive correlation ($p < 0.05$) with the bioavailable contents of
268 Cd, Mn, and Sb (Table S13). A rich organic C in soil could lead to the release of heavy metal
269 ions from the mineral matrix, and then be re-adsorbed to organic C (as well as the surface of
270 other minerals) functional groups (Yin et al., 2023).

271 The bioavailability of heavy metals in soil can be increased in the presence of plant root
272 exudates (such as organic acids) and therefore could be affected by the diversity and
273 composition of indigenous plant species (Yin et al., 2023). The percentages of bioavailable
274 content (EXC fraction expressed as %) of As, Cd, Fe, Pb, and V in the inactive sites (YN and
275 GX) were higher than those in the active site (Table S11), whereas those of Cd were SC
276 (0.63), YN (30.50), GX (51.02) and GZ (17.44) sites, and of Mn were SC (7.69), YN (7.31),
277 GX (7.40), and GZ (4.41) sites. Compared to the other heavy metal(loid)s, Cd had the highest
278 bioavailability in the YN, GX, and GZ sites, probably because Cd can be mobilized in soil
279 following competition and/or ligand-induced desorption (Kubier et al., 2019). Overall, the

280 bioavailability of heavy metal(loid)s in soils collected close to the inactive sites (YN and GX)
281 was generally higher than that of soils collected close to the active sites (SC and GZ).
282 Fugitive dust particles carrying the measured heavy metals (including the total and
283 bioavailable fractions) were likely transferred off-site from the nearby smelter dump sites and
284 accumulated in the surrounding studied forest soils. By design, it is unlikely that the source of
285 the measured heavy metals from forest soil was from vehicular emissions or debris, but
286 dispersion from local agricultural sources should not be under-estimated.

287 The Contamination factor (CF) was calculated as the ratio of the measured total heavy
288 metal(loid)s contents with the corresponding local geochemical background values (CNEMC,
289 1990) and was used to assess the pollution level (Fig. 2C, Table S12). The CF index for As,
290 Cd, Pb, and Sb reached a “high pollution level” in soils proximal to the active (GZ and SC)
291 and inactive (GX and YN) sites. In addition, the Cr (10.12), Cu (27.23), Mn (3.57), Ni
292 (29.24) and Zn (65.46) in the GX site, and Cu (430.10), and Zn (10.86) in YN, and Zn
293 (19.97) in GZ reached “high pollution levels.”

294 The overall heavy metal pollution level of the surface soils was further assessed using the
295 pollution load index (PLI), which was calculated from the total contents of heavy metals and
296 local geochemical background values (CNEMC, 1990). The pollution index profile of the
297 four study sites was YN (1.81) > SC (1.74) > GX (1.68) > GZ (1.50). The PLI values were >
298 1 and indicated that all study sites were “heavily polluted” by heavy metal(loid)s, which may
299 be attributed to the weathering of metal minerals and the transport of flying dust that
300 contributes to the transfer of heavy metals from the smelter sites into the nearby collected soil
301 sites (Zhao et al., 2019; Liu et al., 2022b).

302 **3.3.1 Soil enzyme activities**

303 The microbial enzyme activities of microorganisms among the four research sites were
304 different (Fig. 3, Tables S1-S4). A previous study reported that soil geochemical properties,
305 geographical spatial distance, and metal(loid) concentrations are the main factors affecting
306 microbial differences among three non-ferrous metal-contaminated areas (Liu et al., 2022a).
307 The Spearman correlation analysis showed that the urease activity (UA) was negatively
308 related to MC and pH ($p < 0.01$) (Tables S13-S18), indicating that low MC or pH inhibited
309 UA. The TOC was positively related to FDA, APA, and INV activities ($p < 0.05$). It has been
310 reported that pH and TOC are important factors affecting soil enzyme activity and that TOC
311 could stimulate enzyme activity (Batista et al., 2020; Aponte et al., 2021). The FDA activity
312 was negatively correlated with Ni ($p < 0.05$), and UA activity was negatively related to the
313 bioavailable Mn, as well as total Mn, Pb, Sb, and Zn contents ($p < 0.05$). Enzymes related to
314 soil C-, N-, and P- cycling can be inhibited by heavy metal(loid)s, resulting in differences in
315 enzyme activities in the sampled soils (Aponte et al., 2021; Li et al., 2022b). The observed
316 enzymic inhibition likely involves the binding of metal(loid)s to the active site in the enzyme
317 leading to a more stable complex. Alternatively, the metal(loid)s could also decrease enzyme
318 synthesis and secretion leading to an inhibition of the soil microbial growth and reproduction
319 (Zhao et al., 2015). The enzyme activities (FDA, INV, APA, and UA) were correlated with
320 the total heavy metal(loid) concentrations (As, Mn, Ni, Pb, Sb, and Zn) as well as with the
321 bioavailable Mn and Cd (Tables S13-S18), confirming that forest soil enzyme activities can
322 be used as sensitive biological indicators of aerial heavy metal transfer (by fugitive dust
323 particles) from the neighboring active and inactive smelter facilities, similar to other reports

324 (Wahsha et al., 2017; Zhao et al., 2020).

325 **3.3.2 Total microbial activity using isothermal microcalorimetry**

326 The heat production curves reflecting the metabolic growth of the soil microbial community
327 among different research sites were different (Fig. 3E, Tables S1-S4). On the other hand, the
328 k and P were higher in the inactive sites (Fig. S5, Tables S1-S4). Other researchers noted that
329 the microbial characteristics of non-ferrous metal-contaminated areas in different regions are
330 affected by spatial geography, heavy metal(loid) contents, and edaphic factors (Liu et al.,
331 2022a). Spearman correlation showed that the P and k were significantly and negatively
332 related to the MC and pH ($p < 0.01$), whereas they were positively related to the UA activity
333 ($p < 0.05$) (Tables S13-S18). The bioavailable contents (EXC fractions) of Cr, Cu, and Fe
334 were negatively related to Q and T values ($p < 0.05$), which agreed with the fact that the high
335 concentrations of heavy metal(loid)s decreased the total activity of soil microbial
336 communities (Harris et al., 2012). Also, Q values were negatively related to the total contents
337 of As and Cu ($p < 0.05$), while T values were negatively related to total As contents ($p <$
338 0.05). Such observations suggest that the total content of As and Cu are likely the main
339 factors affecting the microbial activity in the soils proximal to the active and inactive
340 smelting facilities. High concentrations of metal(loid)s can damage and/or inhibit critical
341 microbial cell functions (Harris et al., 2012; Yan et al., 2020). In addition, Q is significantly
342 ($p < 0.05$) and negatively correlated with the total content of metal(loid)s (Cr, Cu, Fe, Mg,
343 Mn, Pb, and Zn) in a non-ferrous metal smelting contaminated site (Li et al., 2022a). Thus,
344 the thermodynamic parameters correlated with the total As and Cu concentrations and the
345 bioavailable Cr, Cu, and Fe contents may be sensitive indicators of microbial metabolic

346 activity in some but not all heavy metal(loid) polluted soils.

347 ***3.4. Microbial community alpha and beta diversities***

348 A dataset of 997,251 high-quality 16S rRNA gene sequences was generated. The average
349 sequence number per sample was 415 bp. The 8,206 OTUs were obtained from high-quality
350 sequences. Compared to a previous study (Liu et al., 2022a), the number of OTUs was low
351 probably because the high concentration of metal(loid)s can reduce microbial richness. The
352 platform sparse curve shown in the Pan/Core species curve (Fig. S6) indicated that the
353 sequencing depth collected most of the microbial community diversity and that the sample
354 size was sufficient. The α -diversity parameters significantly differed according to the site
355 (Fig. 4; Tables S14 and S15), suggesting that the toxic metal(loid)s concentration can shape
356 the microbial community as observed in a dynamic study (Xu et al., 2019). The microbial α -
357 diversity Simpson index (Table S15) was negatively correlated with bioavailable Cd and Mn
358 concentrations ($p < 0.05$). This is consistent with a previous report that toxic metal(loid)s
359 pollution harmed the microbial community (Li et al., 2020). The α -diversity indices were
360 significantly and positively related to the FDA, INV, and APA activities ($p < 0.05$) (Table
361 S14) in the active and inactive smelter sites, suggesting that differences in microbial enzyme
362 activity could reflect microbial diversity, as reported previously (Xiao et al., 2020). Venn
363 diagrams show that there are 1111 shared core OTUs between the four sites (Fig. 5A).
364 Principal co-ordinates analysis (PCoA), based on OTU distances, showed a separation
365 according to sites (Figs. 5B and 8; ANOSIM with 999 iterations, $R = 0.2343$, $p = 0.001$),
366 indicating that the microbial communities of the sites were distinct. Such observations
367 confirmed the possibility that the composition of bacterial communities was affected by the

368 land use, soil geochemical properties, and metal(loid)s content (Zhao et al., 2019). Off-site
369 transfer of heavy metals to the collected forest soil samples probably led to direct (e.g.,
370 decreased host site indigenous microbial metabolic activity and community abundance) and
371 indirect (e.g., stimulation of metal resistance traits and adapted abundance) effects on the new
372 host soil microbial community. This possibility is supported by the observed effects on soil
373 enzyme activities and microbial abundance. Data suggests that the microorganisms sensitive
374 to metal(loid) stress will decrease in abundance, whereas that of insensitive microorganisms
375 will increase. The following studies were conducted to determine the effects of the off-site
376 transfer on the microbial community composition.

377 **3.5. Microbial taxa distribution**

378 We identified OTUs belonging to 48 phyla, 152 classes, 348 orders, 539 families, and 1082
379 genera in soil samples around the four (two active and two inactive) contaminated sites. It
380 was challenging to identify or monitor control (reference) soils in this study. The microbial
381 community in typical healthy soils was considered as a reference for comparison with the
382 present results. The *Proteobacteria*, *Acidobacteria*, *Actinobacteria*, and *Chloroflexi* were the
383 most abundant bacterial phyla in healthy soil, with average relative abundances of 39%, 20%,
384 13%, and 3%, respectively (Janssen, 2006). Specifically, the average relative abundances (%)
385 of *Proteobacteria* in the contaminated forest soil around sites were SC (25.10), YN (15.01),
386 GX (21.84), and GZ (20.13), which is lower than that in healthy soil (39) (Fig. 5C). The
387 average relative abundances (%) of *Acidobacteria* in the contaminated soil around the SC,
388 YN, GX, and GZ sites were 18.33, 14.13, 11.59, and 17.29, respectively, which are lower
389 than those of healthy soil. However, the average relative abundances (%) of *Actinobacteria* in

390 the contaminated soil around sites were SC (21.61) YN (35.07), GX (23.19), and GZ (30.42),
391 higher than those in healthy soil (Fig. 5C). *Actinobacteria*, the most dominant phyla in the
392 soil surrounding mining and smelting activities in the current study, showed remarkable
393 resilience in heavy metal(loid)s environments with low nutrient contents (Qiao et al., 2021),
394 consistent with other studies (Zhang et al., 2019a). The relative abundance of dominant phyla
395 among the active/inactive sites (Fig. 5) may be due to the different adaptabilities of
396 microorganisms to survive in environments having sub-optimal pH, low nutrient conditions,
397 and metal(loid)s stress. *Actinobacteria* was unusually abundant in neutral and slightly acidic
398 environments (Chen et al., 2013). The relative abundance of *Actinobacteria* was significantly
399 and negatively correlated with pH ($p < 0.05$), indicating that changes in soil pH might have
400 affected the *Actinobacteria* enrichment (Fig. 6). Our data indicate that members of the
401 *Actinobacteria* can adapt to or resist high levels of heavy metal(loid)s pollution as previously
402 shown in marine sediments (Duran et al., 2015). This is evidenced by the inhibition of growth
403 and development at high metal(loid)s concentrations that would decrease their proportion in
404 the bacterial community (Chen et al., 2018). Similar main microbial communities were found
405 in abandoned non-ferrous metal tailings, gold tailings environments, and V-Ti magnetite
406 tailings (Kang et al., 2020; Yan et al., 2020). The ubiquity of *Actinobacteria* is mainly due to
407 the adsorption and complexation capacity of microorganisms, which aids in their adaptability
408 to harsh metal-rich environments (Wu et al., 2021).

409 Interestingly, the average relative abundances (%) of *Chloroflexi* in the contaminated soils
410 around the SC (24.10), YN (14.43), GX (24.79), and GZ (12.91) sites (Fig. 5C) were higher
411 than that in the healthy soil (3). Previous studies showed that *Chloroflexi* as well as a

412 *Proteobacteria* were enriched from sites disturbed by mining (Xiao et al., 2021). In heavy
413 metal-polluted soils, *Chloroflexi* was the main phylum with tolerance and resistance to heavy
414 metal stress (Yin et al., 2023). These studies pointed out that members of *Chloroflexi* are
415 poor-nutrition bacteria that prefer low-nourished soil habitats. The phyla *Actinobacteria* and
416 *Chloroflexi* could be involved in metal detoxification by decreasing the high toxicity found in
417 the present metal-rich environment (Wang et al., 2020; Liu et al., 2021), which could explain
418 why their relative abundance was higher than in the healthy soils. In heavily polluted soil, the
419 number of bacteria susceptible to heavy metal stress will decrease, so that the tolerant or
420 resistant bacteria can become the dominant species (Zhao et al., 2019).

421 At the genus level, the most dominant genera in the soil (%) around the SC site were
422 *norank_o_norank_c_AD3* (8.47), *norank_o_subgroup_2* (6.11), *Xanthobacteraceae* (4.72),
423 *norank_o_Elsterales* (4.43), *Acidothermus* (4.03), *norank_o_Acidobacteriales* (3.99),
424 *HSB_OF53-F07* (3.44), *Bradyrhizobium* (3.21), *FCPS473* (2.63), and *norank_o_Gaiellales*
425 (1.96) (Fig. 5D and S8). The most dominant genera in the soil around the YN site were
426 *norank_o_Gaiellales* (5.75), *norank_o_Vicinamibacterales* (4.86), *Vicinamibacteraceae*
427 (3.42), *norank_o_Rokubacteriales* (3.37), *Gemmatimonadaceae* (3.25), *norank_f_67-14*
428 (3.23), *Gaiella* (2.93), *unclassified_f_Micromonosporaceae* (2.6), *Xanthobacteraceae* (2.25),
429 and *norank_o_norank_c_MB-A2-108* (2.05). The most dominant genera of soil around the
430 GX site were *JG30-KF-AS9* (5.88), *norank_o_norank_c_AD3* (4.06), *JG30-KF-CM45* (3.74),
431 *Sinomonas* (3.33), *Ktedonobacteraceae* (2.25), *norank_o_Acidobacteriales* (2.16), *Delftia*
432 (2.1), *Bradyrhizobium* (1.99), *Acidothermus* (1.88), and *norank_o_Vicinamibacterales* (1.71).
433 The most dominant genera in the soil around the GZ site were *Arthrobacter* (6.68),

434 *Vicinamibacteraceae* (5.28), *norank_o_Vicinamibacterales* (5.27), *norank_o_Chloroplast*
435 (2.53), *Nocardioides* (2.46), *Gaiella* (2.42), *norank_o_Rokubacterales* (2.25),
436 *norank_o_Gaiellales* (2.17), *norank_o_norank_c_KD4-96* (2.11), and *Roseiflexaceae* (1.88).
437 *Micromonospora* belonging to *Actinobacteria* showed strong resistance to abiotic stress
438 (Stevenson and Hallsworth, 2014). *Arthrobacter* can thrive in environments with high metal
439 pollution through physiological and genetic modifications (Zhang et al., 2004).
440 The *norank_c_Acidobacteria* is one of the top five genera found in gold mining areas (Yan et
441 al., 2020). In the typical antimony ore smelting area in the south of China, at the genus level,
442 the bioindicators were *Ktedonobacteraceae* and *Xanthomonadaceae_unclassified* in the
443 topsoil, and *Gemmatimonadacea* and *norank_o_norank_c_KD4-96* were in the middle soil
444 depth, and *JG30-KF-AS9* and *norank_o_norank_c_AD3* were in deep soil (Wang et al.,
445 2022). In addition, *norank_o_Rokubacterales*, *norank_o_subgroup_2*, and
446 *norank_o_Acidobacteriales* were the main genera in As/Sb contaminated sites (Kalam et al.,
447 2020; Wang et al., 2022).
448 In the contaminated soil around a vanadium smelter, the main genera in the topsoil included
449 *JG30-KF-CM45*, while the dominant genera in profile soils included *norank_o_Gaiellales*,
450 *Gaiella*, and *norank_o_norank_c_KD4-96* (Wang et al., 2020). In abandoned mine soils in
451 Korea, the main bacteria included *norank_o_Vicinamibacterales*, *norank_o_Gaiellales*,
452 *Micrococcales*, *Gemmatimonadales*, *norank_o_Acidobacteriales*, *Bryobacteriales*,
453 *norank_o_subgroup_2*, *Micropepsales*, *Ktedonobacterales*, and *Pseudonocardiales* (Chun et
454 al., 2021). This exemplifies the main groups of bacteria found in heavy metal-contaminated

455 soil.

456 *Ktedonobacteria* can utilize or degrade different carbohydrates (Wang et al., 2022), whereas
457 *Bradyrhizobium* can minimize oxidative stress and enhance N-fixation in particular plants
458 (Rodrigues et al., 2013). *Arthrobacter* can survive and develop for a long time in harsh
459 ecological environments (Guo et al., 2021a). *Nocardioides* is also noted for its ability to
460 promote plant growth. The majority of these genera promote the C-cycle and fix N, which is
461 conducive to survival in a nutrient-poor environment (Sun et al., 2019). In summary, the
462 observed heterogeneous bacterial community involved in nutrient cycling has probably
463 adapted to anthropogenic disturbances. These major bacterial genera are bioindicators for
464 metal(loid)s-contaminated soil. Thus, the advantages of these core groups may reflect the
465 harsh soil ecological environment, representing the general adaptive groups around the non-
466 ferrous metal mining and smelting facilities in Southwest China.

467 ***3.6. Soil properties, heavy metal(loid)s, microbial metabolic activity, and microbial*** 468 ***community relationships***

469 The Spearman correlation heatmap (Fig. 6) and distance-based redundancy (db-RDA) (Fig.
470 7) analyses were performed based on the sequence abundance of OTUs to identify potential
471 relationships between microbial communities and environmental factors in the four studied
472 areas. Based on correlation analysis (Table S13-S18), microbial community α -diversity
473 indices (Sobs, Shannon, Ace, and Chao) were positively correlated with TOC, FDA, APA,
474 and INV ($p < 0.05$), indicating that the enzyme activities were closely related to bacterial
475 community diversity.

476 In soils proximal to the active sites (SC and GZ), the following observations were made. At
477 the phylum level (Fig. 6A), *Proteobacteria* was positively correlated ($p < 0.05$) with As but
478 negatively correlated ($p < 0.05$) with MC, EC, *Q*, APA, bioavailable Sb, and total Sb.
479 *Chloroflexi* was positively correlated ($p < 0.05$) with UA, bioavailable Cr and Cu, and total
480 As and Cd, but negatively correlated ($p < 0.05$) with EC, pH, APA, *Q*, bioavailable Cd, Mn,
481 and V, and total Mn. At the genus level (Fig. 6D), *Xanthobacteraceae*, *norank_o_EIsterales*,
482 *Acidothermus*, *norank_o_norank_c_AD3*, *norank_o_Subgroup_2*, *Acidobacteria* and
483 *Bradyrhizobium* were negatively correlated ($p < 0.05$) with EC, pH, MC, *Q*, APA,
484 bioavailable Cd and Mn, and total Mn, but positively correlated ($p < 0.05$) with UA,
485 bioavailable Cr and Cu, and total As and Cd. *Arthroactor*, *Vicinamibacteraceae*, and
486 *norank_o_Vicinamibacterales* were positively correlated ($p < 0.05$) with pH, EC, APA, *Q*,
487 bioavailable Cd and Mn, and total Mn, but negatively correlated ($p < 0.05$) with bioavailable
488 Cr and Cu, and with total As.

489 The above results were in contrast to soils close to the inactive sites (YN and GX). At the
490 phylum level (Fig. 6B), *Chloroflexi* was positively correlated ($p < 0.05$) with *T*, but
491 negatively correlated ($p < 0.05$) with TOC, UA, and FDA. *Actinobacteriota* was significantly
492 and positively correlated ($p < 0.05$) with Cu, while negatively correlated ($p < 0.05$) with pH,
493 At the genus level (Fig. 6E), *JG30-KF-AS9* and *norank_o_norank_c_AD3*, were negatively
494 correlated ($p < 0.05$) with TOC, Cu, bioavailable As, Cd, Cr, Cu, Mn, Ni, Sb, and Zn, and
495 total Cr and Pb, while positively correlated ($p < 0.05$) with MC and total Cr. The
496 *Vicinamibacteraceae* and *norank_o_Vicinamibacterales* were positively correlated ($p < 0.05$)
497 with bioavailable Cd, Cr, Cu, Mn, and Zn, and total Cd, Pb, and Sb, but negatively correlated

498 with MC ($p < 0.05$). *JG30-KF-CM45* and *Gemmatimonadaceae* were positively correlated (p
499 < 0.05) with bioavailable As, Cu, Mn, and Sb. In addition, the APA and Q showed negative
500 correlations ($p < 0.05$) with the bacterial community composition in the active and inactive
501 sites (Figs. 6 and 7).

502 Soil heavy metal(loid)s (As, Cd, Cr, Cu, Pb, Ni, Sb, and Zn), EC, and pH are the most
503 important factors affecting bacterial communities in the mining area, as reported in previous
504 studies (Zhao et al., 2019; Li et al., 2020; Zeng et al., 2020). High concentrations of Cd, Cu,
505 and Zn can disturb the cell membrane integrity and inhibit the enzyme activity of soil bacteria
506 (Renella et al., 2003; Jose et al., 2011). A previous study noted that the high content of Cd,
507 Cr, Cu, Pb, and Zn increased the abundance of *Chloroflexi* (Zeng et al., 2020). *Chloroflexi* has
508 strong resistance to heavy metals (Yin et al., 2023), which explains the significant positive
509 correlation between *Chloroflexi* and copper. Recent studies found that Cu and Zn have
510 important effects on metal resistance genes (MRGs) in soil bacteria (Li et al., 2022c). For the
511 heavy metal(loid)s in soils, the bioavailable fractions are absorbed by the microorganisms,
512 thus affecting microbial communities (Zhen et al., 2019). Depending on the concentration,
513 heavy metal ions can have beneficial as well as harmful effects on complex microbial
514 biochemistry and metabolism. It was found that Cd and Pb ions can bind to sulfhydryl ($-SH$)
515 groups and inhibit cell enzyme activity (Pan et al., 2020). This can also explain the significant
516 negative correlation between bioavailable Cd and Mn and *Chloroflexi*. On the other hand,
517 bioavailable Cr and Cu have significant positive correlations with *Chloroflexi*. In addition,
518 some heavy metal(loid)s ions (Cu^{2+} , Mn^{2+} , Ni^{2+} , and Zn^{2+}) are essential trace elements for
519 microorganisms and play an important role in bacterial protein composition, electrostatic

520 interaction, osmoregulation, and redox processes (Bruins et al., 2000).

521 At the genus level, *Bradyrhizobium* can minimize oxidative stress (Rodrigues et al., 2013).

522 *Arthrobacter* can thrive in barren and harsh environments and has a strong tolerance to

523 multiple metals (Cd, Cu, Pb, and Zn) through physiological and genetic modification (Zhang

524 et al., 2004). In the typical antimony ore smelting area in the south of China, most of the

525 bioindicators of soil contaminated with heavy metal(loid)s (As, Cd, Cr, Cu, Ni, Pb, and Sb)

526 include *Gemmatimonadacea*, *norank_o_subgroup_2*, *JG30_KF_AS9*, and

527 *norank_o_norank_c_AD3* (Wang et al., 2022). These studies reported that

528 *norank_o_Rokubacterales* and *norank_o_Acidobacterales* showed a positive relationship

529 with the total As and Sb contents (Kalam et al., 2020; Wang et al., 2022). At the abandoned

530 heavy metal(loid)s (As, Cd, Cu, Pb, and Zn) contaminated sites in Korea,

531 *norank_o_Vicinamibacterales* and *Gemmatimonadales* were identified as the main bacterial

532 genera in the heavy metal-tolerant modules, compared to *norank_o_Acidobacterales* and

533 *norank_o_subgroup_2* in the heavy metal-sensitive modules (Chun et al., 2021). In particular,

534 *norank_o_Vicinamibacterales* and *Gemmatimonadales* could work together to resist As, Cd,

535 Cu, Pb, and Zn. In the contaminated soil around the smelter, the main genera in the topsoil

536 included *JG30-KF-CM45*, these bacteria have a strong tolerance to soil heavy metals (Cr, Cu,

537 V, and Zn) (Wang et al., 2020).

538 In summary, total and bioavailability contents of heavy metal(loid)s strongly altered the

539 abundances of soil microbial taxa. Additionally, many bacterial communities can have

540 different reaction modes to heavy metal(loid)s, implying that soils contaminated with

541 multiple metal(loid)s can shape the microbial communities. Based on the information on the

542 assembly process of soil microbial community, a previous study found that the differences in
543 microbial communities in three mining and smelting sites were driven by the joint influence
544 of soil factors, spatial heterogeneity, and metal(loid) levels, among which pH and Sb content
545 were the main parameters affecting the microbial assembly processes (Liu et al., 2022a; Li et
546 al., 2023). These results (Figs. 6 and 7) indicate that TOC, MC, total Cd and Cu contents, and
547 bioavailable As, Cd, Cu, Sb, Mn, and Zn were the main environmental factors affecting the
548 bacterial community in the inactive sites (YN and GX), whereas EC, pH, total contents of As,
549 Cd, Mn, and Zn, and bioavailable Cd, Cu, Cr, and Mn contents were the main environmental
550 factors affecting the bacterial community in the active sites (SC and GZ). In the present
551 study, EC, total As, Cu, and Mn contents, and bioavailable As, Cu, Cd, and Mn contents were
552 the main important environmental factors affecting the bacterial community in the inactive
553 sites (YN and GX) and active sites (SC and GZ).

554 **3.7. Phenotypic-functional prediction of bacterial communities**

555 There were seven major phenotypes, including Potentially Pathogenic, Gram Positive,
556 Contains Mobile Elements, Forms Biofilms, Gram Negative, Stress Tolerant, and Oxygen
557 Utilizing (Aerobic, Anaerobic, and Facultatively anaerobic) communities (Fig. 8). The
558 relative abundance contribution of species to phenotypic function showed that the highest
559 contribution of phenotypic function included *Actinobacteria*, *Proteobacteria*, *Chloroflexi*,
560 and *Acidobacteriota*. The Aerobic and Forms Biofilms phenotypes were significantly and
561 negatively correlated with the α -diversity indices (Tables S13-S18) but were positively
562 correlated with the Simpson index ($p < 0.05$). The Anaerobic phenotype was negatively
563 related to the α -diversity indices ($p < 0.05$) and was positively related to the Simpson index (p

564 < 0.05). Furthermore, microbial community characteristics and phenotypes were closely
565 related in all sites as determined by correlation analyses.

566 The TOC was negatively correlated with Aerobic and Stress Tolerant phenotypes ($p < 0.05$)
567 (Fig. 8, Tables S13-S18), but it also was positively correlated with the Anaerobic and
568 Contains Mobile Elements phenotypes ($p < 0.05$). The EC was positively related to
569 phenotypes (Contains Mobile Elements and Gram Positive) ($p < 0.05$), while it was
570 negatively related to the Facultatively Anaerobic, Forms Biofilms, and Gram Negative
571 phenotypes ($p < 0.05$). Phenotypic changes related to oxygen demand (e.g., Aerobic,
572 Anaerobic, and Facultative Anaerobic) may be related to soil salinity (Bronick and Lal,
573 2005). Soil salinity is closely related to EC. Earlier studies have shown that the relative
574 abundance of anaerobic phenotypes is positively related to salinity, compared to facultative
575 anaerobic and biofilm-forming phenotypes that are negatively correlated with salinity (Zhang
576 et al., 2019b). Although the TOC is closely related to the soil microbial community (Li et al.,
577 2020), further study is needed to investigate the possibility that the soil microbial community
578 phenotype has affected the soil TOC and EC or that changes in soil TOC and EC have shaped
579 the microbial community. An earlier study confirmed that geographical distance and
580 environmental factors can drive microbial structure differences in the three nonferrous metal
581 pollution sites (Liu et al., 2022a).

582 The different phenotypes of soil microbes are closely related to the total and bioavailable
583 contents of heavy metals(loid)s (Tables S13-S18). Soil microbial communities may develop
584 unique survival and community composition strategies during their adaptation to extreme
585 environments. The present study assumes that the changes in soil properties and function

586 (e.g., microbial enzyme activities and bacterial/fungal communities) are related to (or caused
587 by) exposure to toxic heavy metals on fugitive dust particles that were transferred from the
588 active and inactive smelter sites to the surrounding forest soil and elsewhere (Csavina et al.,
589 2012; Lenart-Boroń and Boroń, 2014; Ettler 2016). Based on the genetic acquisition of MRG
590 in down-wind soils studied here, it is interesting to consider the possibility that the fugitive
591 emissions also carry heavy metal-resistant microbes (Hu et al., 2020), like the aerial transfer
592 of microbes from manure feed farms to urban settings (McEachran et al., 2015; Fry et al.,
593 2020). This process could have hazardous effects on human health (Hu et al., 2020) or
594 negatively impact neighboring ecosystems (Behzad et al., 2022). Whether the fugitive MRG-
595 containing microbes propagate within a new host-microbiome of the surrounding forest soils
596 explains the biogeochemical effects observed in the present study requires future
597 confirmation.

598 Another consideration is that toxic heavy metal(loid)s in soil may force microbial
599 communities into competition to cause a trade-off of resource allocation for the growth,
600 survival, and reproduction of the successful community. The species abundance composition
601 of bacterial communities and antibiotic-resistance genes in activated sludge are consistent
602 with environmental adaptation (Zhao et al., 2019). The correlation between the dominant
603 flora and the bacterial community phenotype may be the main reason for their similar spatial
604 distribution pattern. Here it is inferred that adaptive changes in the structure and phenotype of
605 the diverse microbial flora represent a synergistic or symbiotic strategy to support continual
606 adaptation to temporal changes in environmental stressors.

607 Although many studies on the microbial diversity and structure of mining and smelting sites

608 have been investigated, the ecological processes and symbiotic patterns affecting the
609 biogeographic distribution of microbial communities are still unclear. Therefore, in a follow-
610 up study, we plan to increase the number of study sites and soil samples to further explore the
611 ecological characteristics of soil bacterial and fungal communities.

612 **4. Conclusions**

613 In this study, the soil environment surrounding non-ferrous metal mining and smelting
614 activities in Southwest China was barren and heavily polluted by various heavy metals, with
615 different microbial metabolic activities, and soil bacterial community structure and
616 phenotypic characteristics. Selected microbial metabolic activities (enzyme APA and
617 microcalorimetric parameter Q), bacterial community structure, and phenotype varied across
618 all sites. Furthermore, the main bacterial phyla were *Actinobacteria*, *Proteobacteria*,
619 *Chloroflexi*, and *Acidobacteriota*. The TOC, MC, total Cd and Cu contents, and bioavailable
620 As, Cd, Cu, Mn, Sb, and Zn contents were the main environmental factors affecting the
621 bacterial community in the inactive sites, whereas the EC, pH, total As, Cd, Mn, and Zn
622 contents, and bioavailable Cd, Cr, Cu, and Mn contents were the main environmental factors
623 affecting that in the active sites. Many bacterial groups exhibited different response patterns
624 to each heavy metal(loid), implying that the soil microbial communities were shaped jointly
625 by fugitive multiple heavy metal(loid)s and possibly microbes. Species abundances and
626 phenotypes of dominant taxa in soil bacterial communities are involved in potential
627 environmental adaptation consistency. Different advanced gene sequencing techniques will
628 be used in future studies to systematically reveal the microbial biogeography, assembly
629 mechanism, and symbiotic modes of bacterial and fungal communities around mining and

630 smelting areas. This series of studies can provide a more comprehensive and theoretical basis
631 for the microbial treatment of non-ferrous metal-contaminated sites.

632

633 **Acknowledgments**

634 This work was supported in part by grants for the project of the Major National R & D
635 Projects for the Chinese Ministry of Science and Technology (2019YFC1803500,
636 2021YFE0106600), the National Natural Science Foundation of China (42230716), the 111
637 Project (B21017), Centre National de la Recherche Scientifique (CNRS PRC1416, France),
638 and the 1000-Talents Plan project (WQ2017110423).

639

640 **CRedit authorship contribution statement**

- 641 - **Hao Li:** Conceptualization, Methodology, Writing - review & editing, Data Curation,
642 Visualization, Writing - original draft.
- 643 - **Jun Yao:** Conceptualization, Writing – review & editing, Resources, Funding
644 acquisition, Supervision.
- 645 - **Ning Min:** Formal analysis, Review & editing.
- 646 - **Geoffrey Sunahara:** Conceptualization, Visualization, Writing - review & editing.
- 647 - **Robert Duran:** Formal analysis, Writing - review & editing.

648 **Declaration of competing interest**

649 The authors declare that there is no conflict of interest in the publication of this article.

650

651 **References**

- 652 Aponte, H., Mondaca, P., Santander, C., Meier, S., Paolini, J., Butler, B., Rojas, C., Diez,
653 M.C., Cornejo, P., 2021. Enzyme activities and microbial functional diversity in
654 metal(loid) contaminated soils near to a copper smelter. *Sci. Total Environ.* 779, 146423.
655 <https://doi.org/10.1016/j.scitotenv.2021.146423>.
- 656 Batista, D.R., Carneiro, J.J., Pinto, F.A., Santos, J., Carneiro, M., 2020. Environmental
657 drivers of shifts on microbial traits in sites disturbed by a large-scale tailing dam collapse
658 *Sci. Total Environ.* 738, 139453. <https://doi.org/10.1016/j.scitotenv.2020.139453>.
- 659 Behzad, H., Ohyanagi, H., Alharbi, B., Ibarra, M., Alarawi, M., Saito, Y., Duarte, C.M., Bajic,
660 V., Mineta, K., Gojobori, T. 2022. A cautionary signal from the Red Sea on the impact of
661 increased dust activity on marine microbiota. *BMC Genomics.* 23(1), 277.
662 <https://doi.org/10.1186/s12864-022-08485-w>.
- 663 Bronick, C.J., Lal, R., 2005. Soil structure and management: a review. *Geoderma* 124(1-2), 3-
664 22. <https://doi.org/10.1016/j.geoderma.2004.03.005>.
- 665 Bruins, M.R., Kapil, S., Oehme, F.W., 2000. Microbial resistance to metals in the
666 environment. *Ecotox. Environ. Safe.* 45(3), 198-207. <https://doi.org/10.1006/eesa.1999.1860>.
- 667 Chae, Y., Cui, R., Kim, S.W., An, G., Jeong, S.W., An, Y.J., 2017. Exoenzyme activity in
668 contaminated soils before and after soil washing: beta-glucosidase activity as a biological
669 indicator of soil health. *Ecotox. Environ. Safe.* 135, 368-374.
670 <https://doi.org/10.1016/j.ecoenv.2016.10.007>.
- 671 Chen, L.X., Li, J.T., Chen, Y.T., Huang, L.N., Shu, W.S., 2013. Shifts in microbial
672 community composition and function in the acidification of a lead/zinc mine tailings.
673 *Environ. Microbiol.* 15(9), 2431-2444. <https://doi.org/10.1111/1462-2920.12114>.
- 674 Chen, Y., Jiang, Y.M., Huang, H.Y., Mou, L.C., Ru, J.L., Zhao, J.H., Xiao, S., 2018. Long-
675 term and high-concentration heavy-metal contamination strongly influences the
676 microbiome and functional genes in Yellow River sediments. *Sci. Total Environ.* 637,
677 1400-1412. <https://doi.org/10.1016/j.scitotenv.2018.05.109>.

678 Chun, S.J., Kim, Y.J., Cui, Y., Nam, K.H., 2021. Ecological network analysis reveals
679 distinctive microbial modules associated with heavy metal contamination of abandoned
680 mine soils in Korea. *Environ. Pollut.* 289, 117851. <https://doi.org/10.1016/j.envpol.2021.117851>.

681 China National Environmental Monitoring Center (CNEMC), 1990. *Background Values of*
682 *Soil Elements in China*. China Environmental Science Press: Beijing, China (in Chinese).

683 Csavina, J., Field, J., Taylor, M.P., Gao, S., Landázuri, A., Betterton, E.A., Sáez, A.E., 2012.
684 A review on the importance of metals and metalloids in atmospheric dust and aerosol
685 from mining operations. *Sci.Total. Environ.* 433, 58-73.
686 <https://doi.org/10.1016/j.scitotenv.2012.06.013>.

687 Duran, R., Bielen, A., Paradzik, T., Gassie, C., Pustijanac, E., Cagnon, C., Hamer, B.,
688 Vujaklija, D., 2015. Exploring Actinobacteria assemblages in coastal marine sediments
689 under contrasted Human influences in the West Istria Sea, Croatia. *Environ. Sci. Pollut.*
690 *Res.* 22(20), 15215-15229. <https://doi.org/10.1007/s11356-015-4240-1>.

691 Ettler, V., 2016. Soil contamination near non-ferrous metal smelters: A review. *Appl.*
692 *Geochem.* 64, 56-74. <https://doi.org/10.1016/j.apgeochem.2015.09.020>.

693 Fry, K.L., Wheeler, C.A., Gillings, M.M., Flegal, A.R., Taylor, M.P., 2020. Anthropogenic
694 contamination of residential environments from smelter As, Cu and Pb emissions:
695 Implications for human health. *Environ. Pollut.* 262, 114235.
696 <https://doi.org/10.1016/j.envpol.2020.114235>.

697 Guo, J., Zhang, Y., Huang, H., Yang, F., 2021a. Deciphering soil bacterial community
698 structure in subsidence area caused by underground coal mining in arid and semiarid
699 area. *Appl. Soil Ecol.* 163, 103916. <https://doi.org/10.1016/j.apsoil.2021.103916>.

700 Guo, Z., Yang, J., Sarkodie, E.K., Li, K., Deng, Y., Meng, D., Miao, B., Liu, H., Liang, Y.,
701 Yin, H., 2021b. Vertical distribution of the toxic metal(loid)s chemical fraction and
702 microbial community in waste heap at a nonferrous metal mining site. *Ecotox. Environ.*
703 *Safe.* 228, 113037. <https://doi.org/10.1016/j.ecoenv.2021.113037>.

704

705 Harris, J.A., Ritz, K., Coucheney, E., Grice, S.M., Lerch, T.Z., Pawlett, M., Herrmann, A.M.,
706 2012. The thermodynamic efficiency of soil microbial communities subject to long-term
707 stress is lower than those under conventional input regimes. *Soil Biol. Biochem.* 47, 149-
708 157. <https://doi.org/10.1016/j.soilbio.2011.12.017>.

709 Herrmann, A.M., Coucheney, E., Nunan, N., 2014. Isothermal microcalorimetry provides
710 new insight into terrestrial carbon cycling. *Environ. Sci. Technol.* 48(8), 4344-4352.
711 <https://doi.org/10.1021/es403941h>.

712 Hu, B., Shao, S., Ni, H., Fu, Z., Huang, M., Chen, Q., Shi, Z., 2021. Assessment of
713 potentially toxic element pollution in soils and related health risks in 271 cities across
714 China. *Environ. Pollut.* 270, 116196. <https://doi.org/10.1016/j.envpol.2020.116196>.

715 Hu, W., Wang, Z., Huang, S., Ren, L., Yue, S., Li, P., Xie, Q., Zhao, W., Wei, L., Ren, H.,
716 Wu, L., Deng, J., Fu, P., 2020. Biological aerosol particles in polluted regions. *Curr.*
717 *Pollut. Rep.* 6, 65–89. <https://doi.org/10.1007/s40726-020-00138-4>.

718 Janssen, P.H., 2006. Identifying the dominant soil bacterial taxa in libraries of 16S rRNA and
719 16S rRNA genes. *Appl. Environ. Microbiol.* 72(3), 1719-1728.
720 <https://doi.org/10.1128/aem.72.3.1719-1728.2006>.

721 Jiang, X., Liu, W., Xu, H., Cui, X., Zheng, B., 2021. Characterizations of heavy metal
722 contamination, microbial community, and resistance genes in a tailing of the largest
723 copper mine in China. *Environ. Pollut.* 280, 116947.
724 <https://doi.org/10.1016/j.envpol.2021.116947>.

725 Jose, J., Giridhar, R., Anas, A., Bharathi, P.A.L., Nair, S., 2011. Heavy metal pollution exerts
726 reduction/adaptation in the diversity and enzyme expression profile of heterotrophic
727 bacteria in Cochin estuary, India. *Environ. Pollut.* 159(10), 2775-2780.
728 <https://doi.org/10.1016/j.envpol.2011.05.009>.

729 Kalam, S., Basu, A., Ahmad, I., Sayyed, R.Z., El-Enshasy, H.A., Dailin, D.J., Suriani, N.L.,
730 2020. Recent understanding of soil Acidobacteria and their ecological significance: A
731 critical review. *Front. Microbiol.* 11, 580024. <https://doi.org/10.3389/fmicb.2020.580024>.

732 Kang, X., Cui, Y., Shen, T., Yan, M., Yu, X., 2020. Changes of root microbial populations of
733 natively grown plants during natural attenuation of V–Ti magnetite tailings. *Ecotox.*
734 *Environ. Safe.* 201, 110816. <https://doi.org/10.1016/j.ecoenv.2020.110816>.

735 Ke, W.S., Zeng, J.Q., Zhu, F., Luo, X.H., Feng, J.P., He, J., Xue, S.G., 2022. Geochemical
736 partitioning and spatial distribution of heavy metals in soils contaminated by lead
737 smelting. *Environ. Pollut.* 307, 19486. <https://doi.org/10.1016/j.envpol.2022.119486>.

738 Kubier, A., Wilkin, R.T., Pichler, T., 2019. Cadmium in soils and groundwater: A review.
739 *Appl. Geochem.* 108, 104388. <https://doi.org/10.1016/j.apgeochem.2019.104388>.

740 Lenart-Boroń, A., Boroń, P., 2014., The effect of industrial heavy metal pollution on
741 microbial abundance and diversity in soils—A review, in: Hernandez Soriano, M.C.,
742 (Ed). *Environmental Risk Assessment of Soil Contamination*, IntechOpen, Mar 26.
743 <http://dx.doi.org/10.5772/57406>.

744 Li, H., Yao, J., Min, N., Chen, Z.H., Li, M.M., Pang, W.C., Liu, B., Cao, Y., Men, D.Y.,
745 Duran, R., 2022a. Comprehensive evaluation of metal(loid)s pollution risk and microbial
746 activity characteristics in non-ferrous metal smelting contaminated site. *J. Clean. Prod.*
747 344, 130999. <https://doi.org/10.1016/j.jclepro.2022.130999>.

748 Li, H., Yao, J., Min, N., Liu, J.L., Chen, Z.H., Zhu, X.Z., Zhao, C.C., Pang, W.C., Li, M.M.,
749 Cao, Y., Liu, B., Duran, R., 2022b. Relationships between microbial activity, enzyme
750 activities and metal(loid) form in Ni-Cu tailings area. *Sci. Total Environ.* 812, 152326.
751 <https://doi.org/10.1016/j.scitotenv.2021.152326>.

752 Li, M.M., Yao, J., Sunahara, G., Duran, R., Liu, B., Cao, Y., Li, H., Pang, W.C., Liu, H.Q.,
753 Jiang, S., Zhu, J.J., Zhang, Q.H., 2023. Assembly processes of bacterial and fungal
754 communities in metal(loid)s smelter soil. *J. Hazard. Mater.* 451, 131153.
755 <https://doi.org/10.1016/j.jhazmat.2023.131153>.

756 Li, N., Chen, J.G., Liu, C., Yang, J.X., Zhu, C.X., Li, H.N., 2022c. Cu and Zn exert a greater
757 influence on antibiotic resistance and its transfer than doxycycline in agricultural soils. *J.*
758 *Hazard. Mater.* 423, 127042. <https://doi.org/10.1016/j.jhazmat.2021.127042>.

759

760 Li, S., Wu, J., Huo, Y., Zhao, X., Xue, L., 2020. Profiling multiple heavy metal contamination
761 and bacterial communities surrounding an iron tailing pond in Northwest China. *Sci.*
762 *Total Environ.* 752(2), 141827. <https://doi.org/10.1016/j.scitotenv.2020.141827>.

763 Liu, B., Yao, J., Chen, Z., Ma, B., Li, H., Pang, W., Liu, J., Wang, D., Duran, R., 2022a.
764 Biogeography, assembly processes and species coexistence patterns of microbial
765 communities in metalloids-laden soils around mining and smelting sites. *J. Hazard.*
766 *Mater.* 425, 127945. <https://doi.org/10.1016/j.jhazmat.2021.127945>.

767 Liu, B., Yao, J., Ma, B., Chen, Z., Zhu, X., Zhao, C., Li, M., Cao, Y., Pang, W., Li, H.,
768 Mihucz, V.G., Duran, R., 2022b. Metal(loid)s diffusion pathway triggers distinct
769 microbiota responses in key regions of typical karst non-ferrous smelting assembly. *J.*
770 *Hazard. Mater.* 423, 127164. <https://doi.org/10.1016/j.jhazmat.2021.127164>.

771 Liu, B., Yao, J., Ma, B., Chen, Z., Zhao, C., Zhu, X., Li, M., Cao, Y., Pang, W., Li, H., 2021.
772 Microbial community profiles in soils adjacent to mining and smelting areas: Contrasting
773 potentially toxic metals and co-occurrence patterns. *Chemosphere* 282, 130992.
774 <https://doi.org/10.1016/j.chemosphere.2021.130992>.

775 Liu, J.L., Yao, J., Wang, F., Ni, W., Liu, X.Y., Sunahara, G., Duran, R., Jordan, G., Hudson-
776 Edwards, K.A., Alakangas, L., Solevic-Knudsen, T., Zhu, X.Z., Zhang, Y.Y., Li, Z.F.,
777 2018. China's most typical nonferrous organic-metal facilities own specific microbial
778 communities. *Sci. Rep-UK* 8, 12570. <https://doi.org/10.1038/s41598-018-30519-1>.

779 McEachran, A.D., Blackwell, B.R., Hanson, J.D., Wooten, K.J., Mayer, G.D., Cox, S.B.,
780 Smith, P.N., 2015. Antibiotics, bacteria, and antibiotic resistance genes: aerial transport
781 from cattle feed yards via particulate matter. *Environ. Health Perspect.* 123, 337–343.
782 <http://dx.doi.org/10.1289/ehp.1408555>.

783 Pan, X.M., Zhang, S.R., Zhong, Q.M., Gong, G.S., Wang, G.Y., Guo, X., Xu, X.X., 2020.
784 Effects of soil chemical properties and fractions of Pb, Cd, and Zn on bacterial and
785 fungal communities. *Sci. Total Environ.* 715, 136904.
786 <https://doi.org/10.1016/j.scitotenv.2020.136904>.

787

- 788 Qiao, L., Liu, X., Zhang, S., Zhang, L., Yu, C., 2021. Distribution of the microbial
789 community and antibiotic resistance genes in farmland surrounding gold tailings: A
790 metagenomics approach. *Sci. Total Environ.* 779(4), 146502.
791 <https://doi.org/10.1016/j.scitotenv.2021.146502>.
- 792 Renella, G., Ortigoza, A.L.R., Landi, L., Nannipieri, P., 2003. Additive effects of copper and
793 zinc on cadmium toxicity on phosphatase activities and ATP content of soil as estimated
794 by the ecological dose (ED50). *Soil Biol. Biochem.* 35(9), 1203-1210.
795 [https://doi.org/10.1016/s0038-0717\(03\)00181-0](https://doi.org/10.1016/s0038-0717(03)00181-0).
- 796 Rinklebe, J., Antoniadis, V., Shaheen, S.M., Rosche, O., Altermann, M., 2019. Health risk
797 assessment of potentially toxic elements in soils along the Central Elbe River, Germany.
798 *Environ. Int.* 126, 76-88. <https://doi.org/10.1016/j.envint.2019.02.011>.
- 799 Rodrigues, A.C., Bonifacio, A., Antunes, J.E.L., da Silveira, J.A.G., Figueiredo, M.D.B.,
800 2013. Minimization of oxidative stress in cowpea nodules by the interrelationship
801 between *Bradyrhizobium sp* and plant growth-promoting bacteria. *Appl. Soil Ecol.* 64,
802 245-251. <https://doi.org/10.1016/j.apsoil.2012.12.018>.
- 803 Schnurer, J., Rosswall, T., 1982. Fluorescein diacetate hydrolysis as a measure of total
804 microbial activity in soil and litter. *Appl. Environ. Microbiol.* 43(6), 1256-1261.
805 <https://doi.org/10.1128/aem.43.6.1256-1261.19>.
- 806 Stevenson, A., Hallsworth, J.E., 2014. Water and temperature relations of soil Actinobacteria.
807 *Environ. Microbiol. Rep.* 6(6), 744-755. <https://doi.org/10.1111/1758-2229.12199>.
- 808 Sun, X.X., Li, B.Q., Han, F., Xiao, E.Z., Wang, Q., Xiao, T.F., Sun, W.M., 2019. Vegetation
809 type impacts microbial interaction with antimony contaminants in a mining-
810 contaminated soil environment. *Environ. Pollut.* 252, 1872-1881.
811 <https://doi.org/10.1016/j.envpol.2019.06.070>.
- 812 Vinhal-Freitas, I.C., Correa, G.F., Wendling, B., Bobul'Ska, L., Ferreira, A.S., 2017. Soil
813 textural class plays a major role in evaluating the effects of land use on soil quality
814 indicators. *Ecol. Indic.* 74(Mar.), 182-190. <https://doi.org/10.1016/j.ecolind.2016.11.020>.

- 815 Wahsha, M., Nadimi-Goki, M., Fornasier, F., Al-Jawasreh, R., Hussein, E.I., Bini, C., 2017.
816 Microbial enzymes as an early warning management tool for monitoring mining site
817 soils. *Catena* 148, 40-45. <https://doi.org/10.1016/j.catena.2016.02.021>.
- 818 Ward, T., Larson, J., Meulemans, J., Hillmann, B., Lynch, J., Sidiropoulos, D., Spear, J.,
819 Caporaso, G., Ran, B., Knight, R., 2017. BugBase predicts organism level microbiome
820 phenotypes. *bioRxiv*. <https://doi.org/10.1101/133462>.
- 821 Wang, S., Zhang, B.G., Li, T.T., Li, Z.Y., Fu, J., 2020. Soil vanadium(V)-reducing related
822 bacteria drive community response to vanadium pollution from a smelting plant over
823 multiple gradients. *Environ. Int.* 138, 105630. <https://doi.org/10.1016/j.envint.2020.105630>.
- 824 Wang, W., Xiao, S., Amanze, C., Anaman, R., Zeng, W., 2022. Microbial community
825 structures and their driving factors in a typical gathering area of antimony mining and
826 smelting in South China. *Environ. Sci. Pollut. Res.* 29, 50070–50084
827 <https://doi.org/10.1007/s11356-022-19394-6>.
- 828 Wu, B., Luo, H., Wang, X., Liu, H., Xu, H., 2021. Effects of environmental factors on soil
829 bacterial community structure and diversity in different contaminated districts of
830 Southwest China mine tailings. *Sci. Total Environ.* 802(16), 149899.
831 <https://doi.org/10.1016/j.scitotenv.2021.149899>.
- 832 Xiao, E.Z., Wang, Y.Q., Xiao, T.F., Sun, W.M., Deng, J.M., Jiang, S.M., Fan, W.J., Tang, J.F.,
833 Ning, Z.P., 2021. Microbial community responses to land-use types and its ecological
834 roles in mining area. *Sci. Total Environ.* 775, 145753.
835 <https://doi.org/10.1016/j.scitotenv.2021.145753>.
- 836 Xiao, L., Yu, Z.J., Liu, H.Q., Tan, T., Yao, J.H., Zhang, Y.X., Wu, J.J., 2020. Effects of Cd and
837 Pb on diversity of microbial community and enzyme activity in soil. *Ecotoxicology*
838 29(5), 551-558. <https://doi.org/10.1007/s10646-020-02205-4>.
- 839 Xu, Y., Seshadri, B., Bolan, N., Sarkar, B., Ok, Y.S., Zhang, W., Rumpel, C., Sparks, D.,
840 Farrell, M., Hall, T., 2019. Microbial functional diversity and carbon use feedback in
841 soils as affected by heavy metals. *Environ. Int.* 125, 478-488.
842 <https://doi.org/10.1016/j.envint.2019.01.071>.

843 Yan, C., Wang, F., Liu, H., Liu, H., Pu, S., Lin, F., Geng, H., Ma, S., Zhang, Y., Tian, Z.,
844 Chen, H., Zhou, B., Yuan, R., 2020. Deciphering the toxic effects of metals in gold
845 mining area: Microbial community tolerance mechanism and change of antibiotic
846 resistance genes. *Environ. Res.* 189, 109869. <https://doi.org/10.1016/j.envres.2020.109869>.

847 Yin, Y., Wang, X.J., Hu, Y.A., Li, F.D., Cheng, H.F., 2023. Soil bacterial community structure
848 in the habitats with different levels of heavy metal pollution at an abandoned
849 polymetallic mine. *J. Hazard. Mater.* 442, 130063.
850 <https://doi.org/10.1016/j.jhazmat.2022.130063>.

851 Yuan, C.Y., Li, F.Y., Yuan, Z.Q., Li, G.Y., Liang, X.Q., 2021. Response of bacterial
852 communities to mining activity in the alpine area of the Tianshan Mountain region,
853 China. *Environ. Sci. Pollut. Res.* 28(13), 15806-15818. [https://doi.org/10.1007/s11356-020-](https://doi.org/10.1007/s11356-020-11744-6)
854 [11744-6](https://doi.org/10.1007/s11356-020-11744-6).

855 Zeng, J.Q., Li, C.X., Wang, J.T., Tang, L., Wu, C., Xue, S.G., 2022. Pollution simulation and
856 remediation strategy of a zinc smelting site based on multi-source information. *J. Hazard.*
857 *Mater.* 433, 128774. <https://doi.org/10.1016/j.jhazmat.2022.128774>.

858 Zeng, X.Y., Li, S.W., Leng, Y., Kang, X.H., 2020. Structural and functional responses of
859 bacterial and fungal communities to multiple heavy metal exposure in arid loess. *Sci.*
860 *Total Environ.* 723, 138081. <https://doi.org/10.1016/j.scitotenv.2020.138081>.

861 Zhang, B., Wang, S., Diao, M., Fu, J., Borthwick, A.G.L., 2019a. Microbial community
862 responses to vanadium distributions in mining geological environments and
863 bioremediation assessment. *J. Geophys. Res-Bioge.* 124(3), 601-615.
864 <https://doi.org/10.1029/2018jg004670>.

865 Zhang, H.B., Duan, C.Q., Shao, Q.Y., Ren, W.M., Sha, T., Cheng, L.Z., Zhao, Z.W., Hu, B.,
866 2004. Genetic and physiological diversity of phylogenetically and geographically distinct
867 groups of *Arthrobacter* isolated from lead-zinc mine tailings. *FEMS Microbiol. Ecol.*
868 49(2), 333-341. <https://doi.org/10.1016/j.femsec.2004.04.009>.

869

870 Zhang, K., Shi, Y., Cui, X., Yue, P., Li, K., Liu, X., Tripathi, B.M., Chu, H., Lozupone, C.,
871 2019b. Salinity is a key determinant for soil microbial communities in a desert
872 ecosystem. *mSystems* 4(1). <https://doi.org/10.1128/mSystems.00225-18>.

873 Zhang, Y.Y., Wang, F., Hudson-Edwards, K.A., Blake, R., Zhao, F.R., Yuan, Z.M., Gao, W.,
874 2020. Characterization of mining-related aromatic contaminants in active and abandoned
875 metal(loid) tailings ponds. *Environ. Sci. Technol.* 54(23), 15097-15107.
876 <https://doi.org/10.1021/acs.est.0c03368>.

877 Zhao, F.J., Ma, Y.B., Zhu, Y.G., Tang, Z., McGrath, S.P., 2015. Soil contamination in China:
878 Current status and mitigation strategies. *Environ. Sci. Technol.* 49(2), 750-759.
879 <https://doi.org/10.1021/es5047099>.

880 Zhao, X., Huang, J., Lu, J., Sun, Y., 2019. Study on the influence of soil microbial
881 community on the long-term heavy metal pollution of different land use types and depth
882 layers in mine. *Ecotox. Environ. Safe.* 170, 218-226.
883 <https://doi.org/10.1016/j.ecoenv.2018.11.136>.

884 Zhao, X.Q., Sun, Y., Huang, J., Wang, H., Tang, D., 2020. Effects of soil heavy metal
885 pollution on microbial activities and community diversity in different land use types in
886 mining areas. *Environ. Sci. Pollut. Res.* 27(16), 20215-20226. [https://doi.org/10.1007/s11356-](https://doi.org/10.1007/s11356-020-08538-1)
887 [020-08538-1](https://doi.org/10.1007/s11356-020-08538-1).

888 Zhen, Z., Wang, S.B., Luo, S.W., Ren, L., Liang, Y.Q., Yang, R.C., Li, Y.T., Zhang, Y.Q.,
889 Deng, S.Q., Zou, L.N., Lin, Z., Zhang, D.Y., 2019. Significant impacts of both total
890 amount and availability of heavy metals on the functions and assembly of soil microbial
891 communities in different land use patterns. *Front. Microbiol.* 10, 02293.
892 <https://doi.org/10.3389/fmicb.2019.02293>.

893 Zhu, X.Z., Yao, J., Wang, F., Yuan, Z.M., Liu, J.L., Jordan, G., Knudsen, T.S., Avdalovic, J.,
894 2018. Combined effects of antimony and sodium diethyldithiocarbamate on soil
895 microbial activity and speciation change of heavy metals. Implications for contaminated
896 lands hazardous material pollution in nonferrous metal mining areas. *J. Hazard. Mater.*
897 349, 160-167. <https://doi.org/10.1016/j.jhazmat.2018.01.044>.

898 **List of Figures**

899 **Fig. 1.** Locations and photos of four non-ferrous metal mining and smelting activities

900 affected areas in Southwest China. The distributions of sampling points of active sites
901 (SC and GZ) and inactive sites (YN and GX) are shown in the top and bottom panels,
902 respectively (also see Supplementary Information, Figs. S1 and S2).

903 **Fig. 2.** Total (A) and bioavailable (Exchangeable fraction) (B) contents of metal(loid)s in the
904 surface soil from active (SC and GZ) and inactive (YN and GX) sites. Panel (C) shows
905 the Contamination factor (CF) and pollution load index (PLI) of metal(loid)s from active
906 (SC and GZ) and inactive (YN and GX) sites. $CF < 1$, low pollution; $1 \leq CF < 3$,
907 moderate pollution; $3 \leq CF < 6$, serious pollution, and $CF \geq 6$, extreme pollution. $PLI > 1$
908 indicates significant pollution.

909 **Fig. 3.** Microbial activities in the SC, YN, GX, and GZ sites. FDA (A), UA (B), APA (C), and
910 INV (D) enzymes activities. Power-time curves (E) for different soil samples in the SC,
911 YN, GX, and GZ sites were recorded using microcalorimetry. Different lowercase letters
912 are used to indicate significant differences between groups ($p < 0.05$). The
913 thermodynamic parameter values for different samples are detailed in Supplementary
914 Information Fig. S5 and Tables S1-S4.

915 **Fig. 4.** Microbial community α -diversity in different soil samples from SC, YN, GX, and GZ
916 sites. (A) Shannon diversity index; (B) Sobs richness at the OTU level; (C) Chao
917 richness at the OTU level; (D) Ace richness at the OTU level; (E) Simpson diversity
918 index; and (F) Coverage's index. Statistical differences between SC, YN, GX, and GZ
919 sites were performed by the Student's *t*-test ($p \leq 0.05$ is marked as *, $p \leq 0.01$ as **, $p \leq$
920 0.001 as ***).

921 **Fig. 5.** Comparison of the microbial communities from GX, GZ, SC, and YN sites. Venn
922 diagram (A) and Principal co-ordinate analysis (PCoA, B) showing the variations of
923 microbial structure at the OTU level. Soil bacterial community composition shows the
924 top 20 most abundant phyla (C) and genera (D).

925

926 **Fig. 6.** Spearman correlation heatmap of the top five most abundant phyla (A: active sites; B:
927 inactive sites; C: active and inactive sites) and the top ten most abundant genera (D:
928 active sites; E: inactive sites; F: active and inactive sites) of the microbial communities,
929 the environmental factors, microbial activity characteristics, and total and bioavailable
930 metal(loid)s contents (E). *r*-values are plotted in different colors; the right side of the
931 legend shows the color range and the corresponding *r*-values. Significant values are
932 shown as * $p < 0.05$; ** $p < 0.01$; *** $p < 0.001$.

933 **Fig. 7.** Comparison of microbial communities. The distance-based redundancy analysis (db-
934 RDA) was performed at the OTUs abundance level. The red line arrows denote the soil
935 characteristics and microbial activity characteristics (A), and total (B), and bioavailable
936 (C) metal(loid)s contents. The length of the arrows represents the degree of relevance
937 between microbial communities and various factors. The percentage in the two axes
938 indicates the eigenvalues of environmental factors.

939 **Fig. 8.** The corresponding OTU contribution plots of the relative abundance of phyla
940 possessing each phenotype (A: Aerobic; B: Potentially Pathogenic; C: Gram Positive; D:
941 Anaerobic; E: Facultatively Anaerobic; F: Contains Mobile Elements; G: Forms
942 Biofilms; and H: Gram Negative; I: Stress Tolerant) in the YN, SC, GZ, and GX sites
943 are also shown. Different lowercase letters indicate significant differences between
944 groups ($p < 0.05$).

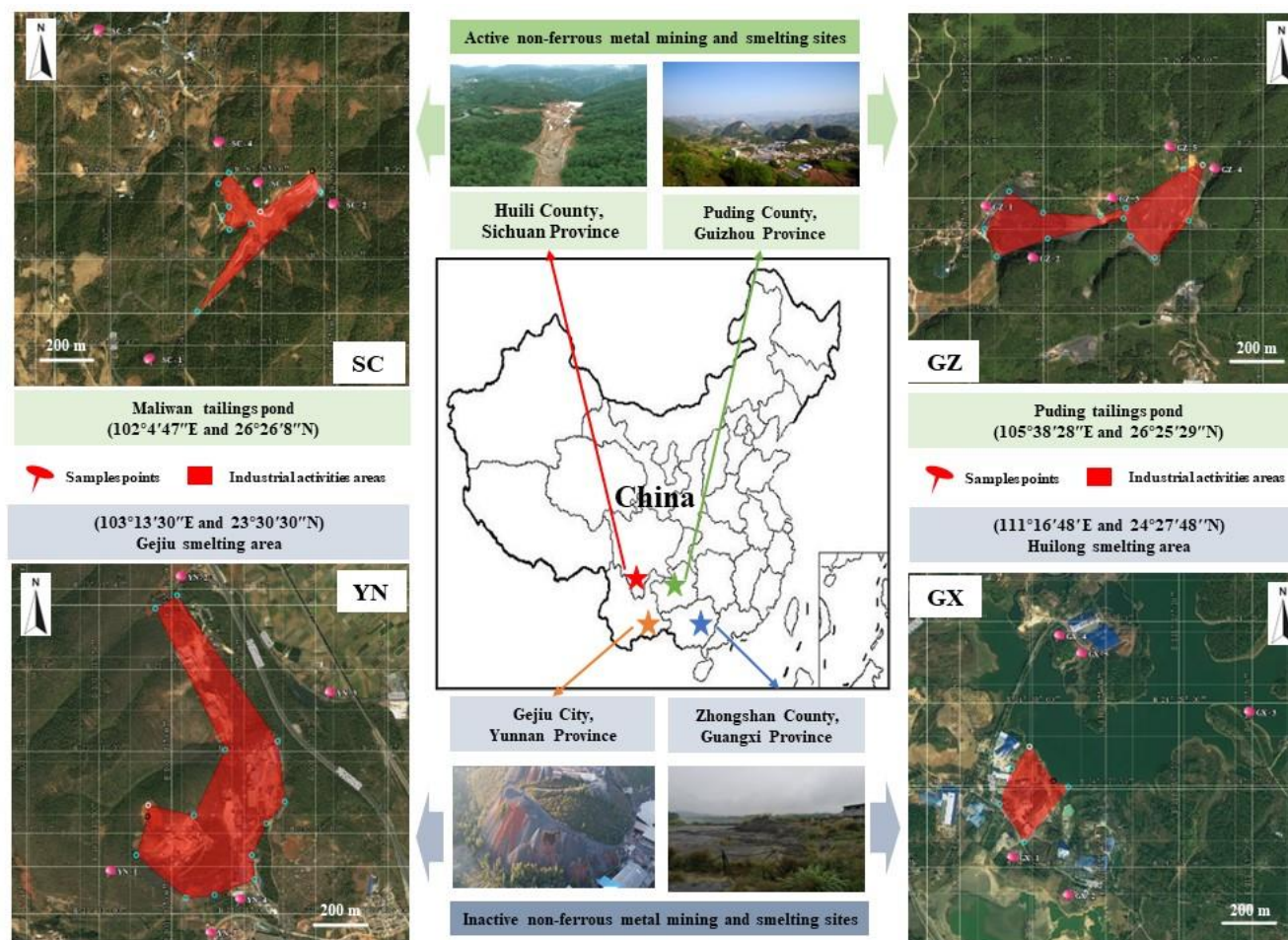


Fig. 1. Locations and photos of four non-ferrous metal mining and smelting activities affected areas in Southwest China. The distributions of sampling points of active sites (SC and GZ) and inactive sites (YN and GX) are shown in the top and bottom panels, respectively (also see Supplementary Information, Figs. S1 and S2).

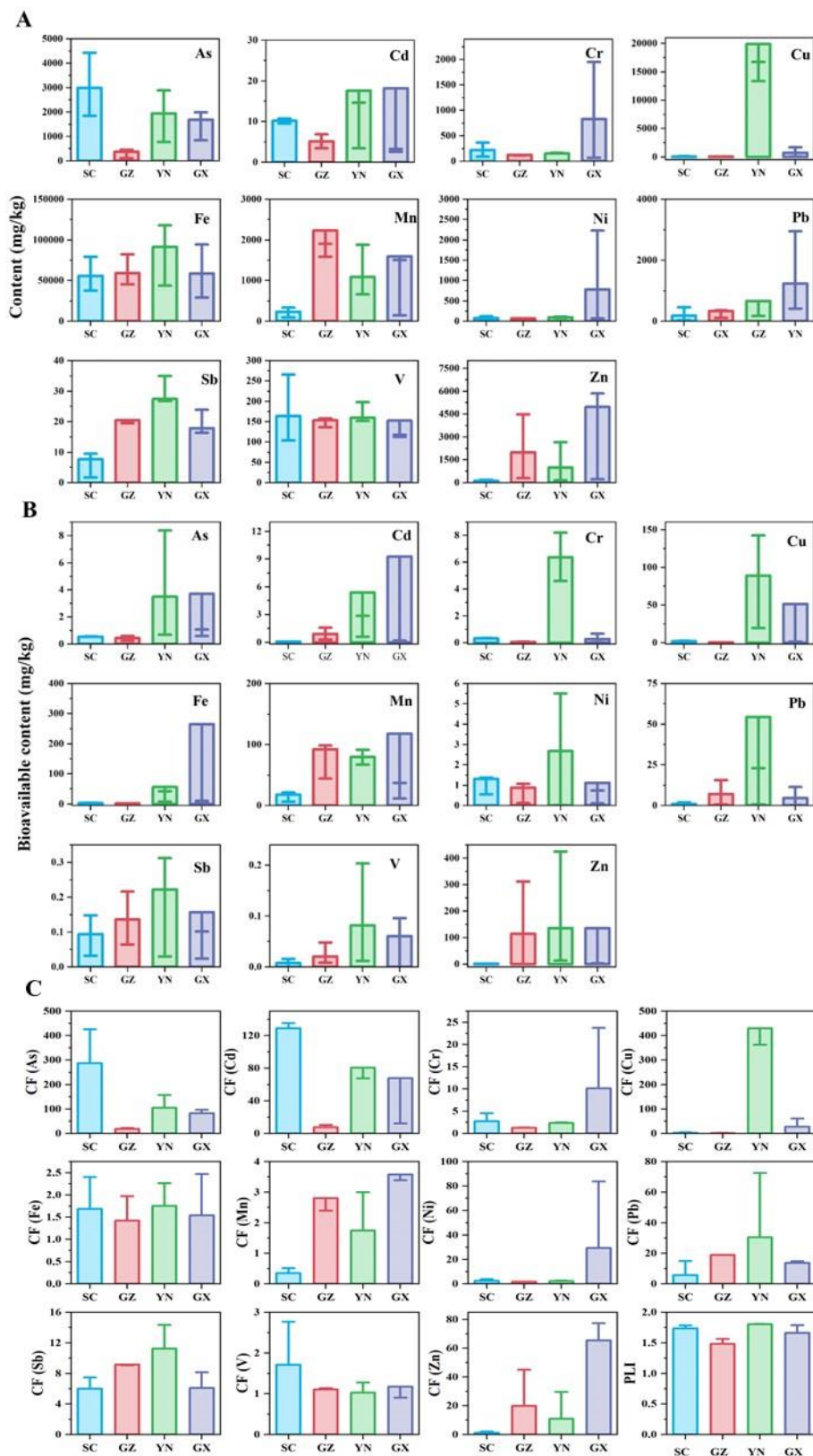


Fig. 2. Total (A) and bioavailable (Exchangeable fraction) (B) contents of metal(loid)s in the surface soil from active (SC and GZ) and inactive (YN and GX) sites. Panel (C) shows the Contamination factor (CF) and pollution load index (PLI) of metal(loid)s from active (SC and GZ) and inactive (YN and GX) sites. $CF < 1$, low pollution; $1 \leq CF < 3$, moderate pollution; $3 \leq CF < 6$, serious pollution, and $CF \geq 6$, extreme pollution. $PLI > 1$ indicates

significant pollution.

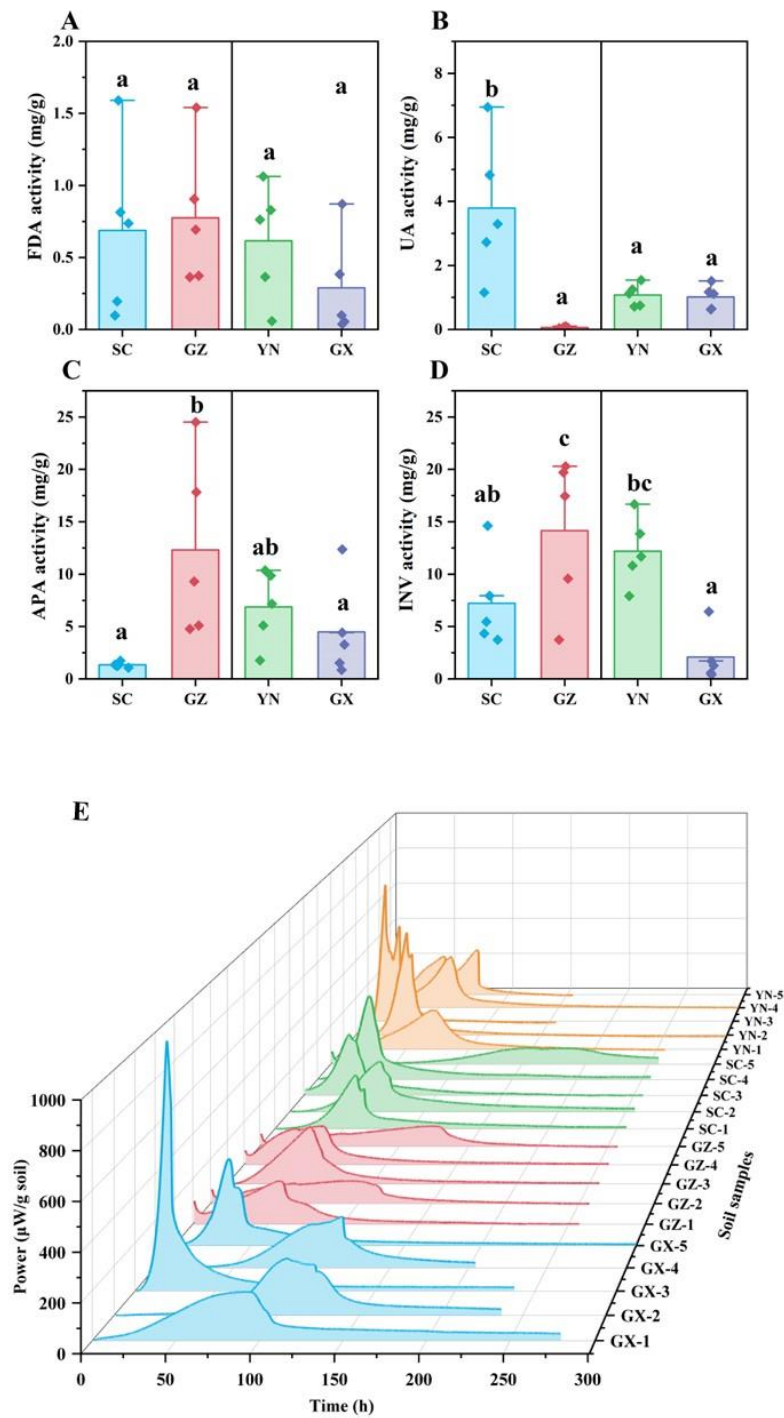


Fig. 3. Microbial activities in the SC, YN, GX, and GZ sites. FDA (A), UA (B), APA (C), and INV (D) enzymes activities. Power-time curves (E) for different soil samples in the SC, YN, GX, and GZ sites were recorded using microcalorimetry. Different lowercase letters are used to indicate significant differences between groups ($p < 0.05$). The different thermodynamic parameter values for different samples are

detailed in Supplementary Information Fig. S5 and Tables S1-S4.

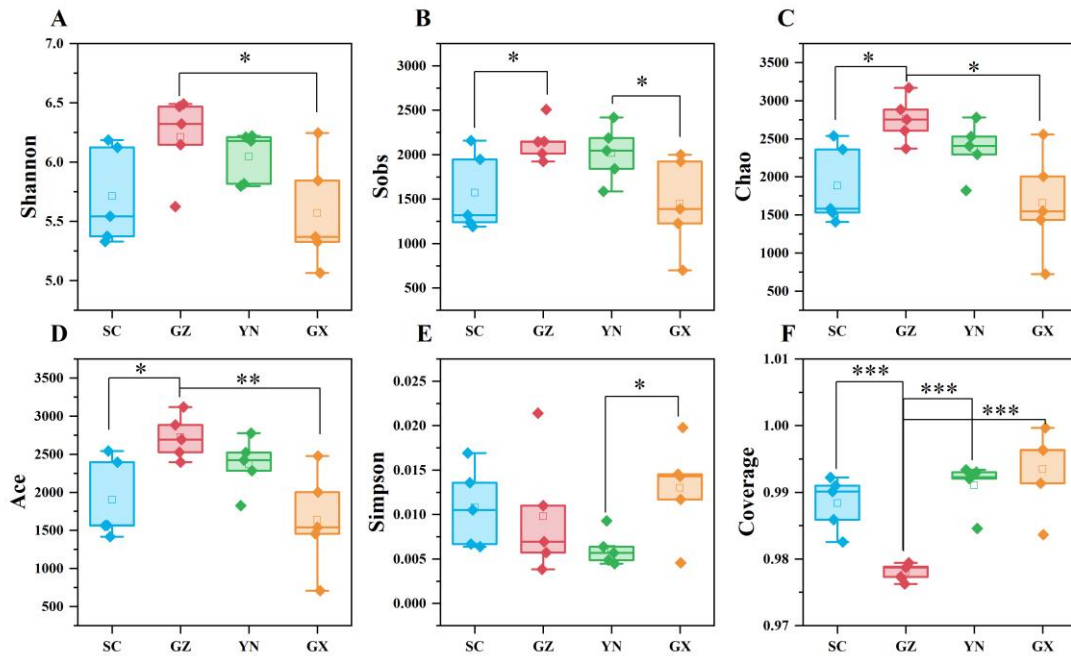


Fig. 4. Microbial community α -diversity in different soil samples from SC, YN, GX, and GZ sites. (A) Shannon diversity index; (B) Sobs richness at the OTU level; (C) Chao richness at the OTU level; (D) Ace richness at the OTU level; (E) Simpson diversity index; and (F) Coverage's index. Statistical differences between SC, YN, GX, and GZ sites were performed using the Student's *t*-test ($p \leq 0.05$ is marked as *, $p \leq 0.01$ as **, $p \leq 0.001$ as ***).

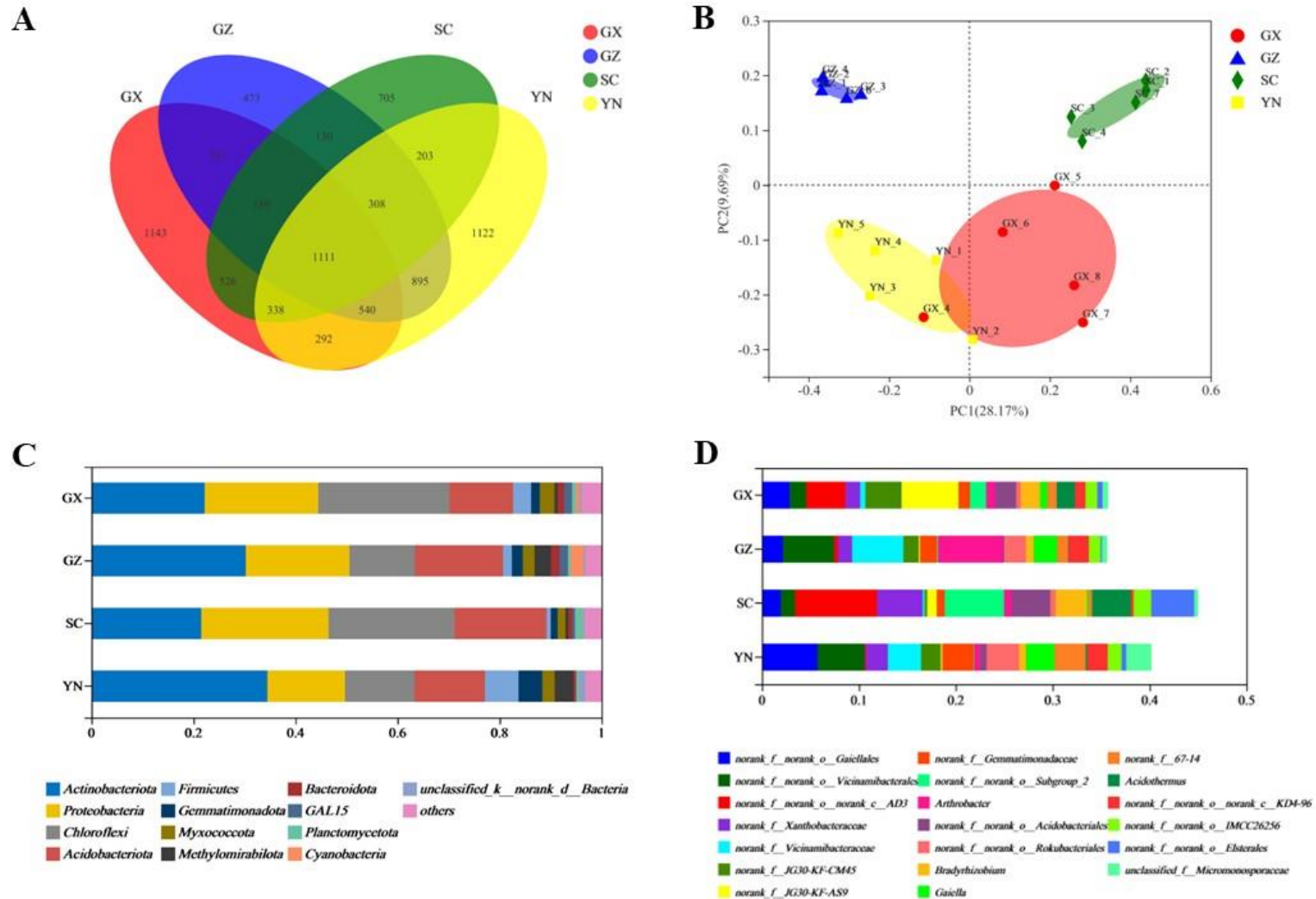


Fig. 5. Comparison of the microbial communities from GX, GZ, SC, and YN sites. Venn diagram (A) and Principal co-ordinate analysis (PCoA, B) showing the variations of microbial structure at the OTU level. Soil bacterial community composition shows the top 20 most abundant phyla (C) and genera (D).

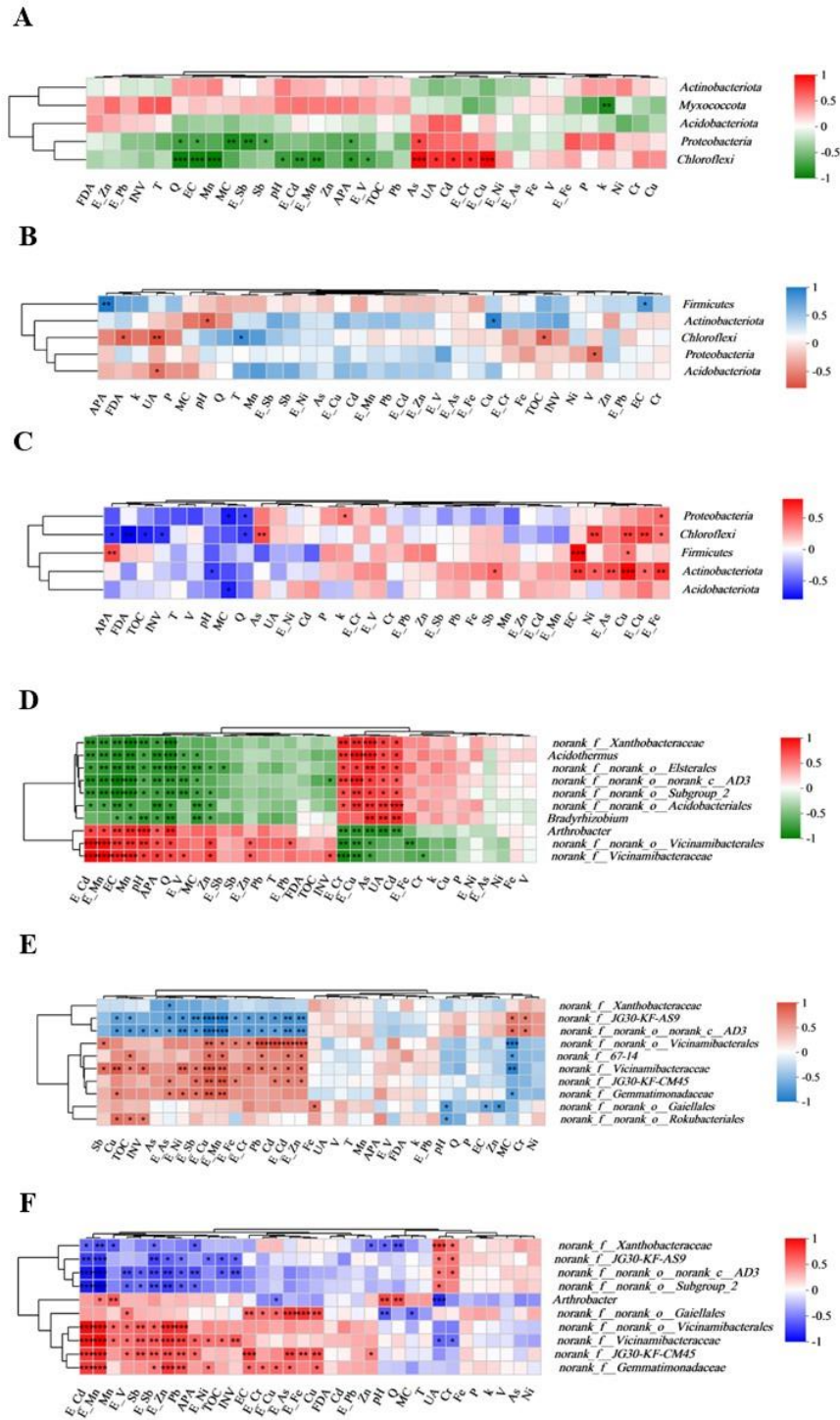


Fig. 6. Spearman correlation heatmap of the top five most abundant phyla (A: active sites; B: inactive sites; C: active and inactive sites) and the top ten most abundant genera (D: active sites; E: inactive sites; F: active and inactive sites) of the microbial communities, the environmental factors, microbial activity characteristics, and total and bioavailable metal(loid)s contents (E). *r*-values are plotted in different colors; the right side of the legend shows the color range and the corresponding *r*-values. Significant values are shown as * $p < 0.05$; ** $p < 0.01$; *** $p < 0.001$.

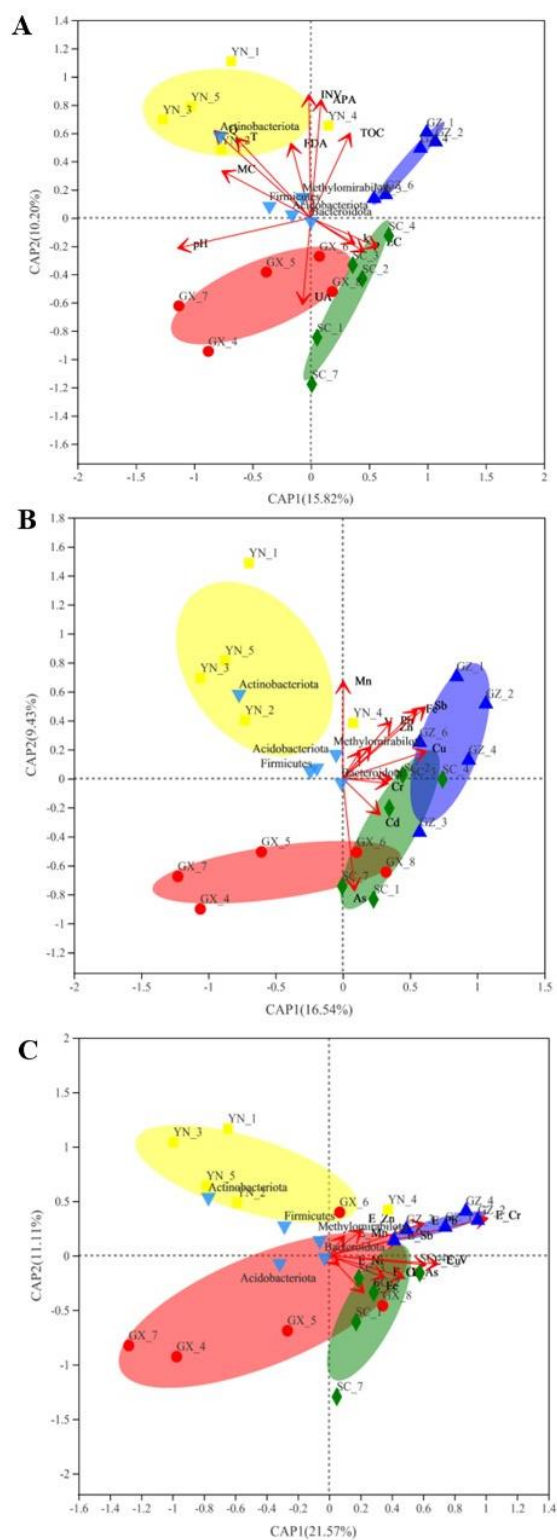


Fig. 7. Comparison of microbial communities. The distance-based redundancy analysis (db-RDA) was performed at the OTUs abundance level. The red line arrows denote the soil characteristics and microbial activity characteristics (A), and total (B) and bioavailable (C) metal(loid)s contents. The length of the arrows represents the degree of relevance between microbial communities and various factors. The percentage in the two axes indicates the eigenvalues of environmental factors.

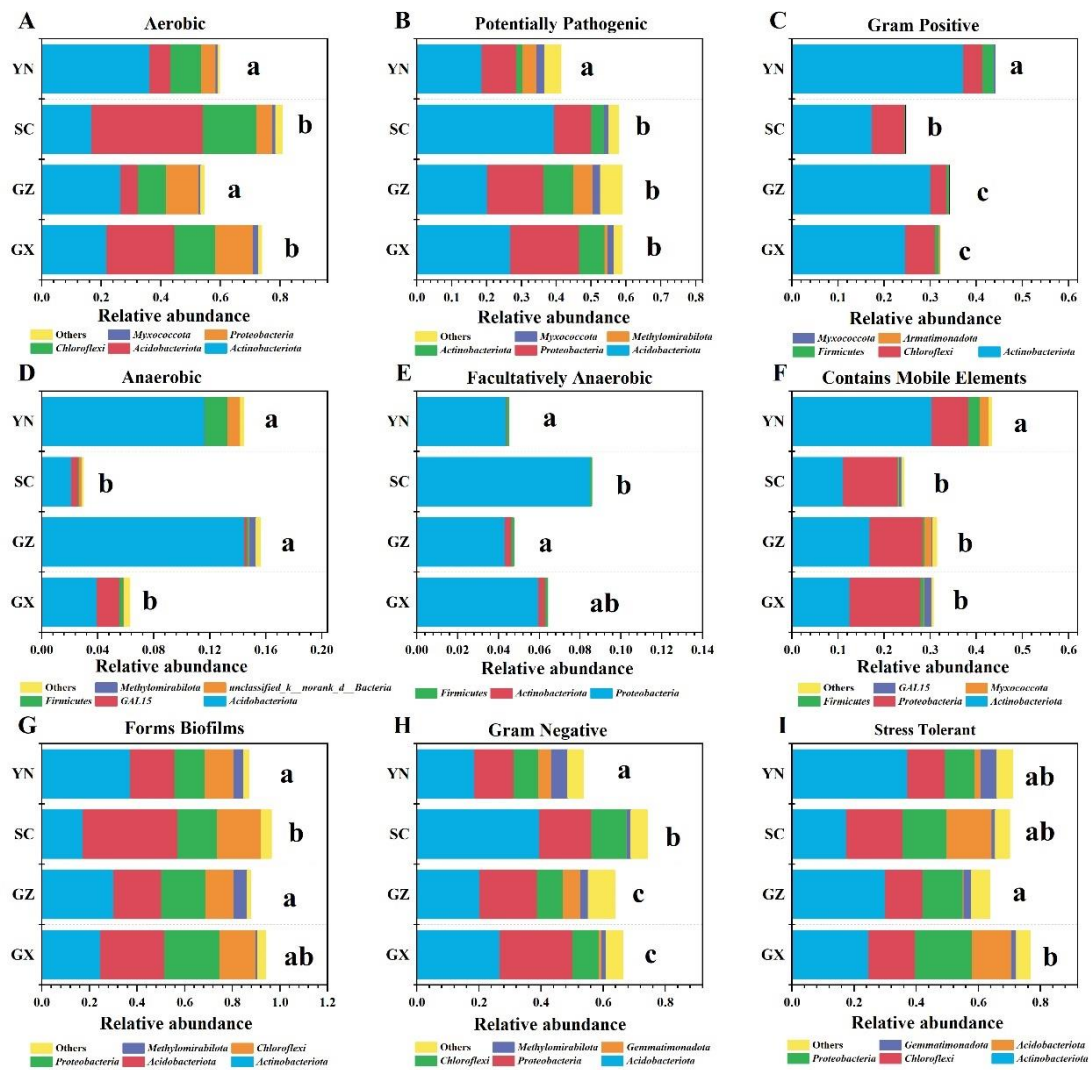


Fig. 8. The corresponding OTU contribution plots of the relative abundance of phyla possessing each phenotype (A: Aerobic; B: Potentially Pathogenic; C: Gram Positive; D: Anaerobic; E: Facultatively Anaerobic; F: Contains Mobile Elements; G: Forms Biofilms; and H: Gram Negative; I: Stress Tolerant) in the YN, SC, GZ, and GX sites are also shown. Different lowercase letters indicate significant differences between groups ($p < 0.05$).

1 New insights on the effect of non-ferrous metal mining and smelting activities
2 on microbial activity characteristics and bacterial community structure

3

4

5 Hao Li^a, Jun Yao^{a,*}, Ning Min^a, Geoffrey Sunahara^{a,b}, Robert Duran^{a,c}

6

7

8 ^a School of Water Resources and Environment, Research Center of Environmental Science
9 and Engineering, China University of Geosciences (Beijing), 29 Xueyuan Road, Haidian
10 District, 100083, Beijing, China

11 ^b Department of Natural Resource Sciences, McGill University, 2111 Lakeshore Drive, Ste-
12 Anne-de-Bellevue, Quebec, H9X 3V9, Canada

13 ^c Universite de Pau et des Pays de l'Adour, E2S-UPPA, IPREM 5254, BP 1155, 64013 Pau
14 Cedex, France

15

16

17

18

19 * Corresponding author. School of Water Resources and Environment, Research Center of
20 Environmental Science and Engineering, China University of Geosciences (Beijing), 29
21 Xueyuan Road, Haidian District, 100083 Beijing, China, E-mail: yaojun@cugb.edu.cn (J.
22 Yao), Tel: +86-10-82321958.

23

24 **Abstract**

25 Mining and smelting activities have brought potentially serious heavy metal(loid) pollution to
26 their surrounding locale. However, studies on microbial metabolic activities, community
27 structure, and adaptation in soils proximal to non-ferrous metal mining and smelting areas are
28 still lacking. Here the effects of biotic and abiotic characteristics of soil taken from sites
29 surrounding inactive and active nonferrous metal mine smelting facilities on microbial
30 enzyme activity, microcalorimetry, and high-throughput sequencing of 16S rRNA gene
31 barcoding were studied. Data indicated that the soils were heavily polluted by toxic
32 metal(loid)s, of which As and Cd are the main contaminants. Microbial acid phosphatase
33 activity and microcalorimetric total heat value were sensitive metabolic indicators in the
34 studied areas. *Actinobacteriota* had the highest relative abundance, followed by
35 *Proteobacteria*, *Chloroflexi*, and *Acidobacteria*. Microbial metabolic activity and bacterial
36 community structure and phenotype varied between inactive and active sites ($p < 0.05$). Such
37 analyses indicated that electrical conductivity, total As, Cu, and Mn contents, and
38 bioavailable As, Cu, Cd, and Mn concentrations were key factors determining microbial
39 activities, bacterial community structure, and phenotypes. Knowledge of microbial adaptation
40 to heavy metal stressors is important for better understanding the aerial transfer of fugitive
41 heavy metals (and possibly microbes) and for designing future strategies for improved soil
42 bioremediation.

43 **Keywords:** Mining and smelting activities, Heavy metal(loid)s pollution, Microbial
44 metabolic activities, Bacterial community, Phenotypes

45 **1. Introduction**

46 Industrial activities including mining and smelting, production of used Pb-acid batteries,
47 tanneries, and dye production, and agriculture are key sources of potentially toxic metal
48 pollution causing serious global environmental issues and have drawn considerable scientific
49 attention (Hu et al., 2021; Guo et al., 2021b). In recent decades, the long-term large-scale
50 non-ferrous metal mining and smelting activities in China have produced a large amount of
51 waste gas and water, as well as waste residues, carrying a variety of toxic heavy metal(loid)s
52 (e.g., As, Cr, Cu, Ni, Pb, and Zn) (Li et al., 2020; Ke et al., 2022; Zeng et al., 2022). These
53 environmental contaminants have invaded farmland and forests causing continuous damage
54 to their surrounding environments (Li et al., 2020; Guo et al., 2021b).

55 The soil ensures important ecosystem services, including material cycling, information
56 transfer, energy flow, and the microbial-mediated biogeochemical cycling of key
57 metal(loid)s (Liu et al., 2021). In environments contaminated by tailings and smelting waste,
58 excess heavy metals can affect microbial metabolic activities in soil (Chun et al., 2021). Soil
59 microbial activities are involved in the storage and cycling of nutrients in the soil (Batista et
60 al., 2020). Soil enzyme activities (phosphatase, invertase, and urease) have been used as
61 biochemical markers (biomarkers) of soil microbial nutrient (C, N, and P) effects and
62 metabolic activity (Chae et al., 2017; Aponte et al., 2021). Other soil biomarkers such as
63 fluorescein diacetate hydrolase (FDA) reflect the total microbial activity (Schnurer and
64 Rosswall, 1982), whereas isothermal microcalorimetry can be used as a quantitative and real-
65 time measure of the total metabolic activity of microbial communities in soil (Herrmann et

66 al., 2014). Microbial enzymatic and total metabolic activities are considered sensitive and
67 effective indicators of soil health in mining and smelting ecosystems (Vinhai-Freitas et al.,
68 2017; Yuan et al., 2021).

69 As important components of soil, microbial communities also play a key role in the
70 ecological functions of energy and nutrient cycling (Guo et al., 2021a; Li et al., 2022b).

71 Bacteria are important members of the soil ecosystem, interacting with plants or fungi to
72 change and adapt to the soil environment (Chun et al., 2021). Therefore, soil microbial
73 characteristics can be used as potential indicators of ecosystem health (Li et al., 2020).

74 Although tailings and smelting sites are often described as metal-rich and nutrient-poor
75 environments, certain microorganisms can tolerate highly toxic environmental conditions by
76 developing specific survival strategies for their growth on contaminated sites (Chun et al.,
77 2021). These strategies include detoxification, metal resistance, and cellular oxidative stress
78 responses (Jiang et al., 2021). Many heavy metal-resistant microorganisms (e.g., dominant
79 soil phyla including *Actinobacteria*, *Proteobacteria*, *Chloroflexi*, and *Acidobacteriota*) can be
80 found in various polluted environments (Li et al., 2020; Yin et al., 2023). Differences in
81 microbial community structure between active and inactive nonferrous metal smelting sites
82 have been reported earlier (Liu et al., 2018). Phenotypic plasticity is widespread in the
83 biological world, but relatively few studies have been conducted in the field of
84 microorganisms (Ward et al., 2017). Phenotypic predictive research based on soil bacterial
85 communities is important for understanding the adaptability of microbial populations, as well
86 as for protecting the ecological environment and maintaining species coexistence (Zhang et
87 al., 2019b).

88 The soil properties including the bioavailable and total contents of heavy metal(loid)s may
89 vary greatly between different mining and smelting sites (Liu et al., 2021; Yin et al., 2023).
90 Earlier studies show that the total concentrations of As, Cd, Co, Cr, Cu, Mn, Ni, and Pb are as
91 important as their bioavailable contents by influencing the soil microbial community
92 structure (Yin et al., 2023). The exchangeable (EXC) content of heavy metal(loid)s is often
93 regarded as the bioavailable fraction in soil, using the European Community Bureau of
94 Reference (BCR) sequential extraction procedure (Zhu et al., 2018). The pollution load index
95 (PLI) and contamination factor (CF) can be used to assess the pollution degree of heavy
96 metal(loid)s in soil (Rinklebe et al., 2019). Although complex interactions between soil
97 properties, heavy metal(loid)s, microbial metabolic activities, and microbial communities
98 have been reported (Yan et al., 2020), few studies have addressed how these important factors
99 (heavy metal(loid)s and soil properties) and processes affect microbial metabolic activities
100 and bacterial communities in contaminated soils surrounding active and inactive nonferrous
101 metal mining and smelting sites.

102 Most nonferrous metal smelting and collection activities in Southwest China are located in
103 karst landforms, so mobile heavy metals are often highly diffusible and can disperse within
104 the environment, especially through runoff or atmospheric deposition. Long-term mining and
105 smelting of non-ferrous metals have caused serious damage to the health of the local soil
106 environment (Liu et al., 2022a; Zhang et al., 2020). Compared to active nonferrous metal
107 smelting sites, microbial communities present in mine tailings at inactive or abandoned
108 facilities can adapt (by long-term natural attenuation) to their nonferrous metal(loid)s-
109 containing environments (Liu et al., 2018). Therefore, there are few studies on the microbial

110 characteristics and bacterial community structure of the surrounding soil caused by the non-
111 ferrous metal activities in different states (inactive and active).

112 Here we hypothesize that the microbial communities in soils proximal to nonferrous metal
113 mining and smelting sites are influenced by these neighboring activities. The research aims
114 were to 1) Determine the microbial metabolic activity and bacterial communities structure
115 characteristics in contaminated soil around active and inactive nonferrous metal mining and
116 smelting sites in Southwest China, and 2) Identify and compare the main factors affecting the
117 microbial characteristics of the studied nonferrous metal-contaminated sites. The results
118 described here will provide new insights into soil microbial characteristics after
119 environmental disturbances from different mining and smelting activities.

120 **2. Materials and methods**

121 *2.1. Study areas*

122 The soil samples were collected in triplicate from the topsoil (depth of 0-20 cm) of forest land
123 proximal to two active, and two inactive sites non-ferrous metal mining and smelting sites
124 (Fig. 1). It was assumed that the forest land surrounding the smelter sites were not influenced
125 by extraneous anthropogenic factors such as agricultural tilling, use of chemical and
126 biological fertilizers, domestic hazardous waste, and roadside emissions.

127 The active Lumaolin Pb-Zn tailing pond (GZ) was located in Puding County, Guizhou
128 Province (105°38'28"E, 26°25'29"N) (Figs. 1 and S1). The metal minerals are mainly
129 sphalerite, smithsonite, and galena. The site GZ started production after 2008. Samples were
130 collected from five representative points (GZ-1, GZ-2, GZ-3, GZ-4, and GZ-5). Additional

131 information is provided in Supplementary Information (Text S1.1). The active Maliwan Cu-
132 Ni tailing pond (SC) was located in Huili County, Sichuan Province (102°4'47"E, 26°26'8"N)
133 (Figs. 1 and S1). The tailings are mainly copper-nickel beneficiation smelting slag, nickel-
134 iron processing plant waste, and calcium sulfate slag. Samples were collected from five
135 representative points (SC-1, SC-2, SC-3, SC-4, and SC-5).

136 The inactive Gejiu Pb smelting site (YN) was located in Gejiu City, Yunnan Province
137 (103°13'30"E, 23°30'30"N) (Figs. 1 and S2). A large amount of waste residue was stored at
138 this smelting area typical of the lead smelting industry. Samples were collected from five
139 representative points (YN-1, YN-2, YN-3, YN-4, and YN-5). The inactive Huilong As
140 smelting site (GX) was located in Zhongshan County, Guangxi Province (111°16'48"E,
141 24°27'48"N) (Figs. 1 and S2). This site opened operations (producing metal arsenic, arsenic
142 trioxide, and other products) in 1994 but stopped production in 2003. Samples were collected
143 from five representative points (GX-1, GX-2, GX-3, GX-4, and GX-5).

144 All samples were collected using sterile tools and placed in biological storage bags (□ 1 kg
145 per sample), stored in ice packs, and quickly transported to the laboratory. Each collected soil
146 sample was divided into two sub-samples for subsequent testing, one of which was air-dried
147 (for 10 d) at room temperature, sieved (100-mesh) to remove rocks, animal, and plant debris,
148 etc., and stored at 4°C for geochemical and microbial analyses, and the other aliquot was
149 stored at -80°C for high-throughput sequencing. All chemicals and reagents were purchased
150 from commercial sources and were at least analytical grade purity.

151 ***2.2. Geochemical analyses and heavy metal(loid) pollution assessment***

152 The electrical conductivity (EC, expressed as $\mu\text{S}/\text{cm}$) and the pH of the soil were determined
153 in the slurry with the soil-to-water ratio of 1:2.5 and 1:5, respectively. The soil moisture
154 content (MC, as %) was measured by drying the soil sample in an oven ($105 \pm 2^\circ\text{C}$) for 8 h
155 until the weight remains constant (Li et al., 2020). The soil total organic carbon (TOC, mg/g)
156 in soil was determined using a TOC instrument (Shimadzu SSM-5000, Japan) (Zhu et al.,
157 2018). To determine the total amount of heavy metal(loid)s in soil, the following digestion
158 steps were taken. The air-dried soil sample was ground and sieved, and 0.100 g of pretreated
159 soil sample was weighed, and then added into a digestion tube containing $\text{HNO}_3\text{-HCl}$ (1:3,
160 volume/ volume). The tube was placed in a $140\text{-}180^\circ\text{C}$ heater for 2 h. If a solid residue
161 remained in the tube, a 2 mL volume of HF was added until a white sediment was formed.
162 The digested residue was then dissolved in a 1% HNO_3 solution and made up to 50 mL in a
163 volumetric flask. All experimental data were corrected by subtracting the blank group of
164 mixed acids prepared using the same digestion steps described above. The recovery rate of
165 total As, Cd, Cr, Cu, Fe, Mn, Ni, Pb, Sb, V, and Zn concentration in soil was between 92.5%
166 and 107.5%, and the relative standard deviation (RSD) was $< 5\%$. The concentrations of As,
167 Cd, Cr, Cu, Fe, Ni, Pb, Sb, V, and Zn were measured using an inductively coupled plasma
168 atomic emission spectrometer, with the detection limits of 0.03, 0.002, 0.004, 0.002, 0.002,
169 0.009, 0.03, 0.03, 0.004, and 0.005 mg/kg, respectively. The quality assurance and quality
170 control procedures are described in Text S1.2.

171 The bioavailable metal(loid) contents (EXC, Exchangeable fraction) (expressed as mg/g or
172 as % of total) were determined by using 0.11 M acetic acid solution of the BCR sequential
173 extraction method, as described in Text S1.2. The pollution load index (PLI) and

174 contamination factor (CF) were used to assess the pollution degree of heavy metal(loid)s in
175 the soil (Rinklebe et al., 2019). The calculation of these indices is described in Text S2.

176 **2.3. Microbial metabolic activity characteristics**

177 **2.3.1. Microcalorimetric measurements**

178 The total metabolic activity of microorganisms was measured using a Model TAM-IV (Fig.
179 S3) isothermal multichannel microcalorimeter (TA Instruments, Delaware, USA), as
180 described earlier (Herrmann et al., 2014). This technique provides qualitative and quantitative
181 information on microbial metabolic processes by generating power-time curves based on
182 microbial growth processes (see Text S3). Using the power-time curve, a variety of
183 thermodynamic parameters can be obtained, including peak time (T , expressed as h), total
184 heat (Q , J/g), growth rate (k , h^{-1}), and peak power (P , $\mu\text{W/g}$) (Zhu et al., 2018). The research
185 data calculated using microcalorimetry are similar to conventional microbiological methods
186 and can provide more detailed information on complex biological processes.

187 **2.3.2. Soil enzyme activity measurements**

188 Fluorescent diacetate hydrolase (FDA, expressed as mg fluorescein/g) was measured as a
189 reflection of the overall microbial activity. The following soil enzyme activities involved in
190 the metabolic cycling of nutrient elements (C, N, and P) were measured, as described by
191 others (Chae et al., 2017; Li et al., 2022a): invertase (INV; hydrolyzes sucrose to fructose and
192 glucose, expressed as mg glucose/g), urease (UA; hydrolyzes urea to carbon dioxide and
193 ammonia, mg NH_4/g), and acid phosphatase (APA; catalyzes the release of phosphate by
194 hydrolysis, mg p -nitrophenyl phosphate/g). Methodological details of the enzyme assays are

195 described in Text S4.

196 ***2.4. DNA extraction, 16S rRNA gene sequencing***

197 Genomic DNA was extracted from the selected samples by 1% agarose gel electrophoresis,
198 and the V3-V4 hypervariable region fragment of the 16S rRNA gene was amplified by the
199 polymerase chain reaction (PCR). The primer sequence was 338F (5'-ACT CCT ACG GGA
200 GGC AGC AG-3') and 806R (5'-GGA CTA CHV GGG TWT CTA AT-3'). The 2% agarose
201 gel electrophoresis was used to verify the qualified PCR amplification. The PCR product was
202 further purified with E.Z.N.A.[™] Gel Extraction Kit (OMEGA Bio-Tek Inc., USA). Bacterial
203 sequencing was carried out on the Illumina MiSeq platform of Majorbio Bio-Pharm
204 Technology Co., Ltd (Shanghai, China).

205 ***2.5. Data processing and statistical analyses***

206 The raw sequencing data were optimized using Fastp software (v0.19.6,
207 <https://github.com/OpenGene/fastp>; accessed 22-March-2023) to filter raw reads. The raw
208 pair-end reads were processed with Flash software (v1.2.11)
209 (<https://ccb.jhu.edu/software/FLASH/index.shtml>; accessed 22-March-2023). During the
210 merging process, the allowable error rate for the pairing of overlapping regions was ≤ 0.2 and
211 resulted in high-quality sequences. Bacterial community diversity indexes, including alpha
212 (α) richness and diversity indices (Ace, Chao, Coverage, Shannon, Sobs, and Simpson) were
213 calculated using the "vegan" package. The calculation of the beta (β) diversity of the
214 microbial community was based on Bray Curtis distance similarity. The Analysis of
215 Similarity (ANOSIM) was used to analyze the availability of sample groupings. Hierarchical

216 clustering and principal coordinates analysis (PcoA) was used to analyze the differences in
217 bacterial communities among samples. Spearman's correlation and distance-based
218 redundancy (db-RDA) analyses were processed using the vegan package in R version 3.4.2 to
219 identify important environmental variables affecting bacterial community structure.
220 Differences between groups were considered significant at $p < 0.05$. **Data were expressed as**
221 **the average \pm standard deviation (SD) unless otherwise stated.** BugBase is a microbiome
222 analysis tool to identify high-level phenotypes in microbiome samples **and enable** phenotype
223 prediction. SPSS 22.0 software was used to calculate the statistical tests, as described in Text
224 S5.

225 **3. Results and discussion**

226 ***3.1. Geochemical characterization of the studied soils***

227 The geochemical properties of the soil from the different site soils are shown in Fig. S4 and
228 Tables S1-S4. The soil pH of sites GX, GZ, and YN was either weakly acidic or weakly
229 alkaline, whereas the SC soil was acidic (pH 4.84 – pH 5.89). These acidic and alkaline pH
230 signatures are typical of forest soils surrounding contaminated sites such as non-ferrous metal
231 smelting sites and tailing ponds (Zhao et al., 2020). The MC and EC values of sites GX, GZ,
232 SC, and YN differed greatly because the soil structure around the polluted sites was
233 heterogenous and complex (Zhao et al., 2020). The TOC contents of all samples were lower
234 than the average generic local soil background level (CNEMC, 1990), which agrees with the
235 fact that the surrounding soils of non-ferrous metal-contaminated sites are often nutrient-poor
236 (Batista et al., 2020). The large differences in soil properties are consistent with the high

237 degree of soil heterogeneity in the affected areas surrounding the studied mining and smelting
238 activities.

239 **3.2. Heavy metal(loid) contents**

240 The total heavy metal contents of soils sampled from the four study sites are summarized in
241 Fig. 2A and Tables S5-S9. The average total contents of As, Cd, Cr, Cu, Fe, Ni, Pb, Sb, V, and
242 Zn in the soil exceeded the local soil background value (CNEMC, 1990), especially the total
243 As, Cd, and Pb content that exceeded the standard values of Grade II for agricultural land.
244 This observation is not surprising given that nonferrous metal smelter sites are enriched with
245 nonferrous metal ores.

246 In soils from the inactive sites (respectively YN and GX), the average total contents (mg/kg)
247 of Cd (17.61 ± 19.72 and 18.14 ± 35.52), Cu (19913.52 ± 11650.05 and 756.99 ± 647.79),
248 and Ni (94.14 ± 13.61 and 782.63 ± 997.05) were higher than those from the active areas (SC
249 and GZ) (Fig. 2A). The average contents (mg/kg) of Cu (19913.52 ± 11650.05), Fe (91468.16
250 ± 30496.68), Pb (1234.48 ± 1053.83), and Sb (27.46 ± 8.14) in the YN site were higher than
251 in the other sites, whereas As (2985.16 ± 1214.52 mg/kg) in SC site was higher than that in
252 the other sites. Such results are consistent with earlier reports that As, Cd, Cu, Pb, Sb, and Zn
253 (especially As, Cu, and Cd) are the major heavy metal pollutants in nonferrous metal mining
254 and smelting areas (Liu et al., 2022a; Yin et al., 2023).

255 In the inactive site soils (respectively YN and GX), the average bioavailable metal contents
256 (mg/kg) of As (3.51 ± 3.29 and 3.70 ± 6.47), Cd (5.37 ± 8.54 and 9.25 ± 20.53), Cu ($88.66 \pm$
257 50.34 and 51.03 ± 111.35), Fe (56.01 ± 81.58 and 264.10 ± 574.69), Sb (0.22 ± 0.12 and 0.16

258 ± 0.23), and Zn (135.78 ± 176.17 and 136.39 ± 301.36) were significantly higher (Fig. 2B,
259 Table S10) than the active sites (respectively SC and GZ) as evidenced by As (0.44 ± 0.16
260 and 0.55 ± 0.03), Cd (0.89 ± 0.51 and 0.06 ± 0.05), Cu (0.19 ± 0.16 and 1.50 ± 0.37), Fe
261 (1.66 ± 1.21 and 3.26 ± 1.13), Sb (0.14 ± 0.06 and 0.09 ± 0.05), and Zn (115.08 ± 125.53 and
262 1.80 ± 0.36). In addition, the average bioavailable contents (mg/kg) of Cr (6.37 ± 1.43), Ni
263 (2.67 ± 2.61), Pb (54.32 ± 97.46), and V (0.08 ± 0.08) were highest in the soils from the YN
264 area.

265 The correlation analyses (Tables S11-S14) show that the total contents of Cd, Cu, Mn, and Ni
266 were significantly and positively correlated ($p < 0.05$) with their bioavailable metal contents.
267 The TOC had a significant positive correlation ($p < 0.05$) with the bioavailable contents of
268 Cd, Mn, and Sb (Table S13). A rich organic C in soil could lead to the release of heavy metal
269 ions from the mineral matrix, and then be re-adsorbed to organic C (as well as the surface of
270 other minerals) functional groups (Yin et al., 2023).

271 The bioavailability of heavy metals in soil can be increased in the presence of plant root
272 exudates (such as organic acids) and therefore could be affected by the diversity and
273 composition of indigenous plant species (Yin et al., 2023). The percentages of bioavailable
274 content (EXC fraction expressed as %) of As, Cd, Fe, Pb, and V in the inactive sites (YN and
275 GX) were higher than those in the active site (Table S11), whereas those of Cd were SC
276 (0.63), YN (30.50), GX (51.02) and GZ (17.44) sites, and of Mn were SC (7.69), YN (7.31),
277 GX (7.40), and GZ (4.41) sites. Compared to the other heavy metal(loid)s, Cd had the highest
278 bioavailability in the YN, GX, and GZ sites, probably because Cd can be mobilized in soil
279 following competition and/or ligand-induced desorption (Kubier et al., 2019). Overall, the

280 bioavailability of heavy metal(loid)s in soils collected close to the inactive sites (YN and GX)
281 was generally higher than that of soils collected close to the active sites (SC and GZ).
282 Fugitive dust particles carrying the measured heavy metals (including the total and
283 bioavailable fractions) were likely transferred off-site from the nearby smelter dump sites and
284 accumulated in the surrounding studied forest soils. By design, it is unlikely that the source of
285 the measured heavy metals from forest soil was from vehicular emissions or debris, but
286 dispersion from local agricultural sources should not be under-estimated.

287 The Contamination factor (CF) was calculated as the ratio of the measured total heavy
288 metal(loid)s contents with the corresponding local geochemical background values (CNEMC,
289 1990) and was used to assess the pollution level (Fig. 2C, Table S12). The CF index for As,
290 Cd, Pb, and Sb reached a “high pollution level” in soils proximal to the active (GZ and SC)
291 and inactive (GX and YN) sites. In addition, the Cr (10.12), Cu (27.23), Mn (3.57), Ni
292 (29.24) and Zn (65.46) in the GX site, and Cu (430.10), and Zn (10.86) in YN, and Zn
293 (19.97) in GZ reached “high pollution levels.”

294 The overall heavy metal pollution level of the surface soils was further assessed using the
295 pollution load index (PLI), which was calculated from the total contents of heavy metals and
296 local geochemical background values (CNEMC, 1990). The pollution index profile of the
297 four study sites was YN (1.81) > SC (1.74) > GX (1.68) > GZ (1.50). The PLI values were >
298 1 and indicated that all study sites were “heavily polluted” by heavy metal(loid)s, which may
299 be attributed to the weathering of metal minerals and the transport of flying dust that
300 contributes to the transfer of heavy metals from the smelter sites into the nearby collected soil
301 sites (Zhao et al., 2019; Liu et al., 2022b).

302 **3.3.1 Soil enzyme activities**

303 The microbial enzyme activities of microorganisms among the four research sites were
304 different (Fig. 3, Tables S1-S4). A previous study reported that soil geochemical properties,
305 geographical spatial distance, and metal(loid) concentrations are the main factors affecting
306 microbial differences among three non-ferrous metal-contaminated areas (Liu et al., 2022a).
307 The Spearman correlation analysis showed that the urease activity (UA) was negatively
308 related to MC and pH ($p < 0.01$) (Tables S13-S18), indicating that low MC or pH inhibited
309 UA. The TOC was positively related to FDA, APA, and INV activities ($p < 0.05$). It has been
310 reported that pH and TOC are important factors affecting soil enzyme activity and that TOC
311 could stimulate enzyme activity (Batista et al., 2020; Aponte et al., 2021). The FDA activity
312 was negatively correlated with Ni ($p < 0.05$), and UA activity was negatively related to the
313 bioavailable Mn, as well as total Mn, Pb, Sb, and Zn contents ($p < 0.05$). Enzymes related to
314 soil C-, N-, and P- cycling can be inhibited by heavy metal(loid)s, resulting in differences in
315 enzyme activities in the sampled soils (Aponte et al., 2021; Li et al., 2022b). The observed
316 enzymic inhibition likely involves the binding of metal(loid)s to the active site in the enzyme
317 leading to a more stable complex. Alternatively, the metal(loid)s could also decrease enzyme
318 synthesis and secretion leading to an inhibition of the soil microbial growth and reproduction
319 (Zhao et al., 2015). The enzyme activities (FDA, INV, APA, and UA) were correlated with
320 the total heavy metal(loid) concentrations (As, Mn, Ni, Pb, Sb, and Zn) as well as with the
321 bioavailable Mn and Cd (Tables S13-S18), confirming that forest soil enzyme activities can
322 be used as sensitive biological indicators of aerial heavy metal transfer (by fugitive dust
323 particles) from the neighboring active and inactive smelter facilities, similar to other reports

324 (Wahsha et al., 2017; Zhao et al., 2020).

325 **3.3.2 Total microbial activity using isothermal microcalorimetry**

326 The heat production curves reflecting the metabolic growth of the soil microbial community
327 among different research sites were different (Fig. 3E, Tables S1-S4). On the other hand, the
328 k and P were higher in the inactive sites (Fig. S5, Tables S1-S4). Other researchers noted that
329 the microbial characteristics of non-ferrous metal-contaminated areas in different regions are
330 affected by spatial geography, heavy metal(loid) contents, and edaphic factors (Liu et al.,
331 2022a). Spearman correlation showed that the P and k were significantly and negatively
332 related to the MC and pH ($p < 0.01$), whereas they were positively related to the UA activity
333 ($p < 0.05$) (Tables S13-S18). The bioavailable contents (EXC fractions) of Cr, Cu, and Fe
334 were negatively related to Q and T values ($p < 0.05$), which agreed with the fact that the high
335 concentrations of heavy metal(loid)s decreased the total activity of soil microbial
336 communities (Harris et al., 2012). Also, Q values were negatively related to the total contents
337 of As and Cu ($p < 0.05$), while T values were negatively related to total As contents ($p <$
338 0.05). Such observations suggest that the total content of As and Cu are likely the main
339 factors affecting the microbial activity in the soils proximal to the active and inactive
340 smelting facilities. High concentrations of metal(loid)s can damage and/or inhibit critical
341 microbial cell functions (Harris et al., 2012; Yan et al., 2020). In addition, Q is significantly
342 ($p < 0.05$) and negatively correlated with the total content of metal(loid)s (**Cr, Cu, Fe, Mg,**
343 **Mn, Pb, and Zn**) in a non-ferrous metal smelting contaminated site (Li et al., 2022a). Thus,
344 the thermodynamic parameters correlated with the total As and Cu concentrations and the
345 bioavailable Cr, Cu, and Fe contents may be sensitive indicators of microbial metabolic

346 activity in some but not all heavy metal(loid) polluted soils.

347 ***3.4. Microbial community alpha and beta diversities***

348 A dataset of 997,251 high-quality 16S rRNA gene sequences was generated. The average
349 sequence number per sample was 415 bp. The 8,206 OTUs were obtained from high-quality
350 sequences. Compared to a previous study (Liu et al., 2022a), the number of OTUs was low
351 probably because the high concentration of metal(loid)s can reduce microbial richness. The
352 platform sparse curve shown in the Pan/Core species curve (Fig. S6) indicated that the
353 sequencing depth collected most of the microbial community diversity and that the sample
354 size was sufficient. The α -diversity parameters significantly differed according to the site
355 (Fig. 4; Tables S14 and S15), suggesting that the toxic metal(loid)s concentration can shape
356 the microbial community as observed in a dynamic study (Xu et al., 2019). The microbial α -
357 diversity Simpson index (Table S15) was negatively correlated with bioavailable Cd and Mn
358 concentrations ($p < 0.05$). This is consistent with a previous report that toxic metal(loid)s
359 pollution harmed the microbial community (Li et al., 2020). The α -diversity indices were
360 significantly and positively related to the FDA, INV, and APA activities ($p < 0.05$) (Table
361 S14) in the active and inactive smelter sites, suggesting that differences in microbial enzyme
362 activity could reflect microbial diversity, as reported previously (Xiao et al., 2020). Venn
363 diagrams show that there are 1111 shared core OTUs between the four sites (Fig. 5A).
364 Principal co-ordinates analysis (PCoA), based on OTU distances, showed a separation
365 according to sites (Figs. 5B and 8; ANOSIM with 999 iterations, $R = 0.2343$, $p = 0.001$),
366 indicating that the microbial communities of the sites were distinct. Such observations
367 confirmed the possibility that the composition of bacterial communities was affected by the

368 land use, soil geochemical properties, and metal(loid)s content (Zhao et al., 2019). Off-site
369 transfer of heavy metals to the collected forest soil samples probably led to direct (e.g.,
370 decreased host site indigenous microbial metabolic activity and community abundance) and
371 indirect (e.g., stimulation of metal resistance traits and adapted abundance) effects on the new
372 host soil microbial community. This possibility is supported by the observed effects on soil
373 enzyme activities and microbial abundance. Data suggests that the microorganisms sensitive
374 to metal(loid) stress will decrease in abundance, whereas that of insensitive microorganisms
375 will increase. The following studies were conducted to determine the effects of the off-site
376 transfer on the microbial community composition.

377 **3.5. Microbial taxa distribution**

378 We identified OTUs belonging to 48 phyla, 152 classes, 348 orders, 539 families, and 1082
379 genera in soil samples around the four (two active and two inactive) contaminated sites. It
380 was challenging to identify or monitor control (reference) soils in this study. The microbial
381 community in typical healthy soils was considered as a reference for comparison with the
382 present results. The *Proteobacteria*, *Acidobacteria*, *Actinobacteria*, and *Chloroflexi* were the
383 most abundant bacterial phyla in healthy soil, with average relative abundances of 39%, 20%,
384 13%, and 3%, respectively (Janssen, 2006). Specifically, the average relative abundances (%)
385 of *Proteobacteria* in the contaminated forest soil around sites were SC (25.10), YN (15.01),
386 GX (21.84), and GZ (20.13), which is lower than that in healthy soil (39) (Fig. 5C). The
387 average relative abundances (%) of *Acidobacteria* in the contaminated soil around the SC,
388 YN, GX, and GZ sites were 18.33, 14.13, 11.59, and 17.29, respectively, which are lower
389 than those of healthy soil. However, the average relative abundances (%) of *Actinobacteria* in

390 the contaminated soil around sites were SC (21.61) YN (35.07), GX (23.19), and GZ (30.42),
391 higher than those in healthy soil (Fig. 5C). *Actinobacteria*, the most dominant phyla in the
392 soil surrounding mining and smelting activities in the current study, showed remarkable
393 resilience in heavy metal(loid)s environments with low nutrient contents (Qiao et al., 2021),
394 consistent with other studies (Zhang et al., 2019a). The relative abundance of dominant phyla
395 among the active/inactive sites (Fig. 5) may be due to the different adaptabilities of
396 microorganisms to survive in environments having sub-optimal pH, low nutrient conditions,
397 and metal(loid)s stress. *Actinobacteria* was unusually abundant in neutral and slightly acidic
398 environments (Chen et al., 2013). The relative abundance of *Actinobacteria* was significantly
399 and negatively correlated with pH ($p < 0.05$), indicating that changes in soil pH might have
400 affected the *Actinobacteria* enrichment (Fig. 6). Our data indicate that members of the
401 *Actinobacteria* can adapt to or resist high levels of heavy metal(loid)s pollution as previously
402 shown in marine sediments (Duran et al., 2015). This is evidenced by the inhibition of growth
403 and development at high metal(loid)s concentrations that would decrease their proportion in
404 the bacterial community (Chen et al., 2018). Similar main microbial communities were found
405 in abandoned non-ferrous metal tailings, gold tailings environments, and V-Ti magnetite
406 tailings (Kang et al., 2020; Yan et al., 2020). The ubiquity of *Actinobacteria* is mainly due to
407 the adsorption and complexation capacity of microorganisms, which aids in their adaptability
408 to harsh metal-rich environments (Wu et al., 2021).

409 Interestingly, the average relative abundances (%) of *Chloroflexi* in the contaminated soils
410 around the SC (24.10), YN (14.43), GX (24.79), and GZ (12.91) sites (Fig. 5C) were higher
411 than that in the healthy soil (3). Previous studies showed that *Chloroflexi* as well as a

412 *Proteobacteria* were enriched from sites disturbed by mining (Xiao et al., 2021). In heavy
413 metal-polluted soils, *Chloroflexi* was the main phylum with tolerance and resistance to heavy
414 metal stress (Yin et al., 2023). These studies pointed out that members of *Chloroflexi* are
415 poor-nutrition bacteria that prefer low-nourished soil habitats. The phyla *Actinobacteria* and
416 *Chloroflexi* could be involved in metal detoxification by decreasing the high toxicity found in
417 the present metal-rich environment (Wang et al., 2020; Liu et al., 2021), which could explain
418 why their relative abundance was higher than in the healthy soils. In heavily polluted soil, the
419 number of bacteria susceptible to heavy metal stress will decrease, so that the tolerant or
420 resistant bacteria can become the dominant species (Zhao et al., 2019).

421 At the genus level, the most dominant genera in the soil (%) around the SC site were
422 *norank_o_norank_c_AD3* (8.47), *norank_o_subgroup_2* (6.11), *Xanthobacteraceae* (4.72),
423 *norank_o_Elsterales* (4.43), *Acidothermus* (4.03), *norank_o_Acidobacteriales* (3.99),
424 *HSB_OF53-F07* (3.44), *Bradyrhizobium* (3.21), *FCPS473* (2.63), and *norank_o_Gaiellales*
425 (1.96) (Fig. 5D and S8). The most dominant genera in the soil around the YN site were
426 *norank_o_Gaiellales* (5.75), *norank_o_Vicinamibacterales* (4.86), *Vicinamibacteraceae*
427 (3.42), *norank_o_Rokubacteriales* (3.37), *Gemmatimonadaceae* (3.25), *norank_f_67-14*
428 (3.23), *Gaiella* (2.93), *unclassified_f_Micromonosporaceae* (2.6), *Xanthobacteraceae* (2.25),
429 and *norank_o_norank_c_MB-A2-108* (2.05). The most dominant genera of soil around the
430 GX site were *JG30-KF-AS9* (5.88), *norank_o_norank_c_AD3* (4.06), *JG30-KF-CM45* (3.74),
431 *Sinomonas* (3.33), *Ktedonobacteraceae* (2.25), *norank_o_Acidobacteriales* (2.16), *Delftia*
432 (2.1), *Bradyrhizobium* (1.99), *Acidothermus* (1.88), and *norank_o_Vicinamibacterales* (1.71).
433 The most dominant genera in the soil around the GZ site were *Arthrobacter* (6.68),

434 *Vicinamibacteraceae* (5.28), *norank_o_Vicinamibacterales* (5.27), *norank_o_Chloroplast*
435 (2.53), *Nocardioides* (2.46), *Gaiella* (2.42), *norank_o_Rokubacteriales* (2.25),
436 *norank_o_Gaiellales* (2.17), *norank_o_norank_c_KD4-96* (2.11), and *Roseiflexaceae* (1.88).
437 *Micromonospora* belonging to *Actinobacteria* showed strong resistance to abiotic stress
438 (Stevenson and Hallsworth, 2014). *Arthrobacter* can thrive in environments with high metal
439 pollution through physiological and genetic modifications (Zhang et al., 2004).
440 The *norank_c_Acidobacteria* is one of the top five genera found in gold mining areas (Yan et
441 al., 2020). In the typical antimony ore smelting area in the south of China, at the genus level,
442 the bioindicators were *Ktedonobacteraceae* and *Xanthomonadaceae_unclassified* in the
443 topsoil, and *Gemmatimonadacea* and *norank_o_norank_c_KD4-96* were in the middle soil
444 depth, and *JG30-KF-AS9* and *norank_o_norank_c_AD3* were in deep soil (Wang et al.,
445 2022). In addition, *norank_o_Rokubacteriales*, *norank_o_subgroup_2*, and
446 *norank_o_Acidobacteriales* were the main genera in As/Sb contaminated sites (Kalam et al.,
447 2020; Wang et al., 2022).
448 In the contaminated soil around a vanadium smelter, the main genera in the topsoil included
449 *JG30-KF-CM45*, while the dominant genera in profile soils included *norank_o_Gaiellales*,
450 *Gaiella*, and *norank_o_norank_c_KD4-96* (Wang et al., 2020). In abandoned mine soils in
451 Korea, the main bacteria included *norank_o_Vicinamibacterales*, *norank_o_Gaiellales*,
452 *Micrococcales*, *Gemmatimonadales*, *norank_o_Acidobacteriales*, *Bryobacteriales*,
453 *norank_o_subgroup_2*, *Micropepsales*, *Ktedonobacterales*, and *Pseudonocardiales* (Chun et
454 al., 2021). This exemplifies the main groups of bacteria found in heavy metal-contaminated

455 soil.

456 *Ktedonobacteria* can utilize or degrade different carbohydrates (Wang et al., 2022), whereas
457 *Bradyrhizobium* can minimize oxidative stress and enhance N-fixation in particular plants
458 (Rodrigues et al., 2013). *Arthrobacter* can survive and develop for a long time in harsh
459 ecological environments (Guo et al., 2021a). *Nocardioides* is also noted for its ability to
460 promote plant growth. The majority of these genera promote the C-cycle and fix N, which is
461 conducive to survival in a nutrient-poor environment (Sun et al., 2019). In summary, the
462 observed heterogeneous bacterial community involved in nutrient cycling has probably
463 adapted to anthropogenic disturbances. These major bacterial genera are bioindicators for
464 metal(loid)s-contaminated soil. Thus, the advantages of these core groups may reflect the
465 harsh soil ecological environment, representing the general adaptive groups around the non-
466 ferrous metal mining and smelting facilities in Southwest China.

467 ***3.6. Soil properties, heavy metal(loid)s, microbial metabolic activity, and microbial*** 468 ***community relationships***

469 The Spearman correlation heatmap (Fig. 6) and distance-based redundancy (db-RDA) (Fig.
470 7) analyses were performed based on the sequence abundance of OTUs to identify potential
471 relationships between microbial communities and environmental factors in the four studied
472 areas. Based on correlation analysis (Table S13-S18), microbial community α -diversity
473 indices (Sobs, Shannon, Ace, and Chao) were positively correlated with TOC, FDA, APA,
474 and INV ($p < 0.05$), indicating that the enzyme activities were closely related to bacterial
475 community diversity.

476 In soils proximal to the active sites (SC and GZ), the following observations were made. At
477 the phylum level (Fig. 6A), *Proteobacteria* was positively correlated ($p < 0.05$) with As but
478 negatively correlated ($p < 0.05$) with MC, EC, *Q*, APA, bioavailable Sb, and total Sb.
479 *Chloroflexi* was positively correlated ($p < 0.05$) with UA, bioavailable Cr and Cu, and total
480 As and Cd, but negatively correlated ($p < 0.05$) with EC, pH, APA, *Q*, bioavailable Cd, Mn,
481 and V, and total Mn. At the genus level (Fig. 6D), *Xanthobacteraceae*, *norank_o_EIsterales*,
482 *Acidothermus*, *norank_o_norank_c_AD3*, *norank_o_Subgroup_2*, *Acidobacteria* and
483 *Bradyrhizobium* were negatively correlated ($p < 0.05$) with EC, pH, MC, *Q*, APA,
484 bioavailable Cd and Mn, and total Mn, but positively correlated ($p < 0.05$) with UA,
485 bioavailable Cr and Cu, and total As and Cd. *Arthroactor*, *Vicinamibacteraceae*, and
486 *norank_o_Vicinamibacterales* were positively correlated ($p < 0.05$) with pH, EC, APA, *Q*,
487 bioavailable Cd and Mn, and total Mn, but negatively correlated ($p < 0.05$) with bioavailable
488 Cr and Cu, and with total As.

489 The above results were in contrast to soils close to the inactive sites (YN and GX). At the
490 phylum level (Fig. 6B), *Chloroflexi* was positively correlated ($p < 0.05$) with *T*, but
491 negatively correlated ($p < 0.05$) with TOC, UA, and FDA. *Actinobacteriota* was significantly
492 and positively correlated ($p < 0.05$) with Cu, while negatively correlated ($p < 0.05$) with pH,
493 At the genus level (Fig. 6E), *JG30-KF-AS9* and *norank_o_norank_c_AD3*, were negatively
494 correlated ($p < 0.05$) with TOC, Cu, bioavailable As, Cd, Cr, Cu, Mn, Ni, Sb, and Zn, and
495 total Cr and Pb, while positively correlated ($p < 0.05$) with MC and total Cr. The
496 *Vicinamibacteraceae* and *norank_o_Vicinamibacterales* were positively correlated ($p < 0.05$)
497 with bioavailable Cd, Cr, Cu, Mn, and Zn, and total Cd, Pb, and Sb, but negatively correlated

498 with MC ($p < 0.05$). *JG30-KF-CM45* and *Gemmatimonadaceae* were positively correlated (p
499 < 0.05) with bioavailable As, Cu, Mn, and Sb. In addition, the APA and *Q* showed negative
500 correlations ($p < 0.05$) with the bacterial community composition in the active and inactive
501 sites (Figs. 6 and 7).

502 Soil heavy metal(loid)s (As, Cd, Cr, Cu, Pb, Ni, Sb, and Zn), EC, and pH are the most
503 important factors affecting bacterial communities in the mining area, as reported in previous
504 studies (Zhao et al., 2019; Li et al., 2020; Zeng et al., 2020). High concentrations of Cd, Cu,
505 and Zn can disturb the cell membrane integrity and inhibit the enzyme activity of soil bacteria
506 (Renella et al., 2003; Jose et al., 2011). A previous study noted that the high content of Cd,
507 Cr, Cu, Pb, and Zn increased the abundance of *Chloroflexi* (Zeng et al., 2020). *Chloroflexi* has
508 strong resistance to heavy metals (Yin et al., 2023), which explains the significant positive
509 correlation between *Chloroflexi* and copper. Recent studies found that Cu and Zn have
510 important effects on metal resistance genes (MRGs) in soil bacteria (Li et al., 2022c). For the
511 heavy metal(loid)s in soils, the bioavailable fractions are absorbed by the microorganisms,
512 thus affecting microbial communities (Zhen et al., 2019). Depending on the concentration,
513 heavy metal ions can have beneficial as well as harmful effects on complex microbial
514 biochemistry and metabolism. It was found that Cd and Pb ions can bind to sulfhydryl (–SH)
515 groups and inhibit cell enzyme activity (Pan et al., 2020). This can also explain the significant
516 negative correlation between bioavailable Cd and Mn and *Chloroflexi*. On the other hand,
517 bioavailable Cr and Cu have significant positive correlations with *Chloroflexi*. In addition,
518 some heavy metal(loid)s ions (Cu^{2+} , Mn^{2+} , Ni^{2+} , and Zn^{2+}) are essential trace elements for
519 microorganisms and play an important role in bacterial protein composition, electrostatic

520 interaction, osmoregulation, and redox processes (Bruins et al., 2000).

521 At the genus level, *Bradyrhizobium* can minimize oxidative stress (Rodrigues et al., 2013).

522 *Arthrobacter* can thrive in barren and harsh environments and has a strong tolerance to

523 multiple metals (Cd, Cu, Pb, and Zn) through physiological and genetic modification (Zhang

524 et al., 2004). In the typical antimony ore smelting area in the south of China, most of the

525 bioindicators of soil contaminated with heavy metal(loid)s (As, Cd, Cr, Cu, Ni, Pb, and Sb)

526 include *Gemmatimonadacea*, *norank_o_subgroup_2*, *JG30_KF_AS9*, and

527 *norank_o_norank_c_AD3* (Wang et al., 2022). These studies reported that

528 *norank_o_Rokubacterales* and *norank_o_Acidobacterales* showed a positive relationship

529 with the total As and Sb contents (Kalam et al., 2020; Wang et al., 2022). At the abandoned

530 heavy metal(loid)s (As, Cd, Cu, Pb, and Zn) contaminated sites in Korea,

531 *norank_o_Vicinamibacterales* and *Gemmatimonadales* were identified as the main bacterial

532 genera in the heavy metal-tolerant modules, compared to *norank_o_Acidobacterales* and

533 *norank_o_subgroup_2* in the heavy metal-sensitive modules (Chun et al., 2021). In particular,

534 *norank_o_Vicinamibacterales* and *Gemmatimonadales* could work together to resist As, Cd,

535 Cu, Pb, and Zn. In the contaminated soil around the smelter, the main genera in the topsoil

536 included *JG30-KF-CM45*, these bacteria have a strong tolerance to soil heavy metals (Cr, Cu,

537 V, and Zn) (Wang et al., 2020).

538 In summary, total and bioavailability contents of heavy metal(loid)s strongly altered the

539 abundances of soil microbial taxa. Additionally, many bacterial communities can have

540 different reaction modes to heavy metal(loid)s, implying that soils contaminated with

541 multiple metal(loid)s can shape the microbial communities. Based on the information on the

542 assembly process of soil microbial community, a previous study found that the differences in
543 microbial communities in three mining and smelting sites were driven by the joint influence
544 of soil factors, spatial heterogeneity, and metal(loid) levels, among which pH and Sb content
545 were the main parameters affecting the microbial assembly processes (Liu et al., 2022a; Li et
546 al., 2023). These results (Figs. 6 and 7) indicate that TOC, MC, total Cd and Cu contents, and
547 bioavailable As, Cd, Cu, Sb, Mn, and Zn were the main environmental factors affecting the
548 bacterial community in the inactive sites (YN and GX), whereas EC, pH, total contents of As,
549 Cd, Mn, and Zn, and bioavailable Cd, Cu, Cr, and Mn contents were the main environmental
550 factors affecting the bacterial community in the active sites (SC and GZ). In the present
551 study, EC, total As, Cu, and Mn contents, and bioavailable As, Cu, Cd, and Mn contents were
552 the main important environmental factors affecting the bacterial community in the inactive
553 sites (YN and GX) and active sites (SC and GZ).

554 **3.7. Phenotypic-functional prediction of bacterial communities**

555 There were seven major phenotypes, including Potentially Pathogenic, Gram Positive,
556 Contains Mobile Elements, Forms Biofilms, Gram Negative, Stress Tolerant, and Oxygen
557 Utilizing (Aerobic, Anaerobic, and Facultatively anaerobic) communities (Fig. 8). The
558 relative abundance contribution of species to phenotypic function showed that the highest
559 contribution of phenotypic function included *Actinobacteria*, *Proteobacteria*, *Chloroflexi*,
560 and *Acidobacteriota*. The Aerobic and Forms Biofilms phenotypes were significantly and
561 negatively correlated with the α -diversity indices (Tables S13-S18) but were positively
562 correlated with the Simpson index ($p < 0.05$). The Anaerobic phenotype was negatively
563 related to the α -diversity indices ($p < 0.05$) and was positively related to the Simpson index (p

564 < 0.05). Furthermore, microbial community characteristics and phenotypes were closely
565 related in all sites as determined by correlation analyses.

566 The TOC was negatively correlated with Aerobic and Stress Tolerant phenotypes ($p < 0.05$)
567 (Fig. 8, Tables S13-S18), but it also was positively correlated with the Anaerobic and
568 Contains Mobile Elements phenotypes ($p < 0.05$). The EC was positively related to
569 phenotypes (Contains Mobile Elements and Gram Positive) ($p < 0.05$), while it was
570 negatively related to the Facultatively Anaerobic, Forms Biofilms, and Gram Negative
571 phenotypes ($p < 0.05$). Phenotypic changes related to oxygen demand (e.g., Aerobic,
572 Anaerobic, and Facultative Anaerobic) may be related to soil salinity (Bronick and Lal,
573 2005). Soil salinity is closely related to EC. Earlier studies have shown that the relative
574 abundance of anaerobic phenotypes is positively related to salinity, compared to facultative
575 anaerobic and biofilm-forming phenotypes that are negatively correlated with salinity (Zhang
576 et al., 2019b). Although the TOC is closely related to the soil microbial community (Li et al.,
577 2020), further study is needed to investigate the possibility that the soil microbial community
578 phenotype has affected the soil TOC and EC or that changes in soil TOC and EC have shaped
579 the microbial community. An earlier study confirmed that geographical distance and
580 environmental factors can drive microbial structure differences in the three nonferrous metal
581 pollution sites (Liu et al., 2022a).

582 The different phenotypes of soil microbes are closely related to the total and bioavailable
583 contents of heavy metals(loid)s (Tables S13-S18). Soil microbial communities may develop
584 unique survival and community composition strategies during their adaptation to extreme
585 environments. The present study assumes that the changes in soil properties and function

586 (e.g., microbial enzyme activities and bacterial/fungal communities) are related to (or caused
587 by) exposure to toxic heavy metals on fugitive dust particles that were transferred from the
588 active and inactive smelter sites to the surrounding forest soil and elsewhere (Csavina et al.,
589 2012; Lenart-Boroń and Boroń, 2014; Ettler 2016). Based on the genetic acquisition of MRG
590 in down-wind soils studied here, it is interesting to consider the possibility that the fugitive
591 emissions also carry heavy metal-resistant microbes (Hu et al., 2020), like the aerial transfer
592 of microbes from manure feed farms to urban settings (McEachran et al., 2015; Fry et al.,
593 2020). This process could have hazardous effects on human health (Hu et al., 2020) or
594 negatively impact neighboring ecosystems (Behzad et al., 2022). Whether the fugitive MRG-
595 containing microbes propagate within a new host-microbiome of the surrounding forest soils
596 explains the biogeochemical effects observed in the present study requires future
597 confirmation.

598 Another consideration is that toxic heavy metal(loid)s in soil may force microbial
599 communities into competition to cause a trade-off of resource allocation for the growth,
600 survival, and reproduction of the successful community. The species abundance composition
601 of bacterial communities and antibiotic-resistance genes in activated sludge are consistent
602 with environmental adaptation (Zhao et al., 2019). The correlation between the dominant
603 flora and the bacterial community phenotype may be the main reason for their similar spatial
604 distribution pattern. Here it is inferred that adaptive changes in the structure and phenotype of
605 the diverse microbial flora represent a synergistic or symbiotic strategy to support continual
606 adaptation to temporal changes in environmental stressors.

607 Although many studies on the microbial diversity and structure of mining and smelting sites

608 have been investigated, the ecological processes and symbiotic patterns affecting the
609 biogeographic distribution of microbial communities are still unclear. Therefore, in a follow-
610 up study, we plan to increase the number of study sites and soil samples to further explore the
611 ecological characteristics of soil bacterial and fungal communities.

612 **4. Conclusions**

613 In this study, the soil environment surrounding non-ferrous metal mining and smelting
614 activities in Southwest China was barren and heavily polluted by various heavy metals, with
615 different microbial metabolic activities, and soil bacterial community structure and
616 phenotypic characteristics. Selected microbial metabolic activities (enzyme APA and
617 microcalorimetric parameter Q), bacterial community structure, and phenotype varied across
618 all sites. Furthermore, the main bacterial phyla were *Actinobacteria*, *Proteobacteria*,
619 *Chloroflexi*, and *Acidobacteriota*. The TOC, MC, total Cd and Cu contents, and bioavailable
620 As, Cd, Cu, Mn, Sb, and Zn contents were the main environmental factors affecting the
621 bacterial community in the inactive sites, whereas the EC, pH, total As, Cd, Mn, and Zn
622 contents, and bioavailable Cd, Cr, Cu, and Mn contents were the main environmental factors
623 affecting that in the active sites. Many bacterial groups exhibited different response patterns
624 to each heavy metal(loid), implying that the soil microbial communities were shaped jointly
625 by fugitive multiple heavy metal(loid)s and possibly microbes. Species abundances and
626 phenotypes of dominant taxa in soil bacterial communities are involved in potential
627 environmental adaptation consistency. Different advanced gene sequencing techniques will
628 be used in future studies to systematically reveal the microbial biogeography, assembly
629 mechanism, and symbiotic modes of bacterial and fungal communities around mining and

630 smelting areas. This series of studies can provide a more comprehensive and theoretical basis
631 for the microbial treatment of non-ferrous metal-contaminated sites.

632

633 **Acknowledgments**

634 This work was supported in part by grants for the project of the Major National R & D
635 Projects for the Chinese Ministry of Science and Technology (2019YFC1803500,
636 2021YFE0106600), the National Natural Science Foundation of China (42230716), the 111
637 Project (B21017), Centre National de la Recherche Scientifique (CNRS PRC1416, France),
638 and the 1000-Talents Plan project (WQ2017110423).

639

640 **CRedit authorship contribution statement**

- 641 - **Hao Li:** Conceptualization, Methodology, Writing - review & editing, Data Curation,
642 Visualization, Writing - original draft.
- 643 - **Jun Yao:** Conceptualization, Writing – review & editing, Resources, Funding
644 acquisition, Supervision.
- 645 - **Ning Min:** Formal analysis, Review & editing.
- 646 - **Geoffrey Sunahara:** Conceptualization, Visualization, Writing - review & editing.
- 647 - **Robert Duran:** Formal analysis, Writing - review & editing.

648 **Declaration of competing interest**

649 The authors declare that there is no conflict of interest in the publication of this article.

650

651 **References**

- 652 Aponte, H., Mondaca, P., Santander, C., Meier, S., Paolini, J., Butler, B., Rojas, C., Diez,
653 M.C., Cornejo, P., 2021. Enzyme activities and microbial functional diversity in
654 metal(loid) contaminated soils near to a copper smelter. *Sci. Total Environ.* 779, 146423.
655 <https://doi.org/10.1016/j.scitotenv.2021.146423>.
- 656 Batista, D.R., Carneiro, J.J., Pinto, F.A., Santos, J., Carneiro, M., 2020. Environmental
657 drivers of shifts on microbial traits in sites disturbed by a large-scale tailing dam collapse
658 *Sci. Total Environ.* 738, 139453. <https://doi.org/10.1016/j.scitotenv.2020.139453>.
- 659 Behzad, H., Ohyanagi, H., Alharbi, B., Ibarra, M., Alarawi, M., Saito, Y., Duarte, C.M., Bajic,
660 V., Mineta, K., Gojobori, T. 2022. A cautionary signal from the Red Sea on the impact of
661 increased dust activity on marine microbiota. *BMC Genomics.* 23(1), 277.
662 <https://doi.org/10.1186/s12864-022-08485-w>.
- 663 Bronick, C.J., Lal, R., 2005. Soil structure and management: a review. *Geoderma* 124(1-2), 3-
664 22. <https://doi.org/10.1016/j.geoderma.2004.03.005>.
- 665 Bruins, M.R., Kapil, S., Oehme, F.W., 2000. Microbial resistance to metals in the
666 environment. *Ecotox. Environ. Safe.* 45(3), 198-207. <https://doi.org/10.1006/eesa.1999.1860>.
- 667 Chae, Y., Cui, R., Kim, S.W., An, G., Jeong, S.W., An, Y.J., 2017. Exoenzyme activity in
668 contaminated soils before and after soil washing: beta-glucosidase activity as a biological
669 indicator of soil health. *Ecotox. Environ. Safe.* 135, 368-374.
670 <https://doi.org/10.1016/j.ecoenv.2016.10.007>.
- 671 Chen, L.X., Li, J.T., Chen, Y.T., Huang, L.N., Shu, W.S., 2013. Shifts in microbial
672 community composition and function in the acidification of a lead/zinc mine tailings.
673 *Environ. Microbiol.* 15(9), 2431-2444. <https://doi.org/10.1111/1462-2920.12114>.
- 674 Chen, Y., Jiang, Y.M., Huang, H.Y., Mou, L.C., Ru, J.L., Zhao, J.H., Xiao, S., 2018. Long-
675 term and high-concentration heavy-metal contamination strongly influences the
676 microbiome and functional genes in Yellow River sediments. *Sci. Total Environ.* 637,
677 1400-1412. <https://doi.org/10.1016/j.scitotenv.2018.05.109>.

678 Chun, S.J., Kim, Y.J., Cui, Y., Nam, K.H., 2021. Ecological network analysis reveals
679 distinctive microbial modules associated with heavy metal contamination of abandoned
680 mine soils in Korea. *Environ. Pollut.* 289, 117851. <https://doi.org/10.1016/j.envpol.2021.117851>.

681 China National Environmental Monitoring Center (CNEMC), 1990. *Background Values of*
682 *Soil Elements in China*. China Environmental Science Press: Beijing, China (in Chinese).

683 Csavina, J., Field, J., Taylor, M.P., Gao, S., Landázuri, A., Betterton, E.A., Sáez, A.E., 2012.
684 A review on the importance of metals and metalloids in atmospheric dust and aerosol
685 from mining operations. *Sci.Total. Environ.* 433, 58-73.
686 <https://doi.org/10.1016/j.scitotenv.2012.06.013>.

687 Duran, R., Bielen, A., Paradzik, T., Gassie, C., Pustijanac, E., Cagnon, C., Hamer, B.,
688 Vujaklija, D., 2015. Exploring Actinobacteria assemblages in coastal marine sediments
689 under contrasted Human influences in the West Istria Sea, Croatia. *Environ. Sci. Pollut.*
690 *Res.* 22(20), 15215-15229. <https://doi.org/10.1007/s11356-015-4240-1>.

691 Ettler, V., 2016. Soil contamination near non-ferrous metal smelters: A review. *Appl.*
692 *Geochem.* 64, 56-74. <https://doi.org/10.1016/j.apgeochem.2015.09.020>.

693 Fry, K.L., Wheeler, C.A., Gillings, M.M., Flegal, A.R., Taylor, M.P., 2020. Anthropogenic
694 contamination of residential environments from smelter As, Cu and Pb emissions:
695 Implications for human health. *Environ. Pollut.* 262, 114235.
696 <https://doi.org/10.1016/j.envpol.2020.114235>.

697 Guo, J., Zhang, Y., Huang, H., Yang, F., 2021a. Deciphering soil bacterial community
698 structure in subsidence area caused by underground coal mining in arid and semiarid
699 area. *Appl. Soil Ecol.* 163, 103916. <https://doi.org/10.1016/j.apsoil.2021.103916>.

700 Guo, Z., Yang, J., Sarkodie, E.K., Li, K., Deng, Y., Meng, D., Miao, B., Liu, H., Liang, Y.,
701 Yin, H., 2021b. Vertical distribution of the toxic metal(loid)s chemical fraction and
702 microbial community in waste heap at a nonferrous metal mining site. *Ecotox. Environ.*
703 *Safe.* 228, 113037. <https://doi.org/10.1016/j.ecoenv.2021.113037>.

704

705 Harris, J.A., Ritz, K., Coucheney, E., Grice, S.M., Lerch, T.Z., Pawlett, M., Herrmann, A.M.,
706 2012. The thermodynamic efficiency of soil microbial communities subject to long-term
707 stress is lower than those under conventional input regimes. *Soil Biol. Biochem.* 47, 149-
708 157. <https://doi.org/10.1016/j.soilbio.2011.12.017>.

709 Herrmann, A.M., Coucheney, E., Nunan, N., 2014. Isothermal microcalorimetry provides
710 new insight into terrestrial carbon cycling. *Environ. Sci. Technol.* 48(8), 4344-4352.
711 <https://doi.org/10.1021/es403941h>.

712 Hu, B., Shao, S., Ni, H., Fu, Z., Huang, M., Chen, Q., Shi, Z., 2021. Assessment of
713 potentially toxic element pollution in soils and related health risks in 271 cities across
714 China. *Environ. Pollut.* 270, 116196. <https://doi.org/10.1016/j.envpol.2020.116196>.

715 Hu, W., Wang, Z., Huang, S., Ren, L., Yue, S., Li, P., Xie, Q., Zhao, W., Wei, L., Ren, H.,
716 Wu, L., Deng, J., Fu, P., 2020. Biological aerosol particles in polluted regions. *Curr.*
717 *Pollut. Rep.* 6, 65–89. <https://doi.org/10.1007/s40726-020-00138-4>.

718 Janssen, P.H., 2006. Identifying the dominant soil bacterial taxa in libraries of 16S rRNA and
719 16S rRNA genes. *Appl. Environ. Microbiol.* 72(3), 1719-1728.
720 <https://doi.org/10.1128/aem.72.3.1719-1728.2006>.

721 Jiang, X., Liu, W., Xu, H., Cui, X., Zheng, B., 2021. Characterizations of heavy metal
722 contamination, microbial community, and resistance genes in a tailing of the largest
723 copper mine in China. *Environ. Pollut.* 280, 116947.
724 <https://doi.org/10.1016/j.envpol.2021.116947>.

725 Jose, J., Giridhar, R., Anas, A., Bharathi, P.A.L., Nair, S., 2011. Heavy metal pollution exerts
726 reduction/adaptation in the diversity and enzyme expression profile of heterotrophic
727 bacteria in Cochin estuary, India. *Environ. Pollut.* 159(10), 2775-2780.
728 <https://doi.org/10.1016/j.envpol.2011.05.009>.

729 Kalam, S., Basu, A., Ahmad, I., Sayyed, R.Z., El-Enshasy, H.A., Dailin, D.J., Suriani, N.L.,
730 2020. Recent understanding of soil Acidobacteria and their ecological significance: A
731 critical review. *Front. Microbiol.* 11, 580024. <https://doi.org/10.3389/fmicb.2020.580024>.

732 Kang, X., Cui, Y., Shen, T., Yan, M., Yu, X., 2020. Changes of root microbial populations of
733 natively grown plants during natural attenuation of V–Ti magnetite tailings. *Ecotox.*
734 *Environ. Safe.* 201, 110816. <https://doi.org/10.1016/j.ecoenv.2020.110816>.

735 Ke, W.S., Zeng, J.Q., Zhu, F., Luo, X.H., Feng, J.P., He, J., Xue, S.G., 2022. Geochemical
736 partitioning and spatial distribution of heavy metals in soils contaminated by lead
737 smelting. *Environ. Pollut.* 307, 19486. <https://doi.org/10.1016/j.envpol.2022.119486>.

738 Kubier, A., Wilkin, R.T., Pichler, T., 2019. Cadmium in soils and groundwater: A review.
739 *Appl. Geochem.* 108, 104388. <https://doi.org/10.1016/j.apgeochem.2019.104388>.

740 Lenart-Boroń, A., Boroń, P., 2014., The effect of industrial heavy metal pollution on
741 microbial abundance and diversity in soils—A review, in: Hernandez Soriano, M.C.,
742 (Ed). *Environmental Risk Assessment of Soil Contamination*, IntechOpen, Mar 26.
743 <http://dx.doi.org/10.5772/57406>.

744 Li, H., Yao, J., Min, N., Chen, Z.H., Li, M.M., Pang, W.C., Liu, B., Cao, Y., Men, D.Y.,
745 Duran, R., 2022a. Comprehensive evaluation of metal(loid)s pollution risk and microbial
746 activity characteristics in non-ferrous metal smelting contaminated site. *J. Clean. Prod.*
747 344, 130999. <https://doi.org/10.1016/j.jclepro.2022.130999>.

748 Li, H., Yao, J., Min, N., Liu, J.L., Chen, Z.H., Zhu, X.Z., Zhao, C.C., Pang, W.C., Li, M.M.,
749 Cao, Y., Liu, B., Duran, R., 2022b. Relationships between microbial activity, enzyme
750 activities and metal(loid) form in Ni-Cu tailings area. *Sci. Total Environ.* 812, 152326.
751 <https://doi.org/10.1016/j.scitotenv.2021.152326>.

752 Li, M.M., Yao, J., Sunahara, G., Duran, R., Liu, B., Cao, Y., Li, H., Pang, W.C., Liu, H.Q.,
753 Jiang, S., Zhu, J.J., Zhang, Q.H., 2023. Assembly processes of bacterial and fungal
754 communities in metal(loid)s smelter soil. *J. Hazard. Mater.* 451, 131153.
755 <https://doi.org/10.1016/j.jhazmat.2023.131153>.

756 Li, N., Chen, J.G., Liu, C., Yang, J.X., Zhu, C.X., Li, H.N., 2022c. Cu and Zn exert a greater
757 influence on antibiotic resistance and its transfer than doxycycline in agricultural soils. *J.*
758 *Hazard. Mater.* 423, 127042. <https://doi.org/10.1016/j.jhazmat.2021.127042>.

759

760 Li, S., Wu, J., Huo, Y., Zhao, X., Xue, L., 2020. Profiling multiple heavy metal contamination
761 and bacterial communities surrounding an iron tailing pond in Northwest China. *Sci.*
762 *Total Environ.* 752(2), 141827. <https://doi.org/10.1016/j.scitotenv.2020.141827>.

763 Liu, B., Yao, J., Chen, Z., Ma, B., Li, H., Pang, W., Liu, J., Wang, D., Duran, R., 2022a.
764 Biogeography, assembly processes and species coexistence patterns of microbial
765 communities in metalloids-laden soils around mining and smelting sites. *J. Hazard.*
766 *Mater.* 425, 127945. <https://doi.org/10.1016/j.jhazmat.2021.127945>.

767 Liu, B., Yao, J., Ma, B., Chen, Z., Zhu, X., Zhao, C., Li, M., Cao, Y., Pang, W., Li, H.,
768 Mihucz, V.G., Duran, R., 2022b. Metal(loid)s diffusion pathway triggers distinct
769 microbiota responses in key regions of typical karst non-ferrous smelting assembly. *J.*
770 *Hazard. Mater.* 423, 127164. <https://doi.org/10.1016/j.jhazmat.2021.127164>.

771 Liu, B., Yao, J., Ma, B., Chen, Z., Zhao, C., Zhu, X., Li, M., Cao, Y., Pang, W., Li, H., 2021.
772 Microbial community profiles in soils adjacent to mining and smelting areas: Contrasting
773 potentially toxic metals and co-occurrence patterns. *Chemosphere* 282, 130992.
774 <https://doi.org/10.1016/j.chemosphere.2021.130992>.

775 Liu, J.L., Yao, J., Wang, F., Ni, W., Liu, X.Y., Sunahara, G., Duran, R., Jordan, G., Hudson-
776 Edwards, K.A., Alakangas, L., Solevic-Knudsen, T., Zhu, X.Z., Zhang, Y.Y., Li, Z.F.,
777 2018. China's most typical nonferrous organic-metal facilities own specific microbial
778 communities. *Sci. Rep-UK* 8, 12570. <https://doi.org/10.1038/s41598-018-30519-1>.

779 McEachran, A.D., Blackwell, B.R., Hanson, J.D., Wooten, K.J., Mayer, G.D., Cox, S.B.,
780 Smith, P.N., 2015. Antibiotics, bacteria, and antibiotic resistance genes: aerial transport
781 from cattle feed yards via particulate matter. *Environ. Health Perspect.* 123, 337–343.
782 <http://dx.doi.org/10.1289/ehp.1408555>.

783 Pan, X.M., Zhang, S.R., Zhong, Q.M., Gong, G.S., Wang, G.Y., Guo, X., Xu, X.X., 2020.
784 Effects of soil chemical properties and fractions of Pb, Cd, and Zn on bacterial and
785 fungal communities. *Sci. Total Environ.* 715, 136904.
786 <https://doi.org/10.1016/j.scitotenv.2020.136904>.

787

- 788 Qiao, L., Liu, X., Zhang, S., Zhang, L., Yu, C., 2021. Distribution of the microbial
789 community and antibiotic resistance genes in farmland surrounding gold tailings: A
790 metagenomics approach. *Sci. Total Environ.* 779(4), 146502.
791 <https://doi.org/10.1016/j.scitotenv.2021.146502>.
- 792 Renella, G., Ortigoza, A.L.R., Landi, L., Nannipieri, P., 2003. Additive effects of copper and
793 zinc on cadmium toxicity on phosphatase activities and ATP content of soil as estimated
794 by the ecological dose (ED50). *Soil Biol. Biochem.* 35(9), 1203-1210.
795 [https://doi.org/10.1016/s0038-0717\(03\)00181-0](https://doi.org/10.1016/s0038-0717(03)00181-0).
- 796 Rinklebe, J., Antoniadis, V., Shaheen, S.M., Rosche, O., Altermann, M., 2019. Health risk
797 assessment of potentially toxic elements in soils along the Central Elbe River, Germany.
798 *Environ. Int.* 126, 76-88. <https://doi.org/10.1016/j.envint.2019.02.011>.
- 799 Rodrigues, A.C., Bonifacio, A., Antunes, J.E.L., da Silveira, J.A.G., Figueiredo, M.D.B.,
800 2013. Minimization of oxidative stress in cowpea nodules by the interrelationship
801 between *Bradyrhizobium sp* and plant growth-promoting bacteria. *Appl. Soil Ecol.* 64,
802 245-251. <https://doi.org/10.1016/j.apsoil.2012.12.018>.
- 803 Schnurer, J., Rosswall, T., 1982. Fluorescein diacetate hydrolysis as a measure of total
804 microbial activity in soil and litter. *Appl. Environ. Microbiol.* 43(6), 1256-1261.
805 <https://doi.org/10.1128/aem.43.6.1256-1261.19>.
- 806 Stevenson, A., Hallsworth, J.E., 2014. Water and temperature relations of soil Actinobacteria.
807 *Environ. Microbiol. Rep.* 6(6), 744-755. <https://doi.org/10.1111/1758-2229.12199>.
- 808 Sun, X.X., Li, B.Q., Han, F., Xiao, E.Z., Wang, Q., Xiao, T.F., Sun, W.M., 2019. Vegetation
809 type impacts microbial interaction with antimony contaminants in a mining-
810 contaminated soil environment. *Environ. Pollut.* 252, 1872-1881.
811 <https://doi.org/10.1016/j.envpol.2019.06.070>.
- 812 Vinhal-Freitas, I.C., Correa, G.F., Wendling, B., Bobul'Ska, L., Ferreira, A.S., 2017. Soil
813 textural class plays a major role in evaluating the effects of land use on soil quality
814 indicators. *Ecol. Indic.* 74(Mar.), 182-190. <https://doi.org/10.1016/j.ecolind.2016.11.020>.

- 815 Wahsha, M., Nadimi-Goki, M., Fornasier, F., Al-Jawasreh, R., Hussein, E.I., Bini, C., 2017.
816 Microbial enzymes as an early warning management tool for monitoring mining site
817 soils. *Catena* 148, 40-45. <https://doi.org/10.1016/j.catena.2016.02.021>.
- 818 Ward, T., Larson, J., Meulemans, J., Hillmann, B., Lynch, J., Sidiropoulos, D., Spear, J.,
819 Caporaso, G., Ran, B., Knight, R., 2017. BugBase predicts organism level microbiome
820 phenotypes. *bioRxiv*. <https://doi.org/10.1101/133462>.
- 821 Wang, S., Zhang, B.G., Li, T.T., Li, Z.Y., Fu, J., 2020. Soil vanadium(V)-reducing related
822 bacteria drive community response to vanadium pollution from a smelting plant over
823 multiple gradients. *Environ. Int.* 138, 105630. <https://doi.org/10.1016/j.envint.2020.105630>.
- 824 Wang, W., Xiao, S., Amanze, C., Anaman, R., Zeng, W., 2022. Microbial community
825 structures and their driving factors in a typical gathering area of antimony mining and
826 smelting in South China. *Environ. Sci. Pollut. Res.* 29, 50070–50084
827 <https://doi.org/10.1007/s11356-022-19394-6>.
- 828 Wu, B., Luo, H., Wang, X., Liu, H., Xu, H., 2021. Effects of environmental factors on soil
829 bacterial community structure and diversity in different contaminated districts of
830 Southwest China mine tailings. *Sci. Total Environ.* 802(16), 149899.
831 <https://doi.org/10.1016/j.scitotenv.2021.149899>.
- 832 Xiao, E.Z., Wang, Y.Q., Xiao, T.F., Sun, W.M., Deng, J.M., Jiang, S.M., Fan, W.J., Tang, J.F.,
833 Ning, Z.P., 2021. Microbial community responses to land-use types and its ecological
834 roles in mining area. *Sci. Total Environ.* 775, 145753.
835 <https://doi.org/10.1016/j.scitotenv.2021.145753>.
- 836 Xiao, L., Yu, Z.J., Liu, H.Q., Tan, T., Yao, J.H., Zhang, Y.X., Wu, J.J., 2020. Effects of Cd and
837 Pb on diversity of microbial community and enzyme activity in soil. *Ecotoxicology*
838 29(5), 551-558. <https://doi.org/10.1007/s10646-020-02205-4>.
- 839 Xu, Y., Seshadri, B., Bolan, N., Sarkar, B., Ok, Y.S., Zhang, W., Rumpel, C., Sparks, D.,
840 Farrell, M., Hall, T., 2019. Microbial functional diversity and carbon use feedback in
841 soils as affected by heavy metals. *Environ. Int.* 125, 478-488.
842 <https://doi.org/10.1016/j.envint.2019.01.071>.

843 Yan, C., Wang, F., Liu, H., Liu, H., Pu, S., Lin, F., Geng, H., Ma, S., Zhang, Y., Tian, Z.,
844 Chen, H., Zhou, B., Yuan, R., 2020. Deciphering the toxic effects of metals in gold
845 mining area: Microbial community tolerance mechanism and change of antibiotic
846 resistance genes. *Environ. Res.* 189, 109869. <https://doi.org/10.1016/j.envres.2020.109869>.

847 Yin, Y., Wang, X.J., Hu, Y.A., Li, F.D., Cheng, H.F., 2023. Soil bacterial community structure
848 in the habitats with different levels of heavy metal pollution at an abandoned
849 polymetallic mine. *J. Hazard. Mater.* 442, 130063.
850 <https://doi.org/10.1016/j.jhazmat.2022.130063>.

851 Yuan, C.Y., Li, F.Y., Yuan, Z.Q., Li, G.Y., Liang, X.Q., 2021. Response of bacterial
852 communities to mining activity in the alpine area of the Tianshan Mountain region,
853 China. *Environ. Sci. Pollut. Res.* 28(13), 15806-15818. [https://doi.org/10.1007/s11356-020-](https://doi.org/10.1007/s11356-020-11744-6)
854 [11744-6](https://doi.org/10.1007/s11356-020-11744-6).

855 Zeng, J.Q., Li, C.X., Wang, J.T., Tang, L., Wu, C., Xue, S.G., 2022. Pollution simulation and
856 remediation strategy of a zinc smelting site based on multi-source information. *J. Hazard.*
857 *Mater.* 433, 128774. <https://doi.org/10.1016/j.jhazmat.2022.128774>.

858 Zeng, X.Y., Li, S.W., Leng, Y., Kang, X.H., 2020. Structural and functional responses of
859 bacterial and fungal communities to multiple heavy metal exposure in arid loess. *Sci.*
860 *Total Environ.* 723, 138081. <https://doi.org/10.1016/j.scitotenv.2020.138081>.

861 Zhang, B., Wang, S., Diao, M., Fu, J., Borthwick, A.G.L., 2019a. Microbial community
862 responses to vanadium distributions in mining geological environments and
863 bioremediation assessment. *J. Geophys. Res-Bioge.* 124(3), 601-615.
864 <https://doi.org/10.1029/2018jg004670>.

865 Zhang, H.B., Duan, C.Q., Shao, Q.Y., Ren, W.M., Sha, T., Cheng, L.Z., Zhao, Z.W., Hu, B.,
866 2004. Genetic and physiological diversity of phylogenetically and geographically distinct
867 groups of *Arthrobacter* isolated from lead-zinc mine tailings. *FEMS Microbiol. Ecol.*
868 49(2), 333-341. <https://doi.org/10.1016/j.femsec.2004.04.009>.

869

870 Zhang, K., Shi, Y., Cui, X., Yue, P., Li, K., Liu, X., Tripathi, B.M., Chu, H., Lozupone, C.,
871 2019b. Salinity is a key determinant for soil microbial communities in a desert
872 ecosystem. *mSystems* 4(1). <https://doi.org/10.1128/mSystems.00225-18>.

873 Zhang, Y.Y., Wang, F., Hudson-Edwards, K.A., Blake, R., Zhao, F.R., Yuan, Z.M., Gao, W.,
874 2020. Characterization of mining-related aromatic contaminants in active and abandoned
875 metal(loid) tailings ponds. *Environ. Sci. Technol.* 54(23), 15097-15107.
876 <https://doi.org/10.1021/acs.est.0c03368>.

877 Zhao, F.J., Ma, Y.B., Zhu, Y.G., Tang, Z., McGrath, S.P., 2015. Soil contamination in China:
878 Current status and mitigation strategies. *Environ. Sci. Technol.* 49(2), 750-759.
879 <https://doi.org/10.1021/es5047099>.

880 Zhao, X., Huang, J., Lu, J., Sun, Y., 2019. Study on the influence of soil microbial
881 community on the long-term heavy metal pollution of different land use types and depth
882 layers in mine. *Ecotox. Environ. Safe.* 170, 218-226.
883 <https://doi.org/10.1016/j.ecoenv.2018.11.136>.

884 Zhao, X.Q., Sun, Y., Huang, J., Wang, H., Tang, D., 2020. Effects of soil heavy metal
885 pollution on microbial activities and community diversity in different land use types in
886 mining areas. *Environ. Sci. Pollut. Res.* 27(16), 20215-20226. [https://doi.org/10.1007/s11356-](https://doi.org/10.1007/s11356-020-08538-1)
887 [020-08538-1](https://doi.org/10.1007/s11356-020-08538-1).

888 Zhen, Z., Wang, S.B., Luo, S.W., Ren, L., Liang, Y.Q., Yang, R.C., Li, Y.T., Zhang, Y.Q.,
889 Deng, S.Q., Zou, L.N., Lin, Z., Zhang, D.Y., 2019. Significant impacts of both total
890 amount and availability of heavy metals on the functions and assembly of soil microbial
891 communities in different land use patterns. *Front. Microbiol.* 10, 02293.
892 <https://doi.org/10.3389/fmicb.2019.02293>.

893 Zhu, X.Z., Yao, J., Wang, F., Yuan, Z.M., Liu, J.L., Jordan, G., Knudsen, T.S., Avdalovic, J.,
894 2018. Combined effects of antimony and sodium diethyldithiocarbamate on soil
895 microbial activity and speciation change of heavy metals. Implications for contaminated
896 lands hazardous material pollution in nonferrous metal mining areas. *J. Hazard. Mater.*
897 349, 160-167. <https://doi.org/10.1016/j.jhazmat.2018.01.044>.

898 **List of Figures**

899 **Fig. 1.** Locations and photos of four non-ferrous metal mining and smelting activities

900 affected areas in Southwest China. The distributions of sampling points of active sites
901 (SC and GZ) and inactive sites (YN and GX) are shown in the top and bottom panels,
902 respectively (also see Supplementary Information, Figs. S1 and S2).

903 **Fig. 2.** Total (A) and bioavailable (Exchangeable fraction) (B) contents of metal(loid)s in the

904 surface soil from active (SC and GZ) and inactive (YN and GX) sites. **Panel (C) shows**
905 **the** Contamination factor (CF) and pollution load index (PLI) of metal(loid)s from active
906 (SC and GZ) and inactive (YN and GX) sites. $CF < 1$, low pollution; $1 \leq CF < 3$,
907 moderate pollution; $3 \leq CF < 6$, serious pollution, and $CF \geq 6$, extreme pollution. $PLI > 1$
908 indicates significant pollution.

909 **Fig. 3.** Microbial activities in the SC, YN, GX, and GZ sites. FDA (A), UA (B), APA (C), and

910 INV (D) enzymes activities. Power-time curves (E) for different soil samples in the SC,
911 YN, GX, and GZ sites were recorded using microcalorimetry. Different lowercase letters
912 are used to indicate significant differences between groups ($p < 0.05$). The
913 thermodynamic parameter values for different samples are detailed in Supplementary
914 Information Fig. S5 and Tables S1-S4.

915 **Fig. 4.** Microbial community α -diversity in different soil samples from SC, YN, GX, and GZ

916 sites. (A) Shannon diversity index; (B) Sobs richness at the OTU level; (C) Chao
917 richness at the OTU level; (D) Ace richness at the OTU level; (E) Simpson diversity
918 index; **and** (F) Coverage's index. Statistical differences between SC, YN, GX, and GZ
919 sites were performed by the Student's *t*-test ($p \leq 0.05$ is marked as *, $p \leq 0.01$ as **, $p \leq$
920 0.001 as ***).

921 **Fig. 5.** Comparison of the microbial communities from GX, GZ, SC, and YN sites. Venn

922 diagram (A) and Principal co-ordinate analysis (PCoA, B) showing the variations of
923 microbial structure at **the** OTU level. Soil bacterial community composition shows the
924 top 20 most abundant phyla (C) and genera (D).

925

926 **Fig. 6.** Spearman correlation heatmap of the top five most abundant phyla (A: active sites; B:
927 inactive sites; C: active and inactive sites) and the top ten most abundant genera (D:
928 active sites; E: inactive sites; F: active and inactive sites) of the microbial communities,
929 the environmental factors, microbial activity characteristics, **and** total and bioavailable
930 metal(loid)s contents (E). *r*-values are plotted in different colors; the right side of the
931 legend shows the color range and the corresponding *r*-values. Significant values are
932 shown as * $p < 0.05$; ** $p < 0.01$; *** $p < 0.001$.

933 **Fig. 7.** Comparison of microbial communities. The distance-based redundancy analysis (db-
934 RDA) was performed at the OTUs abundance level. The red line arrows denote the soil
935 characteristics and microbial activity characteristics (A), and total (B), and bioavailable
936 (C) metal(loid)s contents. The length of the arrows represents the degree of relevance
937 between microbial communities and various factors. The percentage in the two axes
938 indicates the eigenvalues of environmental factors.

939 **Fig. 8.** The corresponding OTU contribution plots of the relative abundance of phyla
940 possessing each phenotype (A: Aerobic; B: Potentially Pathogenic; C: Gram Positive; D:
941 Anaerobic; E: Facultatively Anaerobic; F: Contains Mobile Elements; G: Forms
942 Biofilms; **and** H: Gram Negative; I: Stress Tolerant) in the YN, SC, GZ, and GX sites
943 are also shown. Different lowercase letters indicate significant differences between
944 groups ($p < 0.05$).

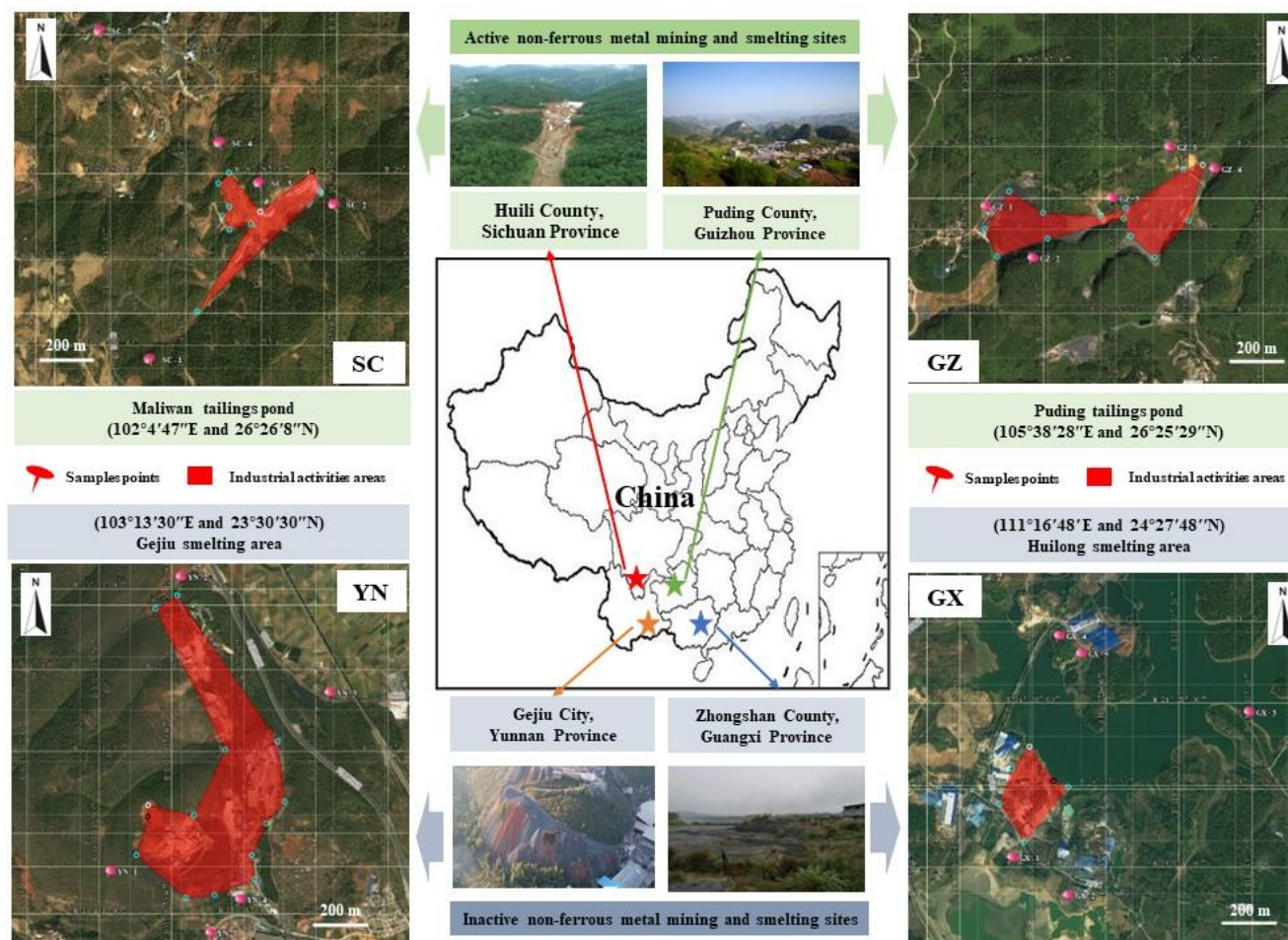


Fig. 1. Locations and photos of four non-ferrous metal mining and smelting activities affected areas in Southwest China. The distributions of sampling points of active sites (SC and GZ) and inactive sites (YN and GX) are shown in the top and bottom panels, respectively (also see Supplementary Information, Figs. S1 and S2).

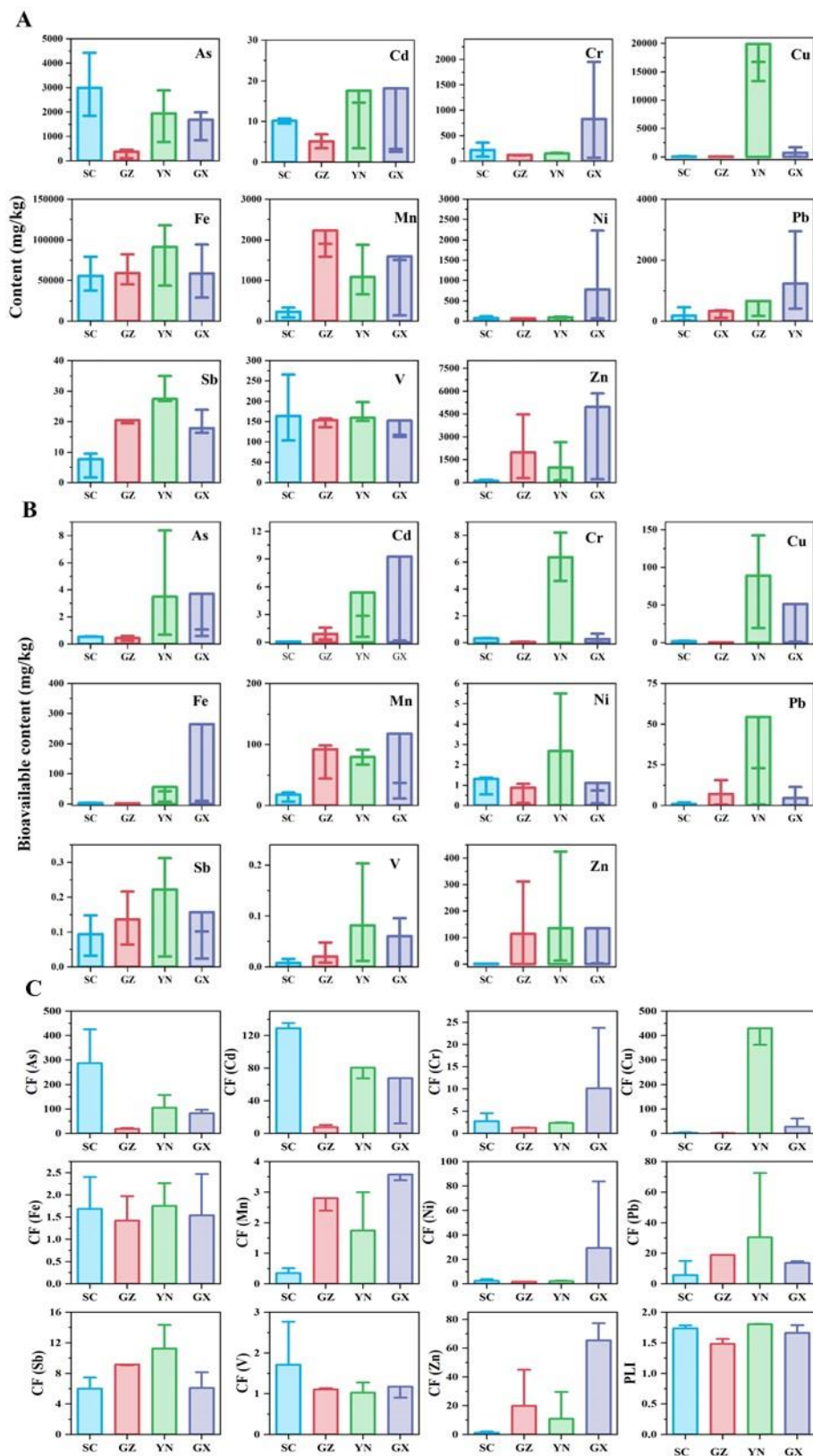


Fig. 2. Total (A) and bioavailable (Exchangeable fraction) (B) contents of metal(loid)s in the surface soil from active (SC and GZ) and inactive (YN and GX) sites. Panel (C) shows the Contamination factor (CF) and pollution load index (PLI) of metal(loid)s from active (SC and GZ) and inactive (YN and GX) sites. $CF < 1$, low pollution; $1 \leq CF < 3$, moderate pollution; $3 \leq CF < 6$, serious pollution, and $CF \geq 6$, extreme pollution. $PLI > 1$ indicates

significant pollution.

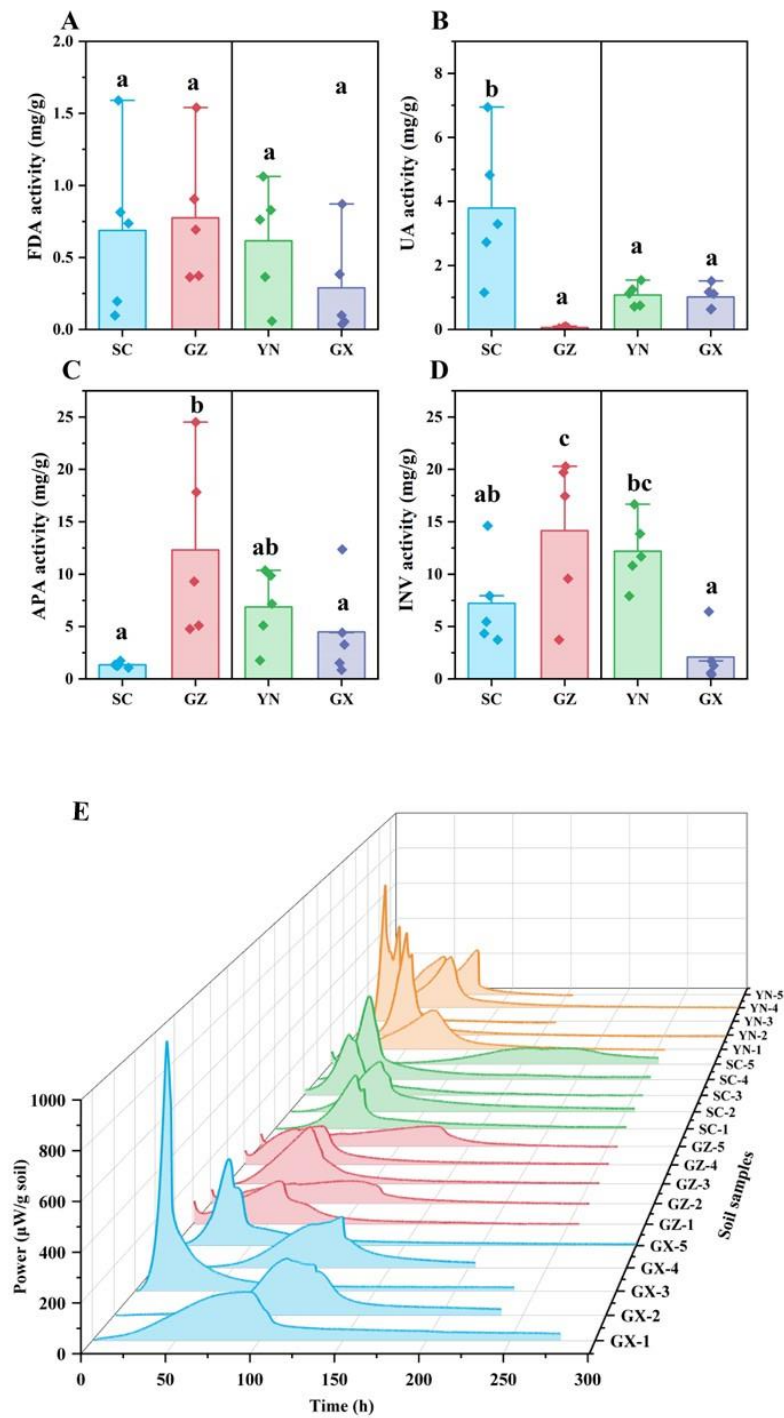


Fig. 3. Microbial activities in the SC, YN, GX, and GZ sites. FDA (A), UA (B), APA (C), and INV (D) enzymes activities. Power-time curves (E) for different soil samples in the SC, YN, GX, and GZ sites were recorded using microcalorimetry. Different lowercase letters are used to indicate significant differences between groups ($p < 0.05$). The different thermodynamic parameter values for different samples are

detailed in Supplementary Information Fig. S5 and Tables S1-S4.

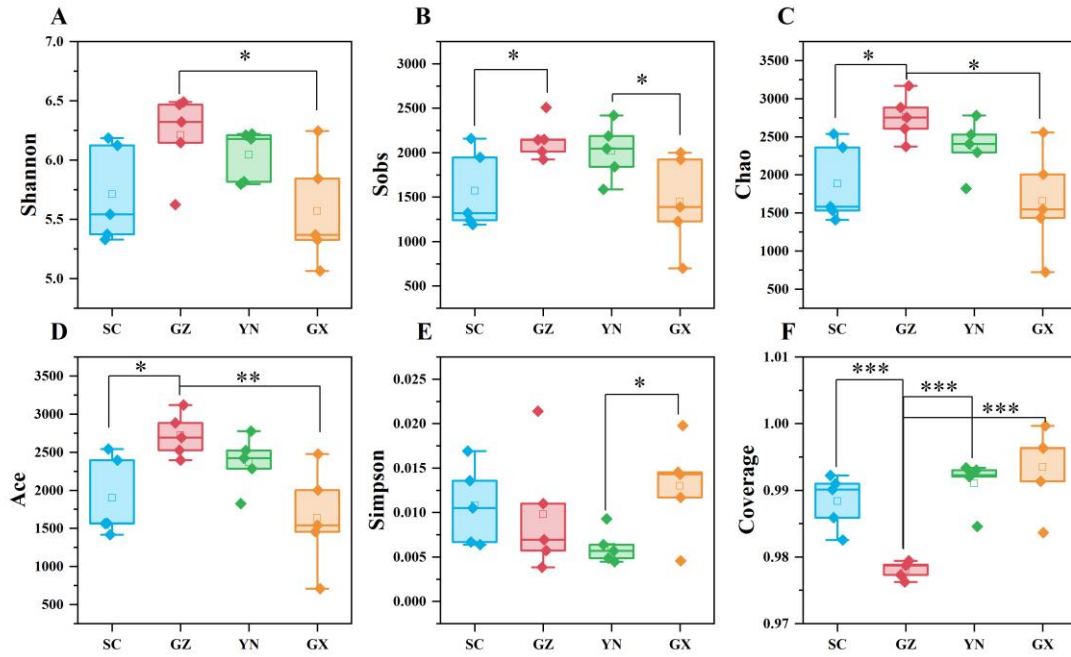


Fig. 4. Microbial community α -diversity in different soil samples from SC, YN, GX, and GZ sites. (A) Shannon diversity index; (B) Sobs richness at the OTU level; (C) Chao richness at the OTU level; (D) Ace richness at the OTU level; (E) Simpson diversity index; and (F) Coverage's index. Statistical differences between SC, YN, GX, and GZ sites were performed using the Student's *t*-test ($p \leq 0.05$ is marked as *, $p \leq 0.01$ as **, $p \leq 0.001$ as ***).

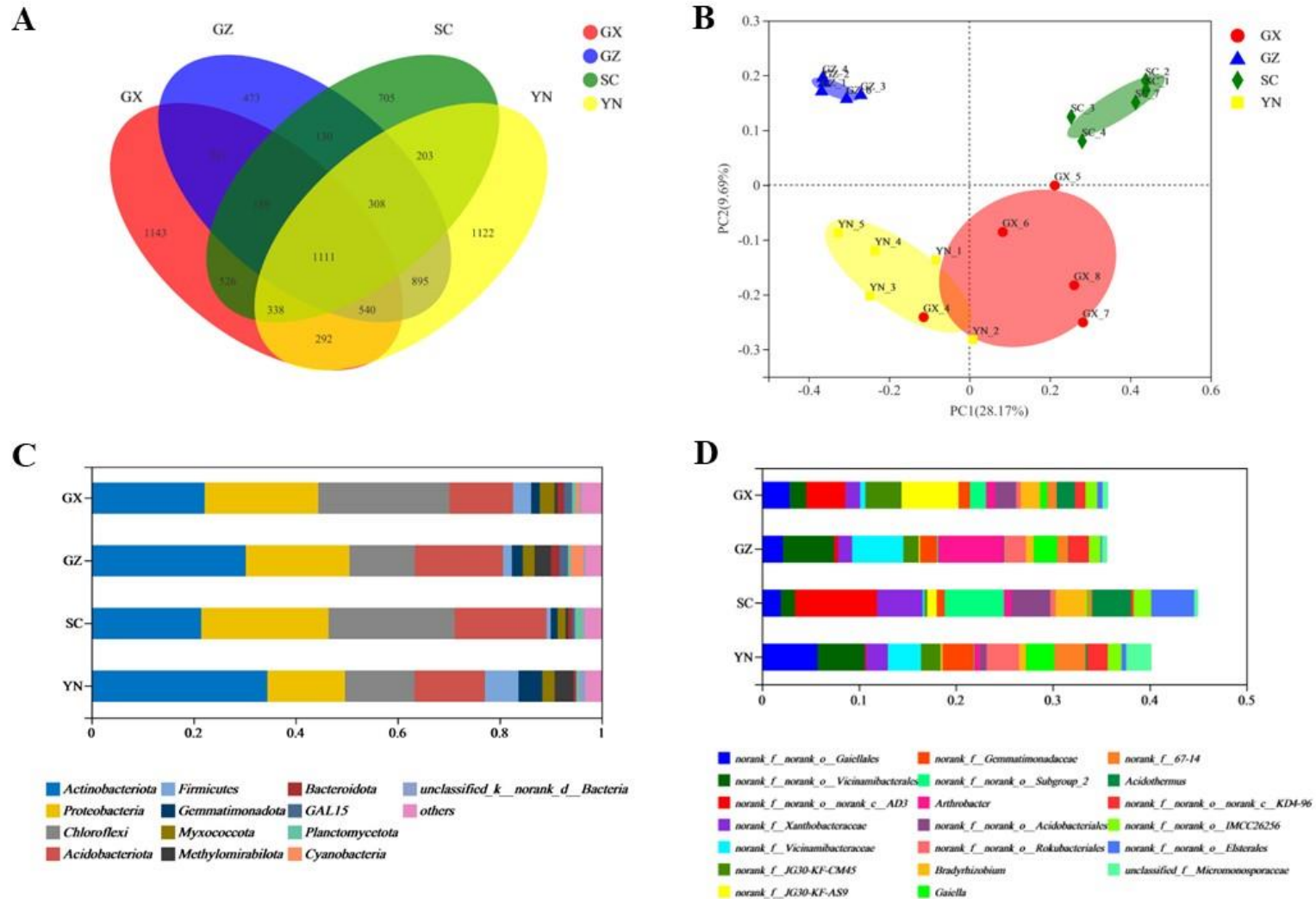


Fig. 5. Comparison of the microbial communities from GX, GZ, SC, and YN sites. Venn diagram (A) and Principal co-ordinate analysis (PCoA, B) showing the variations of microbial structure at the OTU level. Soil bacterial community composition shows the top 20 most abundant phyla (C) and genera (D).

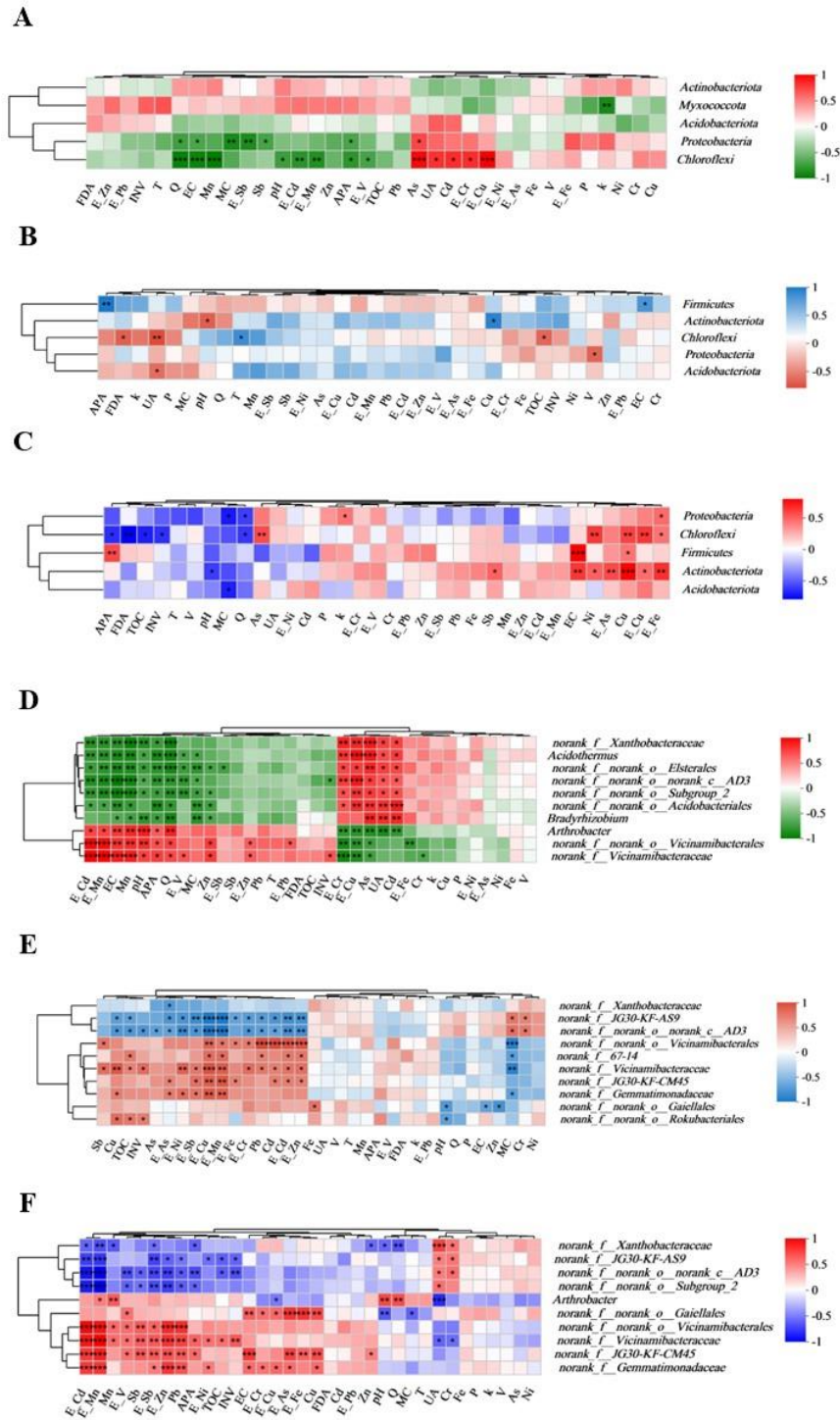


Fig. 6. Spearman correlation heatmap of the top five most abundant phyla (A: active sites; B: inactive sites; C: active and inactive sites) and the top ten most abundant genera (D: active sites; E: inactive sites; F: active and inactive sites) of the microbial communities, the environmental factors, microbial activity characteristics, and total and bioavailable metal(loid)s contents (E). *r*-values are plotted in different colors; the right side of the legend shows the color range and the corresponding *r*-values. Significant values are shown as * $p < 0.05$; ** $p < 0.01$; *** $p < 0.001$.

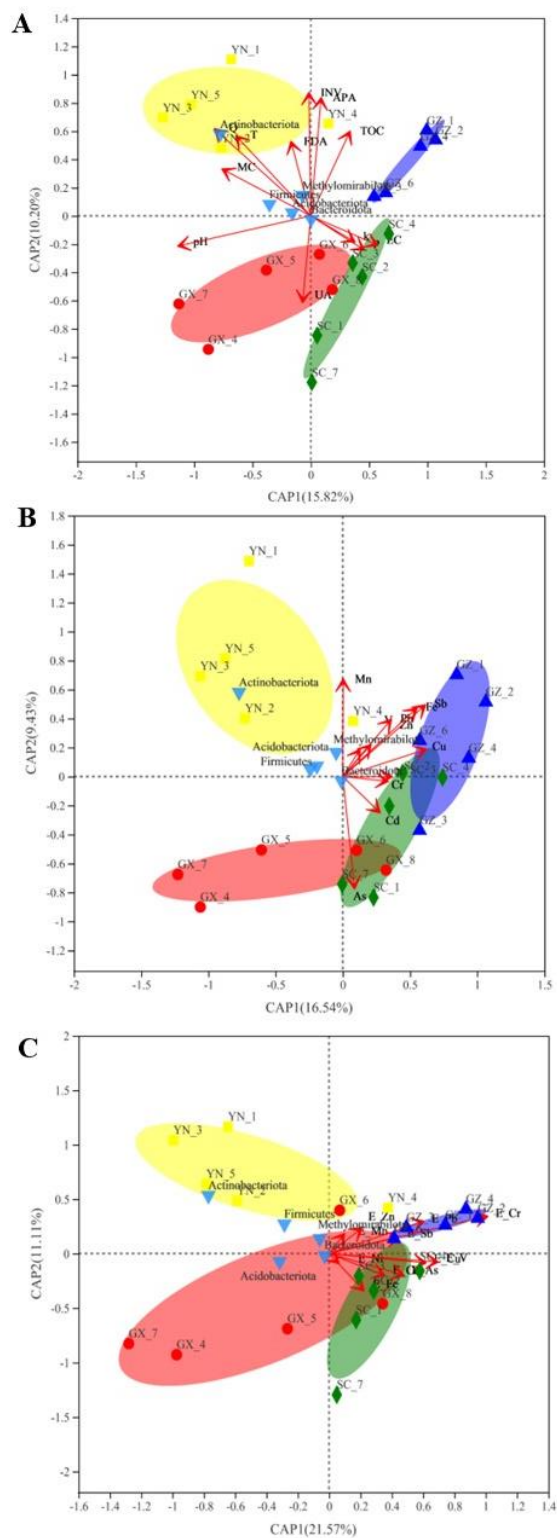


Fig. 7. Comparison of microbial communities. The distance-based redundancy analysis (db-RDA) was performed at the OTUs abundance level. The red line arrows denote the soil characteristics and microbial activity characteristics (A), and total (B) and bioavailable (C) metal(loid)s contents. The length of the arrows represents the degree of relevance between microbial communities and various factors. The percentage in the two axes indicates the eigenvalues of environmental factors.

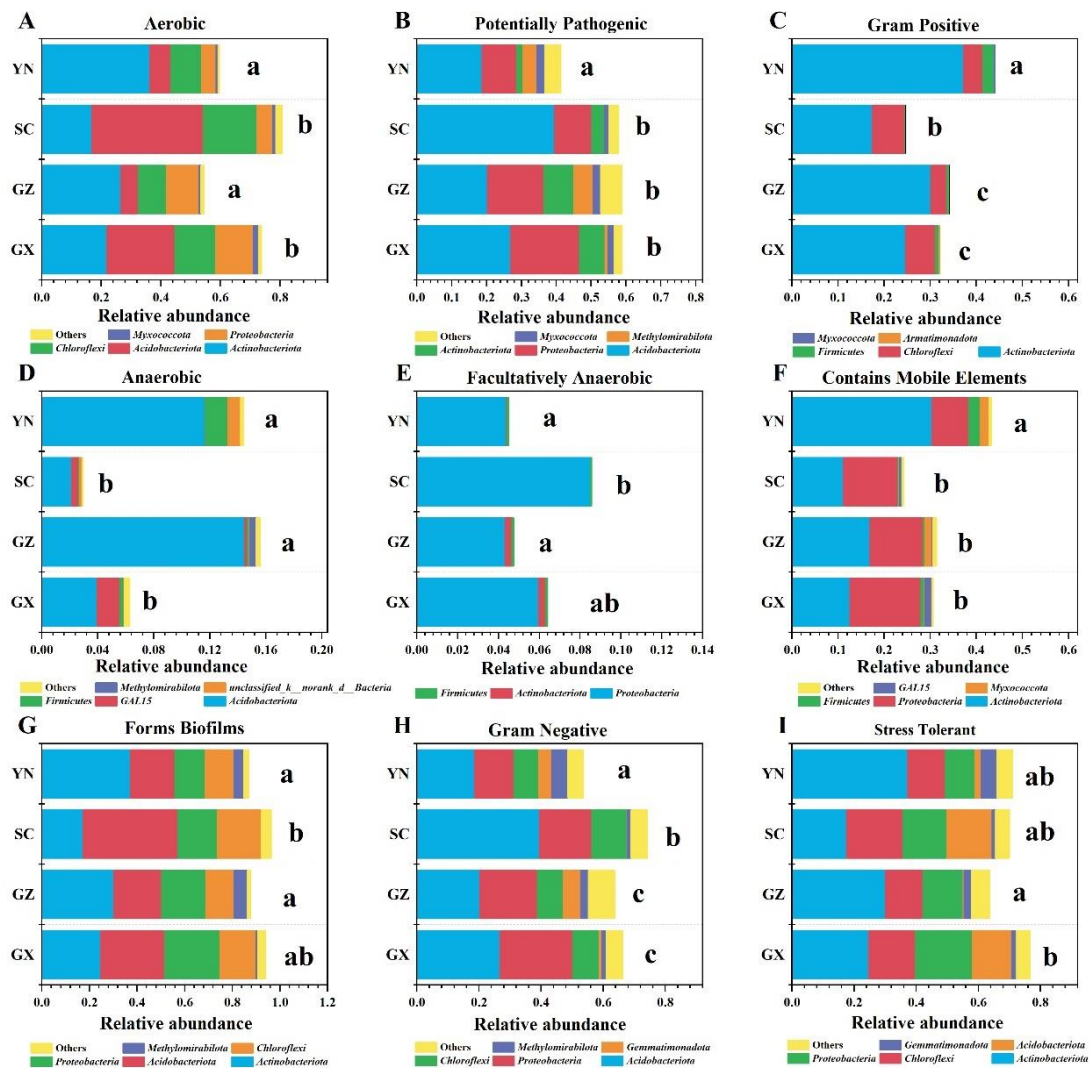


Fig. 8. The corresponding OTU contribution plots of the relative abundance of phyla possessing each phenotype (A: Aerobic; B: Potentially Pathogenic; C: Gram Positive; D: Anaerobic; E: Facultatively Anaerobic; F: Contains Mobile Elements; G: Forms Biofilms; and H: Gram Negative; I: Stress Tolerant) in the YN, SC, GZ, and GX sites are also shown. Different lowercase letters indicate significant differences between groups ($p < 0.05$).



Click here to access/download
Supplementary Material
Supplementary Material.docx



CRedit authorship contribution statement

- **Hao Li:** Conceptualization, Methodology, Writing - review & editing, Data Curation, Visualization, Writing - original draft.
- **Jun Yao:** Conceptualization, Writing – review & editing, Resources, Funding acquisition, Supervision.
- **Ning Min:** Formal analysis, Review & editing.
- **Geoffrey Sunahara:** Conceptualization, Visualization, Writing - review & editing.
- **Robert Duran:** Formal analysis, Writing - review & editing.

Declaration of interests

The authors declare that they have no known competing financial interests or personal relationships that could have appeared to influence the work reported in this paper.

The authors declare the following financial interests/personal relationships which may be considered as potential competing interests: